A STUDY ON STERILE INFLAMMATION IN THE ZEBRAFISH LIVER

A Dissertation

Presented to the Faculty of the Weill Cornell Graduate School

of Medical Sciences

in Partial Fulfillment of the Requirements for the Degree of

Doctor of Philosophy

by

Michelina Diona Stoddard

August 2018

A STUDY ON STERILE INFLAMMATION IN THE ZEBRAFISH LIVER

Michelina Diona Stoddard, PhD.

Cornell University 2018

Sterile inflammation (SI), or inflammation in the absence of microbial pathogens, is responsible for the morbidity and mortality of millions of Americans every year. Decades of pathologic research have shown that innate immune cells play a critical role in the initiation and resolution of SI; however, researchers do not understand why SI exists or what stimulates this process. A barrier to progress in the field has been the lack of a suitable intra-vital system with which to image SI. *In vitro* systems poorly recapitulate complex tissue-level inflammatory responses, and murine models require surgical procedures to perform intra-vital imaging. To address these issues, we have developed a system with which to study SI in zebrafish larvae.

Zebrafish larvae are an ideal system in which to study SI because their small size and transparency allows for intravital imaging without causing damage to the animal. We adapted the Nitroreductase/Metronidazole (NTR/Mtz) system in order to induce tissue damage via production of reactive oxygen species (ROSs) in the livers of zebrafish larvae. Transgenic leukocyte reporter lines and fluorescent dyes were crossed with animals that express NTR in hepatocytes and imaged intra-vitally using our spinning disk confocal microscope.

We found that the NTR/Mtz system induces apoptosis and necrosis in hepatocytes within 24hrs of Mtz exposure, and that reactive oxygen species are present during this process. Leukocyte recruitment to the liver corresponds with the onset of these cell death processes. Furthermore, neutrophils and macrophages show distinct behaviors in both the timing of their recruitment and their morphology upon

arriving to the damaged liver. Macrophages appear to patrol the liver and phagocytose (presumably damaged) hepatocytes within 24hrs of Mtz exposure. Neutrophils are generally not recruited to the liver unless Mtz has been removed from the bathing media and the larvae are allowed ~24hrs to recover. This system has enabled us to observe cell death and inflammation in vivo and in real time in the larval zebrafish liver. We believe that this adaptation of the NTR/Mtz system will enable progress in the field of SI.

BIOGRAPHICAL SKETCH

Michelina Diona Stoddard is a student in the Tri-Institutional MD/PhD program at Weill Cornell Medical College. She graduated from Mount Baker Senior High School in 2005, and after a year studying classical voice at Cornish College of the Arts in Seattle realized that her true passion was science and medicine. She changed her major to Biochemistry and studied at Seattle Central Community College for two years to obtain her Associate's degree in Science. After her first experience in a research laboratory, Michelina decided to pursue the MD/PhD educational path. In the summer of 2008 Michelina participated in the competitive undergraduate research program Hooked on Photonics. During the program she worked in Dr. Christine Luscombe's laboratory at the University of Washington (UW) and published a paper on her work with organic photovoltaic polymers. Michelina then transferred to UW that Fall and was accepted into the highly competitive Neurobiology major in 2009. Michelina continued her research at UW, where she received the Mary Gates Research Scholarship to support her research endeavors. Michelina graduated with a Bachelor's degree in Neurobiology in 2011 with Departmental Distinction. In the summer of 2012 Michelina enrolled in the Tri-Institutional MD/PhD program and joined Dr. Philipp Niethammer's laboratory in the Fall of 2014. Presently, Michelina will be returning to medical school to complete her medical degree. Michelina has not yet decided upon a medical specialty, but she is confident that her training in Dr. Niethammer's laboratory will guide her clinical reasoning and research questions throughout her career.

This work is dedicated to all of the individuals in my life who have supported my passions and made my education possible. Dr. Brad Stone, Dr. Christine Luscombe, Dr. Gwenn Garden and Dr. Suman Jayadev, who mentored and supported my undergraduate research and without whom I would not have a scientific career. Dr. John Ravits, who inspired me to pursue the MD/PhD career path. Tess Cabasco-Cebrian and Dr. Thomas Schultz for being the best bosses a TA could ask for. To my other undergraduate professors and advisors: Dr. Wendy Rockhill, Dr. Nada Oakley, Dr. Michael Kennedy, Dr. Mary-Claire King, and many others. To my friends and family who have supported and encouraged me during this journey: Robert Michael Stoddard, Lora Jean Stoeckl, Victoria Stoddard, Crystal Stoddard, Evan Stoddard, Emma Stoeckl, David Stoeckl, Heather Maas, Dr. Amy Kwon, Dr. Zoe Chung, Dr. Annabel Chang, and Jack Vorhies. To my fellow classmates, who have been like family to me these past five years: Dr. Andrew Milewski, Dr. Jim Castellanos, Lisa Noble, Phillip Nussenzweig, Dr. Diana Wang, Doowon Huh, Mytrang Do, Dr. Anfei Li, Raul Martinez, Margaret Fabiszak, Dr. Gustav Cedarquist, Dr. Alexendar Perez, and John Zhuang (rest in peace). To the administrators and supportive staff at the Tri-Institutional MD/PhD Program and Weill Cornell Medical College, especially Dr. Ruth Gotian, Renee Horton, Dr. Olaf Andersen, Dean Sibel Klimstra, Dean Dana Zappetti, Dean Barbara Hempstead, and Dean Yoon Kang. To Dr. Nelson Sanchez, my mentor and collaborator with LGBT health initiatives. To my therapist Dr. Carolyn Feigelson, who has made it possible for me to continue my studies. And last but not least, to my dog, Geordi LaForge, who has provided immeasurable support while writing this dissertation.

ACKNOWLEDGEMENTS

I would like to thank my primary mentor, Dr. Philipp Niethammer for his guidance, mentorship, and enthusiasm since I joined his lab. I would also like to acknowledge my thesis committee, Dr. Todd Evans, Dr. Michael Overholzer, Dr. Jaime Chu, and Dr. Jennifer Zallen, for their feedback and contributions to this project. Financial and administrative support was provided in part by the Tri-Institutional MD/PhD Program.

TABLE OF CONTENTS

LIST OF FIGURES

LIST OF ILLUSTRATIONS

LIST OF TABLES

CHAPTER 1: INTRODUCTION

Sterile inflammation (SI), defined as inflammation that occurs in the absence of microbial pathogens[1–4] is a growing problem. Each year, millions of individuals in the United States alone will suffer from the effects of SI due to disease processes such as myocardial infarction (MI), stroke, asthma, non-alcoholic fatty liver disease (NAFLD), and gout[3,5–8]. SI has been documented to worsen outcomes for patients suffering from these, and other, disease processes. Although the precise mechanisms by which SI worsens tissue damage remains unclear, the hallmarks of SI (cell swelling, tissue damage, leukocyte infiltration, and cytokine and chemokine production (Figure 1.1)) remain consistent among various disease processes and suggest innate immune system involvement. The innate immune system has been shown to contribute to the major hallmarks of SI[3,5–7,9], yet researchers are only

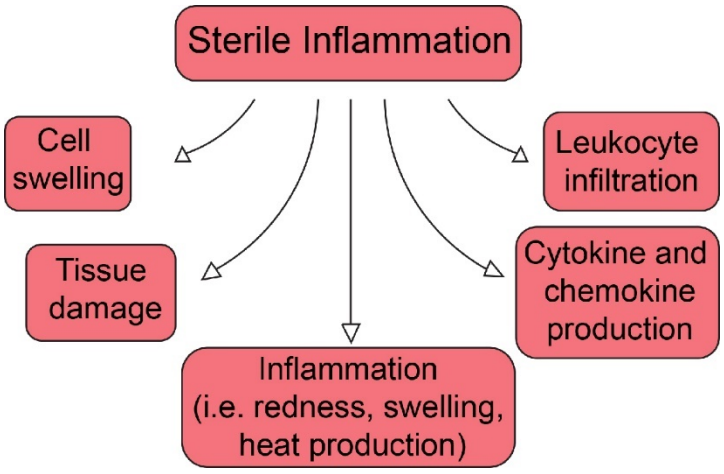

Figure 1.1: Schematic representation of the hallmarks of sterile inflammation.

beginning to understand the intricacies of this process. The main justification for studying SI has been to identify novel therapeutic targets to treat disease, but SI is also intriguing from a basic science perspective. This thesis will explore relevant questions and progress in the field of SI. Primary data from a novel intravital imaging system in zebrafish will be presented and discussed, along with a thorough description of the

methods used in this study. Finally, this thesis will discuss how this system can contribute to the scientific and medical understanding of SI.

The importance of understanding SI

SI has become interesting to scientists for two main reasons. First, it is of medical interest because of its prevalence in non-infectious disease in the US, and that the prevalence of diseases with SI processes is expected to rise in coming decades[10–13]. In the United States infection is no longer a leading cause of death; therefore, people die at an older age due to complications of chronic disease (heart attack, cancer, etc)[10,14]. SI plays an integral role in these processes, as it has been associated with poorer prognosis for patients[3,5]. These phenomena lead one to ask why SI is so prevalent in human diseases since it seems to have only negative outcomes for the host. The signaling pathways that become active in SI are present throughout the animal kingdom, including invertebrates[15]. Therefore, if SI produces only negative outcomes for the host, it seems unlikely that SI would be highly conserved across the phyla. This observation begs the question of whether SI provides an evolutionary advantage to the host, or whether SI is a coincidence of inflammatory activity in a host whose immune system adapted to fight infection. This project attempts to address the question of which process(es), signal(s), and inflammatory mediator(s) may be active in the zebrafish in circumstances of oxidative damage *in vivo*, allowing us to better understand SI in a live animal.

SI as an evolutionarily advantageous process

The question of whether SI is representative of a process that may be beneficial to the host has been raised in recent years. A recent review indicated that inflammation is beneficial—and perhaps even necessary—in the healing and resolution phase of certain disease processes in the liver[8]. One example in their discussion is that liver failure (acute or chronic) can increase an organism's susceptibility to infection, so

inflammation may occur prophylactically to prevent infection. Generally speaking, however, liver compromise is unnecessary for microbes to infect a host. For infection to take place, pathogens must overcome several obstacles. In most circumstances, external epithelial surfaces provide an effective barrier that prevents most pathogenic infections[16]. However, if the epithelial barrier has been breached, pathogens could

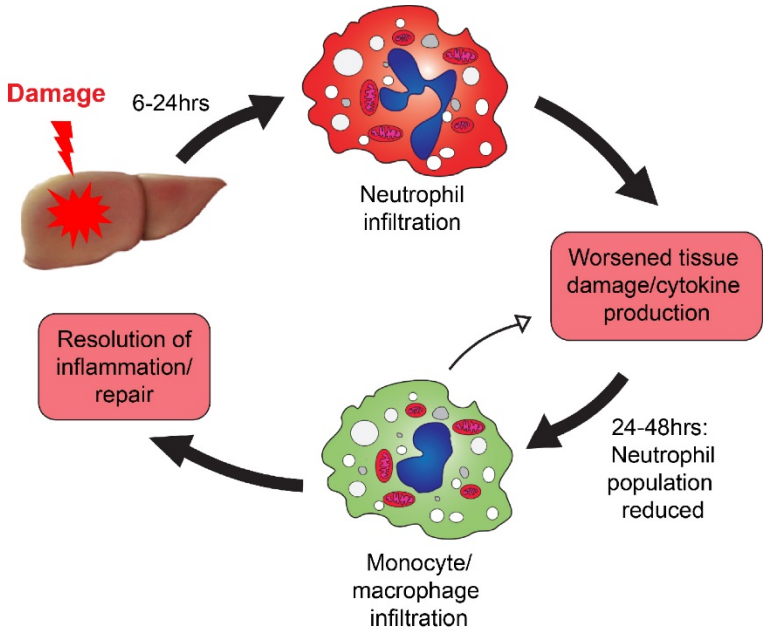

Figure 1.2: Canonical representation of neutrophil and macrophage involvement during SI. Neutrophil recruitment to the site of injury occurs 6-25hrs post-injury followed by macrophage recruitment. Depending on the macrophage's state of activation it can either worsen or resolve inflammation by initiating the repair and healing process.

then cross the barrier and infect the host. Mucosal surfaces are more vulnerable to infection and generally have a significant amount of immune activity associated with the epithelial barrier (such as the production of IgA antibodies and antigen-presenting cells near the epithelium)[16]. Since epithelial barriers are so important for protecting a host against pathogens, and since most pathogenic microbes cannot cross the epithelium unless it is breached, perhaps it is more effective for leukocytes to respond to an epithelial injury rather than the pathogen itself. Essentially, a sterile wound is

capable of becoming infected after the initial injury. If leukocytes could only travel to sites of infection, the pathogen would have a bit of time to replicate and invade the host. Leukocyte migration to signals from the injury, rather than the pathogen, would be of immense benefit to the host because leukocytes already present in the wound can neutralize pathogens as soon as they arrive.

Experimental evidence for benefits of SI

Other members of our laboratory also questioned whether neutrophils could mount an immune response to pathogen-associated molecular patterns (PAMPs) agents alone, or if additional signals were needed to stimulate robust neutrophil recruitment. In this study, Pseudomonas aeruginosa (PA) was injected into the otic cavity of zebrafish larvae expressing fluorescent leukocyte markers[17]. The study suggested that sterile and infectious stimuli together generate an inflammatory response that is stronger than that generated by either sterile or infectious stimuli alone[17]. Furthermore, sterile and infectious signals are not equally capable of activating inflammation *in vivo*; in fact, SI signals may be more effective than pathogenic signals[17]. After extensive experimentation, the authors found that injecting PA into the otic cavity was much more effective at inducing leukocyte recruitment if the otic cavity was ruptured during the injection[17]. In other words, the addition of damage-associated molecular patterns (DAMPs) from epithelial cells lining the otic cavity augmented the immune response to bacteria. Injecting bacteria in a solution of hypotonic injection medium (as opposed to injection medium that is isotonic to the zebrafish larval intestinal fluid) produced a stronger immune response[17], perhaps by causing local tissues to swell. Bacterial stimulation provides some input for the inflammatory process: injecting PA with null mutations of lipopolysaccharide (LPS) reduced neutrophil recruitment, whereas injecting multi-flagellated PA did not change the immune response[17]. The authors also discovered that blocking $cPLA_2$ transcription

using a morpholino reduced leukocyte recruitment in this model, and that injecting $cPLA_2$ mRNA into the single-cell staged embryo increased leukocyte recruitment[17]. This is consistent with a prior study from our lab that showed that nuclear swelling is sufficient to induce $cPLA_2$ translocation to the nuclear membrane, where it liberates arachidonic acid (AA) from the nuclear membrane[18] to drive inflammation. Finally, mortality in larvae with a ruptured otic cavity was much lower (44% survival) in larvae that did not suffer damage to the otic cavity (15% survival) [17]. Therefore, DAMPs/SI signaling promotes survival, indicating that DAMP signaling may be beneficial for the host. Inflammation in this infection model is greatly enhanced by sterile signals (i.e. otic cavity rupture during the injection), indicating that bacterial insults play a smaller role in this process.

Evidence for SI as maladaptive response

SI signals may provide benefit in protecting a host from pathogenic infection in the case of epithelial barrier breach. When we consider this process in the context of SI in the absence of epithelial barrier breach, however, it becomes less clear whether SI provides an advantage for the host. Since processes like MI and gout typically occur in sterile environments, it is difficult to rationalize the presence of neutrophils in these injuries[5,19–21]. While the concept of neutrophils migrating to necrotic tissue to remove debris is reasonable, the question of whether (and/or how) neutrophils exacerbate inflammation and tissue damage remains. A recent study in mice showed that while neutrophil activation may not contribute significantly to liver damage during paracetamol (APAP) toxicity, it may actually be a critical part of host defense or injury resolution following APAP overdose[22]. It has been known for some time that macrophages can switch from an activated pro-inflammatory state into a healing, anti-inflammatory state during SI[6,23], and that they may require inflammatory signals from neutrophils to do so[8,24,25]. The processes are actively being researched, but one of the

central questions (how and why neutrophils are recruited to the site of sterile injury) has yet to be fully addressed. In order to discuss this process in more detail, it is useful to review the innate immune system and its role in SI and disease pathogenesis.

Innate Immunity in SI

SI has been of increasing interest to investigators as the leading causes of death in the United States have shifted from infectious etiology (such as tuberculosis and influenza) to sterile etiology (such as heart disease and cancer)[10]. Although the innate immune system has been recognized as an integral component of SI[26,27], the mechanism of how the innate immune system contributes to SI did not become of interest to investigators until recently. In order to understand how the innate immune system functions during SI, it is helpful to review the overall functioning of the innate immune system, which has been best characterized in terms of its anti-microbial functions.

The innate inflammatory response

The inflammatory response is induced by tissue injury or pathogenic invasion of the host. The diameter of blood vessels near the site of injury increase, causing heat, swelling, and redness[16]. The release of inflammatory cytokines, chemokines, and bradykinins causes pain and leukocyte recruitment to the injury[16]. Neutrophils are the first responders to injury and infection[2,25,28,29]. They respond to tissue damage and/or pathogens within approximately 30min and remain at the wound site for 12-24hr to clear debris and protect the host against opportunistic infection[4]. Within the first hour of the process, macrophages (sometimes from surrounding tissues) are recruited to the site of injury and begin to clear the remnants of necrotic cells[30]. 8-12h later pro-inflammatory monocytes enter the wound and transition into regulatory monocytes over the course of 48hrs[31]. While in the wound, monocytes mature and engulf cytotoxic cellular debris and pathogens to prevent further damage to the host. In this

way, macrophages prevent dead and damaged cells from releasing cytotoxic intracellular DAMPs into the extracellular space while producing anti-inflammatory cytokines such as TGF-β[3,5,7].

Innate immunity in infection

Historically, the innate immune system's primary role in a host is thought to be infection clearance[16]. This function is vital to the survival of the host; without it, the host would succumb to infection. In order to respond to pathogenic threat, leukocytes rely on a limited set of receptors (called pattern recognition receptors (PRRs)) to recognize and attack viruses and bacteria[16,32]. PRRs specifically respond to molecules known as PAMPs, which are simple, regular patterns of molecular structure (such as mannose-rich oligosaccharides and LPS) that are almost exclusively produced by pathogens[16,17,32–36]. PRRs also identify and respond to "self" proteins during SI, as will be discussed in more detail below.

The process of tissue infection can be described in fairly general terms, although it is important to note that many pathogens have developed unique pathophysiology for evading the immune response. As previously discussed, pathogens must first gain entry into the host, whether it be incidentally after an injury to the epithelial barrier or by overcoming host defenses[16]. After entry the pathogen will be able to migrate into a tissue, where it will likely be recognized by tissue macrophages[37]. These macrophages produce inflammatory signals to recruit other inflammatory cells to the site of infection. Of these, activated neutrophils will be the first leukocyte subpopulation to arrive to the site of infection[37].

Immune effector functions such as complement and antibody production are also initiated. The complement cascade can be activated by either the classical, lectin, or alternative pathways, at which time a few key processes occur[16]. The release of complement proteins C3a and C5a can cause inflammation and induce leukocyte

recruitment[38]. Additionally, the complement proteins C5b and C6-C9 can assemble on the surface of a pathogen and generate pores that directly lyse the pathogen[16]. Complement protein C3b binds to the surface of pathogens, making them visible to phagocytes, which opsonize (that is, engulf) the pathogen[37,38]. Both macrophages and neutrophils can phagocytose pathogens, taking them up into phagosomes. Phagosomes can fuse with lysosomes within the cells, which contain noxious substances like the O_2^- superanion and H_2O_2 to neutralize the pathogen—a process known as the oxidative burst[7,8,39]. Macrophages and neutrophils then produce cytokines and chemokines that perpetuate the inflammatory response[16,40,41].

Pattern recognition in innate immunity

A theme in both sterile and non-sterile inflammation is the ability of the innate immune system's ability to recognize and respond to molecular motifs in both pathogenic and "self" structures. Researchers have traditionally thought that PRRs existed primarily to recognize PAMPs. Many PAMPs have been identified to date. In addition to LPS and mannose-rich oligosaccharides, researchers have discovered that peptidoglycans, unmethylated CpG DNA, dsRNA, and other molecules activate the innate immune system[16,32–35]. Many PRRs coincidentally recognize host molecular motifs called DAMPs, which are thought to drive SI[5,16,32,36,42]. The fact that these receptors recognize both PAMPs and DAMPs inspires additional questions. One might question whether DAMPs are in some way derived, or evolved from, PAMPs. Additionally, does the innate immune system preferentially respond to PAMPs as opposed to DAMPs, or vice versa? For instance, if tissue injury stimulates innate immunity more robustly than bacterial pathogens, and since these two processes seem to drive inflammation synergistically, shouldn't each DAMP/PAMP be recognized by a different PRR? Or, are there additional co-signaling factors that bolster the immune response that remain to be characterized? There is an added layer of complexity to this

question when we consider the wide variety of PRRs and the molecules that stimulate them.

PRRs are diverse, comprising different receptor families and sub-groups. Each PRR responds to at least one PAMP or DAMP, and different PRRs can induce different effector functions. For example, mannose-binding lectin is a free-circulating PRR. It binds to bacterial mannose, making the bacteria more susceptible to opsonization by phagocytes[37]. There are also mannose receptors on the surface of leukocytes. One, called the macrophage mannose receptor, also acts to facilitate phagocytosis of the pathogen[37,42,43]. PRRs called scavenger receptors are located on the surface of leukocytes and recognize anionic polymers and acetylated LDLs[16,44]. To date, the best studied PRRs are toll-like receptors (TLRs) and Nod-like receptors (NOD).

Several TLRs, especially TLRs 1, 2, 4-7 and TLR 11, activate the NF-κβ transcription factor via the MyD88 signaling adaptor molecule, which causes the cell to produce pro-inflammatory responses (Figure 1.3)[16,33,35]. TLR3 is an exception to this, as it utilizes the TRIF-dependent pathway. Some TLRs are present on the plasma membranes of cells where they can recognize PAMPs/DAMPs in the extracellular space. TLRs can also be present intracellularly in the endosomal membranes[16,35] to induce inflammation in the event that a pathogen has been opsonized by a leukocyte. NOD1/2 are NOD-like receptors that localize to the cytosol of the cell and utilize some of the same pathways as TLRs[32,45]. They belong to the CARD family of genes and can activate NF-κβ to induce expression of inflammatory factors such as IL1, IL6, IL8, and TNF-α[32,33,45,46]. Activation of the TLRs and/or NLRs results in inflammasome formation and subsequently IL-1β and IL-18 release via Caspase 1 signaling[35].

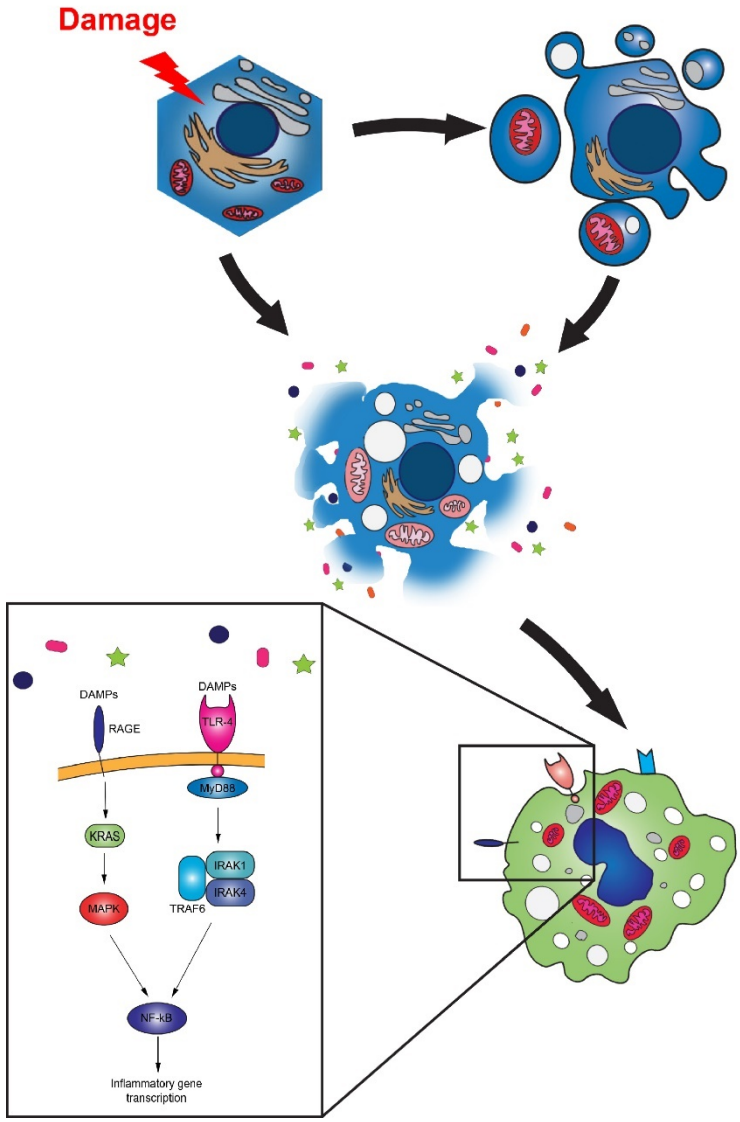

Figure 1.3: Damaged hepatocytes undergo apoptosis or necrosis and release DAMPs. DAMPs are recognized by nearby cells and leukocytes, stimulating the production of inflammatory mediators like IL-1β through the NF-κβ pathway.

Conservation of pattern recognition

PRRs, PAMPs, and DAMPs tend to be conserved across the animal kingdom, although variation among different species is quite common. The TLR family of genes has been described in zebrafish and was recently found to have a subfamily of genes that have a large number of orthologs in TLR signaling[35,47]. Zebrafish also contain at

least 8 non-mammalian TLRs, and may contain more than one genomic copy of each receptor[34]. Overall, TLR and NLR signaling leads to a pro-inflammatory state in the cell. Aside from the non-mammalian TLRs, TLRs and NLRs are fairly conserved in the zebrafish with respect to humans. This PRR ligand specificity is well conserved in zebrafish, increasing the value of zebrafish as a model organism for studies on inflammation[47].

Zebrafish are far from being the only organism for which DAMPs are conserved with mammals. Even invertebrates such as *D. melanogaster* have conserved DAMP/PAMP recognition[15]. Since multiple species of hosts could potentially be infected by some of the same pathogens, it makes sense that PRRs are conserved in the animal kingdom. Similarly, many DAMPs are highly conserved among animal species. This is because DAMPs are essentially normal intracellular proteins that are normally sequestered from the immune system and become immunogenic when they are released from dying cells[3,48]. Several types of DAMPs have been identified to date, ranging in complexity from single molecules such as ATP[49,50] to complex peptides such as S100 proteins[3,4,7,8,26,48,51–54]. Additional DAMPs include nuclear and mitochondrial DNA[55,56], N-formyl peptides[57,58], and heat shock proteins[59,60]. Essentially, if a molecular motif resides in a cell (or other space that prevents recognition from the immune system) is released into the extracellular space, that substance may act as a DAMP[6,61]. Although SI and DAMP spillage is considered to be a result of necrotic cell death, apoptotic cells can release “find me” and “eat me” signals to macrophages. This is part of a non-inflammatory form of cell death[5,51,57] since macrophages function to eliminate apoptotic cells to prevent DAMP release.

Inflammasome activation in SI

PRRs, especially TLRs, are crucial for the activation of SI[6]. For example, TLRs 2 and 4 have been studied in models of ischemia reperfusion injury (IRI) by MI

and acute kidney injury[6]. Most TLRs signal through the IL-1β—MyD88 axis in response to sterile injury; which is responsible for initiating production of pro-inflammatory cytokines and chemokines by activating the inflammasome[62,63]. Inflammasome activation requires two distinct signals. The first signal induces transcriptional upregulation of several molecules (including inflammasome components), pro-IL-1β, and pro-IL-18[3]. The second signal brings the inflammasome components together to form the inflammasome complex and induce Caspase-1 cleavage, which causes cytokine activation and secretion[3,48]. The precise mechanism by which the inflammasome activates neutrophil recruitment is an area of active research. One explanation is that cytokine/chemokine signals directly recruit leukocytes to the site of injury. Alternatively, cytokine/chemokine signals could act indirectly by stimulating sentinel cells near the injury to produce inflammatory cytokines, recruiting leukocytes to the area[3]. In addition to stimulation by DAMPs/PAMPs, there are many layers of complexity to inflammasome activation in SI. For example, there is some evidence to suggest that the IL-1β—MyD88 pathway recruits neutrophils to sites of SI, but not to bacterial infection[54] even though the same surface receptors (eg. TLR-4, etc) are thought to be involved. Thus, there may be additional pathways and signals involved in this process that have yet to be characterized.

Current questions in the role of pattern recognition in SI

Recent work indicates that DAMPs may only represent part of SI. Recently there has been debate regarding whether DAMPs act directly on leukocytes as chemo-attractants or whether they stimulate sentinel cells, which then produce signals that promote inflammation. One study showed that this may be the case with ATP. The authors had hypothesized that ATP released from dying cells acts as a chemoattractant to guide neutrophils to the site of sterile injury[4]. To test this, the authors administered

apyrase, an ATPase, to a mouse liver that had been sterilely damaged. They found that while ATP hydrolysis resulted in fewer neutrophils to the damaged liver, it did not impair their ability to move toward the injury[4]. They then concluded that ATP does not function as a chemotactic signal, but instead initiates inflammation by producing signals that promote neutrophil adhesion. This is only one example of how DAMPs are being tested for their role in SI, but it demonstrates how much work is needed in the field to better understand DAMPs and their molecular interactions.

The story of DAMP signaling in SI is further complicated when we look at

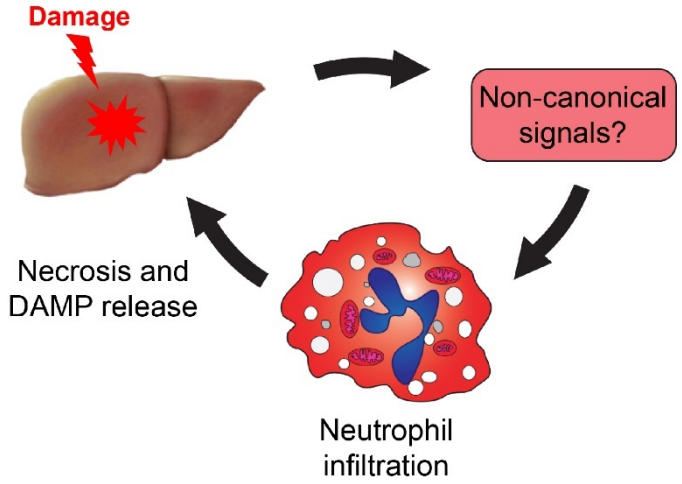

Figure 1.4: Neutrophils may depend on non-canonical signals to travel to the site of sterile injury before cellular necrosis begins. If that is the case, neutrophils may contribute to the tissue damage and worsen SI.

examples of IRI in mice. In IRI, cells in areas of ischemia were known to retain their morphology and metabolic function to some degree; however, restoration of blood flow to the area results in significant necrosis and neutrophil recruitment to the infarct[29,64,65]. Researchers began to ask whether the necrotic cells themselves were recruiting neutrophils, or whether the neutrophils were responding to some other signal that the ischemic cells released upon reperfusion (Figure 1.4), causing neutrophils to enter the ischemic injury and lyse damaged cells via their cytotoxic

functions. Several studies have supported this hypothesis, including one in which researchers knocked out IRF-3 in mice, which is necessary for neutrophil chemotaxis. The study showed that the IRF-3 knockout (KO) mice were consistently protected from IRI in this model, which was similar to the results observed in MyD88 KO mice[64,66]. They also found that the livers from MyD88 KO mice suffered significantly from the IRI, but that the damage was not as severe as that seen in WT controls. Therefore, this is a complex process that likely cannot be attributed to a single pathway or group of receptors.

SI in disease pathology

SI includes a wide variety of injuries and disease processes. For example, inflammation resulting from injuries sustained as a result of sterile surgical procedures are considered SI[7,64,67]. Processes involving subcutaneous/epithelial injury are relatively simple to study *in vivo* because the injury and healing process can be observed directly without surgery. Vertebrate systems such as zebrafish have proven useful for such studies since cutaneous epithelial subtypes can be labeled with transgenic reporters and imaged intravitally[68–71]. As described elsewhere in this chapter, our lab has explored important questions relating to the importance of SI during epithelial barrier breach, which is one of the most direct routes of microbial infection[16,37,72]. The recent paper by Huang, et al., discussed earlier in this chapter, describes a scenario in which SI signals bolster leukocyte recruitment to the otic cavity in a model of infection in zebrafish[17]. Epithelial barrier breach in nonsterile environments poses an important problem to an organism: the host must have a way to clear a potential source of infection (such as a laceration or abrasion) before the pathogen has an opportunity to infect the host. Therefore, it makes sense that breaching the epithelial barrier would induce inflammation in order to prevent microbes in a wound from establishing infection in the host.

However, we also know that SI occurs in instances where the epithelial barrier is not breached[1,2,6,13,21,51,73]. The recruitment of neutrophils and macrophages in clinical cases of IRI has been well known for decades in the field of pathology. It would seem that SI is a harmful, rather than beneficial, process[64,66]. In addition to IRI, non-infectious hepatic insults such as chronic cholestasis, alcoholic fatty liver disease, and drug toxicity contribute to dysregulated inflammatory responses in the liver[5,8,51,52,54,61,74,75]. Non-alcoholic steatohepatitis/non-alcoholic fatty liver disease (NASH/NAFLD) has become a popular system in which to study SI in recent years due to relative ease with which researchers can recapitulate symptoms and pathology in rodents and zebrafish[11,12,76,77]. This work has become increasingly relevant, as up to 25% of Americans are expected to suffer from NASH/NAFLD in coming years due to increasing rates of obesity and fat-rich diet[11,78]. While the mechanisms by which fatty deposits cause inflammation in the liver is an area of ongoing research, the association between NASH and chronic activation of the innate immune system has been well characterized[1].

Crystal deposition into tissues also leads to SI. For example, monosodium urate and calcium pyrophosphate dihydrate crystals cause gout and pseudogout, respectively, when crystal accumulation disrupts joint tissues and causes neutrophilic infiltration of the joint[20,51]. Atherosclerosis, characterized by the hardening and inflammation of major arteries, is a common disease affecting the majority of Americans by late adulthood. Atherosclerosis causes inflammation when excess cholesterol crystals are phagocytosed by macrophages, inducing an inflammatory response when the macrophages are unable to clear the crystals, causing the macrophages to take on a “foamy” appearance and produce inflammatory mediators[13,19]. These processes are also active in the brain. β-amyloid plaque accumulation in the extracellular matrix induces microglial cells (the resident

macrophages of the brain) to activate and produce reactive oxygen species (ROSs), pro-inflammatory cytokines, and chemokines[20,21].

Drug-induced liver injury (DILI) presents another special case in which SI can be induced acutely[6]. Paracetamol (APAP)-induced and idiosyncratic DILI is responsible for roughly 60% of the total cases of liver failure in the United States annually[79]. Of these cases, APAP-induced DILI is roughly four times more common than idiosyncratic DILI. APAP-induced DILI has been well characterized rodent and zebrafish models. In therapeutic doses, APAP is metabolized by UDP-glucuronosyltransferase (UDP) and sulfotransferase (SGT) and excreted in urine. In the context of APAP overdose, UGT and SGT become saturated. APAP then becomes available for metabolization into N-acetyl-p-benzoquinone (NAPQI, a highly reactive metabolite) by CYP2E1 and CYP3A4[44,80–82]. Small amounts of NAPQI are conjugated to glutathione (GSH) by phase II metabolizing enzymes. When these enzymes are saturated by APAP overdose, GSH becomes the limiting reagent of the reaction, as the amount of NAPQI overwhelms GSH neutralizing enzymes and causes GSH depletion in the liver. NAPQI then accumulates, causing mitochondrial oxidative stress by covalently binding to mitochondrial proteins[83]. This mechanism has been documented to induce inflammatory liver disease[84], although it is unclear whether neutrophil recruitment results in worsened liver damage or whether it defends against liver toxicity[44].

IRI is an interesting pathology because it represents a single process with which any tissue that relies on vascular blood supply can be affected. IRI encompasses a wide range of diseases involving SI, in part because the pathophysiology for diseases caused by IRI (e.g. heart attack, graft rejection, etc) is virtually identical among these disease processes[2,25,40,66,85]. IRI occurs when a tissue that has been deprived of blood flow and therefore becomes deplete of oxygen and other nutrients. After experiencing

a restoration of blood flow, the tissue becomes subject to damage and inflammation. The degree of tissue damage can be predicted, to some extent, by the duration of ischemia[2]. The longer the ischemia, the more ROSs are produced by the cell, which increases the degree of tissue damage upon reperfusion[2]. Other signals such as calcium overload contribute to mitochondrial dysfunction and further injury.

Redox signaling

Many disease processes, such as cancer, promote redox signaling in response to ROSs. Redox signaling is an integral part of many disease processes in the liver, including IRI, viral infection, NASH/NAFLD, and alcohol intoxication[51]. Even prolonged periods of starvation can cause NRF cellular necrosis or apoptosis and result in alterations of mitochondrial metabolism[78]. ROSs may also contribute to downstream signaling that initiates SI[54]. For a cell to detect and respond to ROSs, several things must happen. First, the cell must detect ROSs. After ROSs are detected, the cell has the use of two main redox pathways with which it can neutralize the ROSs. In the first arm, GSH conjugation (one of the most important molecules for enabling cellular function to continue during ischemia) assists with converting the ROSs into biologically inactive compounds for excretion by the host[86,87]. In the second major arm of redox signaling, ROSs are neutralized via the enzymes peroxiredoxin 1 (Prdx1) and thioredoxin (Txn)[88,89] (Figure 1.5). These processes are described in more detail below.

The detection of ROSs by the kelch-like ECH-associated protein 1 (KEAP1)/ nuclear factor like 2 (NRF2) signaling pathway is considered to be a major regulator of redox signaling[58,88,90–92]. In the absence of oxidative stress, KEAP1 binds NRF2 in the cytoplasm of the cell and prevents NRF2 from translocating to the nucleus while promoting its degradation by the ubiquitin proteasome pathway[91]. The thiol groups of cysteine-rich proteins are particularly sensitive to ROSs and electrophiles[93,94]. In the

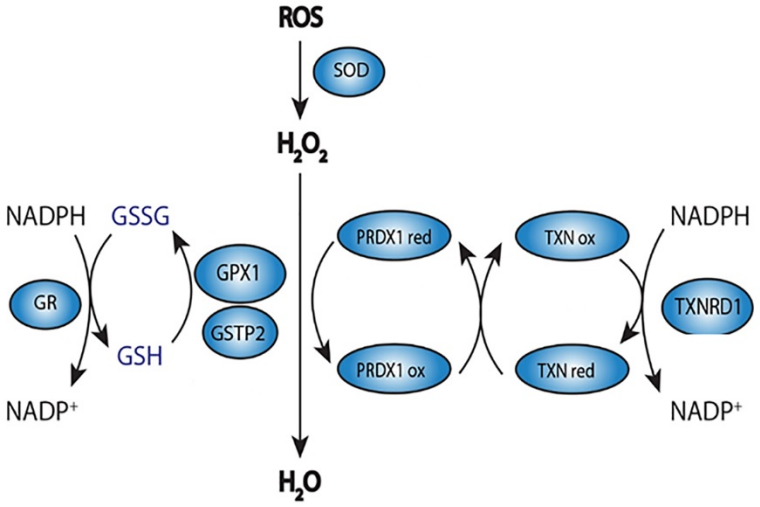

Figure 1.5: ROSs present in cells are neutralized by both the glutathione and peroxiredoxin/thioredoxin pathways.

presence of ROSs KEAP1 undergoes a structural change that releases NRF2, allowing it to enter the nucleus and bind the antioxidant response element (ARE) in promoters of genes involved with the redox response[93,94]. Activation of the KEAP1/NRF2 pathway has been described in models of liver injury, including starvation and IRI[58,64,88]. Additionally, there is evidence to support that the induction of this pathway offers a protective response; for example, KEAP1-null mice have an abundance of NRF2, causing their redox signals to become hyperactive. These mice showed resistance to several hepatotoxins such as cadmium and alcohol[88].

When NRF2 binds to the ARE element of antioxidant genes, GSH-producing and recycling enzymes are upregulated and become active[95]. GSH is oxidized and conjugated with another GSH molecule via covalent binding into GSSG as a means of neutralizing free radical and ROS insults[86]. Under normal physiologic conditions, GSSG is recycled into two GSH molecules by a number of GSH-restoring enzymes, such as glutathione reductase (GR), in what are usually NADPH-dependent processes[95] (Figure 1.5). Therefore, GSH can be recycled and used to detoxify the cell multiple times.

The second arm of redox signaling allows for detoxification of free radicals and ROSs, such as H_2O_2, by utilizing peroxiredoxins (PRDXs) and the thioredoxin/thioredoxin reductase (Trx/TrxR) system[96]. H_2O_2 is formed by NADPH oxidases, which convert O_2 into the O_2^- free radical, and the O_2^- free radical is converted to H_2O_2 by one of the superoxide dismutases (SOD)[54,96,97]. Both arms of redox signaling rely on NADPH oxidases to recycle GSH and to restore the PRDX/Trx/TrxR enzymes to their reduced form[96]. The oxidation-reduction ratio of NADPH to $NADP^+$ and GSH to GSSH controls signaling mechanisms, including transcription factor activity[90,98,99]. During situations of oxidative stress, the cell compensates for the increased demand of $NADP^+$ by producing more via the pentose phosphate pathway[90]. However, if the cell accumulates more ROSs than it can neutralize, the cell will consume all available NADPH, creating an NADPH deficiency. When intracellular NAPDH decreases in the setting of ATP depletion (as in starvation or IRI), the cell begins to decompensate because it can no longer recycle NAPDH [100].

The interactions between GSH, NADPH, and ROSs are complex and may contribute to the development of tissue damage and inflammation in multiple ways. ROSs and free radicals have been associated with cell death and inflammation[1,90,91,98]. ROSs and free radicals are produced physiologically by mitochondria during electron transport[40,44,101] and are quickly neutralized by the pathways described above. In the nitroreductase/metronidazole (NTR/Mtz) system (which will be discussed later in this chapter), ROSs are produced when NTR converts Mtz into a toxic free radical[102–104]. ROSs and free radicals can cause cellular damage in a variety of ways, including direct damage to DNA, phospholipid bilayers, and thiol-rich intracellular proteins[105]. Canonically, the upregulation of KEAP1/NRF2-dependent enzymes is considered to be a protective mechanism against ROS and oxidative stress[58,89,91]. However, there has

been increased evidence that hyperactivation of this pathway can be detrimental to the cell[90,91].

The relationship between oxidative stress and tissue damage

This concept introduces a key question in understanding the relationship between oxidative stress and tissue damage: Does ROS-mediated tissue damage induce leukocyte recruitment to the injury, or does redox signaling recruit leukocytes that travel to the injury and cause the damaged cells to die? If ROS-mediated tissue damage induces leukocyte recruitment via cellular necrosis and DAMP spillage, one would expect the leukocyte influx to correspond with the degree of tissue damage. Although several studies have found this to be the case[7,65,74], this observation does not answer the question of whether leukocytes are responding to, or generating, tissue damage. If leukocytes are being recruited to tissues by redox signals, one would expect that leukocyte recruitment would not correspond with the degree of tissue damage, and also that inhibition of these signals would reduce leukocyte recruitment. This picture is further complicated when we consider the role of oxidative stress and ROSs on cell death. Studies on IRI have revealed insights into these processes. One hypothesis is that redox signaling in the presence of oxidative stressors prevents tissue damage by protecting the cells against cell death[106]. In this scenario, the removal of the oxidative stressor also removes signals necessary to upregulate protective enzymes, thereby allowing the tissue to experience worsening damage, and ultimately, cell death. Another is that severe conditions of oxidative stress can overwhelm the cell's ability to protect itself through redox signaling. To better understand how these processes interact to cause SI, it is important to first review the mechanisms of apoptotic and necrotic cell death and how they interact with the immune system.

Apoptosis

Cells undergo apoptosis physiologically, using this programmed form of cell death to remove unwanted/damaged cells and tissue modeling[1,107]. The process is

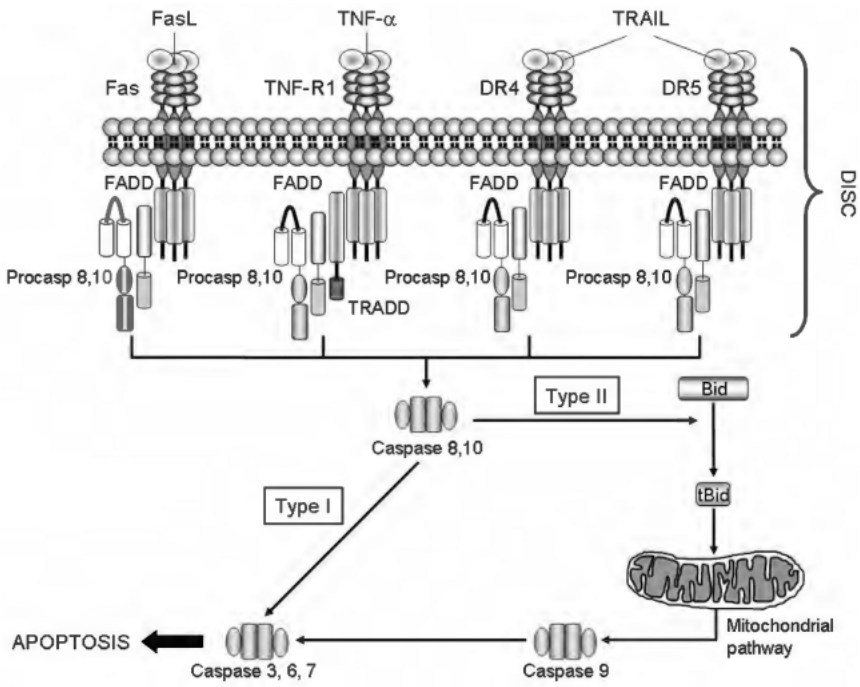

Figure 1.6: The extrinsic pathway of apoptosis is initiated when FasL, TNF-α, and TRAIL bind to their respective receptors. These receptors then trimerize to recruit FADD to the receptor complex, which contributes to the cleavage of procaspases 8 and 10, allowing them to either cleave caspases 3, 6, and 7 and induce apoptosis, or utilize the mitochondrial pathway via caspase 9 activation of caspases 3, 6, and 7. Adapted from Guicciardi, et al., "Apoptosis and necrosis in the liver". *Comr Physiol.* 2013. 3(2).

characterized by chromatin condensation and DNA fragmentation, blebbing of the plasma membrane, cell shrinkage, and finally fragmentation of the entire cell into plasma membrane-bound "apoptotic bodies[1,108]". Apoptosis can be initiated by either the "intrinsic" or "extrinsic" pathways[1,57,109].

The extrinsic pathway of apoptosis

Activation of the Fas, TNF-α and TRAIL receptors initiates the extrinsic pathway when the receptors trimerize (Figure 1.6), recruiting proteins like FADD to the receptor complex[109]. FADD is an example of proteins that contain death domains,

which contribute to the activation of caspases 8 and 10 [1,57,109]. Activation of caspase 8 and caspase 10 then initiate apoptosis by activating caspases 3, 7, and 9, culminating in the degradation of intracellular proteins[1].

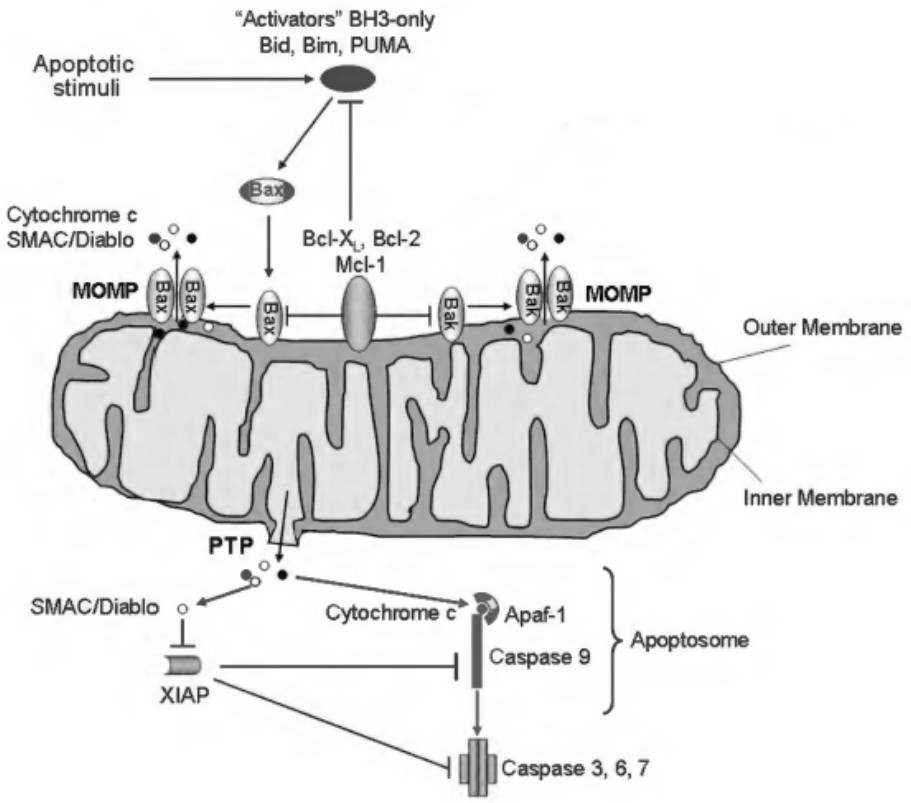

Figure 1.7: The intrinsic pathway of apoptosis is initiated when a stimulus activates Bax and BAK, which form MOMPs on the mitochondrial membrane. Cytochrome C and SMAC/Diablo proteins work on downstream effectors to start apoptosis. Adapted from Guicciardi, et al., "Apoptosis and necrosis in the liver". *Comr Physiol*. 2013. 3(2).

The intrinsic pathway of apoptosis

The intrinsic pathway does not require activation of receptors to initiate apoptosis. Instead, it relies on cytotoxic stimuli such as oxidative stress, DNA damage, and UV radiation to induce translocation of pro-death members of the Bcl2 protein family to the outer mitochondrial membrane[1,108,109]. The Bcl2 family of proteins regulates this process at both the mitochondrial level, and upstream; some proteins have pro-survival activity and some have pro-apoptotic activity[1,109]. Bax and Bak are

two pro-apoptotic peptides that undergo conformational changes upon activation, allowing for their insertion into the mitochondrial membrane[1]. There, they can oligomerize and form pores into the outer mitochondrial membrane. The point at which Bax and Bak become activated marks the "point of no return" for the cell; that is, if these proteins become activated, the cell will fragment and die[109]. Perforation of the outer mitochondrial membrane allows downstream pro-apoptotic proteins, including Cytochrome C, Smac/DIABLO, and endonuclease-G, activate caspases 3 and 9, and induce apoptosis[1,5,109–111]. The activated caspases are then free to cleave their substrates, one of which being the Inhibitor of Caspase Activated DNAse (ICAD), which the activates the Caspase Activated DNAse (CAD)[109,110].

It is the activation of CAD that leads to DNA laddering and the "blebbing" of apoptotic bodies and other characteristic morphologies[109]. These apoptotic bodies are corpses that self-contain cellular fragments that include DNA, cytosolic proteins (such as DAMPs) and organelles[109]. However, they are incapable of maintaining homeostasis for an extended period of time since they do not contain a complete genome. If left in that state, the apoptotic bodies deplete their ATP stores and can no longer maintain the electrochemical gradient across the plasma membrane, leading to a phenomenon known as "secondary necrosis[112]". This leads to DAMP spillage into the extracellular space[30,52,53]. Logically, this would cause DAMP spillage into the extracellular space and drive SI; however, recent work has shown that apoptotic cells maintain a relatively anti-inflammatory state, even during secondary necrosis [113].

Anti-inflammatory signals in apoptotic cells

Recently, researchers have come to understand that apoptotic corpses secrete anti-inflammatory factors that recruit macrophages[113]. Additionally, apoptotic cells secrete several anti-inflammatory molecules such as TGF-β that work to prevent inflammation. TGF-β has anti-inflammatory effects that inhibit neutrophil adhesion

and TNF-α signaling [114] while stimulating macrophage infiltration [115]. Apoptotic bodies release a variety of signals called "find me" signals, including lysophosphatidylcholine, the nucleotides ATP and uridine 5-triphosphate (UTP), and sphingosine 1-phosphate (S1P), that stimulate and direct macrophage recruitment to the apoptotic corpse [50,108]. When the macrophages arrive, "eat me" signals such as phosphatidyl serine are presented on the outer surface of the plasma membrane [108,116]. These signals stimulate phagocytosis of the apoptotic body by the macrophage, thereby preventing secondary necrosis and harmful DAMP release. An important aspect of this process is that macrophages perform anti-inflammatory functions (such as releasing IL-10 and TGFβ) upon phagocytosing the apoptotic corpses[117–119]. Therefore, it is possible that macrophages and apoptotic cells work together to prevent SI by directly discouraging neutrophils from entering the area.

The use of pan-caspase inhibitors prior to liver transplant

Since apoptosis plays a crucial role in the tissue damage induced by ROSs, there have been studies on the use of pan-caspase inhibitors to prevent tissue injury, particularly in cases of IRI. One group used pan-caspase inhibitor IDN-6556 to prevent IRI in the case of clinical liver transplant, and observed reduced SI when the drug was administered to the organ only by delivery through storage and flush solution pre-operatively [107]. However, there was little-to-no benefit when administered intravenously to organ recipients[107]. There are two possible reasons for this: 1) inhibition of apoptosis in the presence of certain proinflammatory factors (such as TNF-α) may allow cell death to occur by more destructive means such as necroptosis[109,120,121]; and 2) that neutrophil apoptosis has been implicated in resolution of inflammation[8,107], so inhibiting apoptosis of all cell types in the recipient may prevent resolution of inflammation.

If inhibiting apoptosis only provides benefit when given to the damaged tissue itself, as opposed to administration to the entire host, new challenges arise. Pan-caspase inhibitors like zVAD-FMK and MX 1013 may have benefit in limited cases (e.g. organ transplant) but would do little for patients suffering from non-transplant IRI (such as MI and stroke). Furthermore, inhibiting certain parts of the apoptotic process may result in other forms of more toxic cell death, like necroptosis, which means that treating patients with systemic pan-caspase inhibitors could cause harm. For example, caspase inhibition in the presence of TNF-α activates a programmable form of necrosis called necroptosis. Necroptosis occurs when the intrinsic pathway of apoptosis cannot activate *caspase 3,* and instead forms a necrosome that contains RIP3. Phosphorylation of RIP3 causes translocation of mixed lineage kinase-like (MLKL) domain to the plasma membrane, where it oligomerizes into a pore-forming protein that induces cell lysis[120,122]. Therefore, activation of apoptosis does not necessarily lead to an immunologically silent cell death, and inhibition of apoptosis may actually worsen the inflammatory effects associated with apoptotic cell death.

Necrosis

As noted in the section describing DAMP release and pattern recognition, necrosis causes DAMPs to leak into the extracellular space, which allows them to be recognized by the innate immune system and neighboring cells. As this mechanism is described at length elsewhere in the chapter, this section will focus on another possible mechanism for tissue damage during IRI— the neutrophilic response itself. Studies involving both DILI and renal IRI have shown that inhibiting neutrophil migration to damaged tissue prevents, or at least greatly reduces, the degree of tissue damage[65,110,123,124]. This hypothesis has gained traction in recent years, as increasing evidence has shown that necrotic cell lysis or apoptosis is unnecessary to induce neutrophil chemotaxis[18,70,125]. Therefore, it is possible that pre-necrotic signals such as

inflammatory lipids and H_2O_2 signaling are responsible for the initial recruitment of neutrophils to the site of tissue damage, and it is neutrophils themselves that initiate tissue necrosis[18,65,70]. The hypothesis of neutrophil-mediated tissue damage is attractive from a clinical perspective because it would enable a therapeutic target to prevent IRI. However, it has been difficult to confirm this hypothesis because few animal models or in vitro systems exist which allow direct observation of this phenomenon.

Challenges associated with studying SI

While DAMP involvement in SI has been known for some time, whether DAMPs are required for SI initiation remains debatable. One of the main barriers to better understanding SI is the lack of a model system that allows for the direct observation of how stressed/dying cells interact with leukocytes in the inflammatory process. Traditionally, SI has been studied using mammalian models and *in vitro* systems. Scores of information have been gathered using traditional methods like histopathology, western blotting, and immunohistochemistry. However, some of the most pressing questions, such as precisely which signals initiate SI and whether leukocytes themselves contribute to the progression of SI, are difficult to answer without the ability to observe these processes directly.

Ischemia reperfusion injury

IRI has been discussed as an example of SI elsewhere in this chapter. Models of MI have been used extensively due to the clinical relevance of the model and relative ease with which MI can be caused in rodent models. This model has shown that DAMP release and PRR signaling are present during MI, and that tissue damage can be reduced by targeting these pathways[126]. Studies on the role of inflammasomes in MI have shown that inhibition of NLRP3 reduces cardiac remodeling and improve LV systolic functioning[127]. Similar work has been performed in rodent models of

stroke, showing that deleting NLRC4 and NLRP3 attenuates inflammasome-mediated neuro-inflammation[128]. Work performed in renal and liver transplant models has shown that tissue damage and infarct size is reduced when neutrophil adhesion is blocked, supporting the hypothesis that neutrophils may be responsible for mediating tissue damage in IRI[25]. With these systems it is fairly straightforward to study the consequences of these injuries. However, due to the nature of working with rodent models, it has been practically infeasible to identify signals that initiate the inflammatory process before the tissues have been damaged.

Zebrafish and the NTR/Mtz system

We therefore set out to identify early recruitment signals for SI by using the NTR/Mtz system to induce damage in the larval zebrafish liver, which can be imaged intravitally without dissecting the animal. The liver is a heterogeneous organ composed of multiple cell types such as Kupffer cells (KCs, resident macrophages of the liver), hepatic stellate cells (HSCs), sinusoidal endothelial cells, and hepatocytes. Because of this, *in vitro* systems rarely recapitulate the complex interaction between multiple cell types. Non-hepatocyte cells comprise approximately half of the cells in the liver and 70-80% of the liver's mass[12,129]. Many cell types, including HSCs, KCs, and endothelial cells play a role in inflammatory signaling[129,130]. For example, HSCs secrete prostaglandins and cytokines in response to stress and surrounding tissue damage[129,131]. Due to the complexity of these interactions, finding a way to image the liver that will not alter inflammatory signals is crucial to understanding these processes. Intravital imaging of the intact organ is one way in which the limitations of *in vitro* systems could be addressed.

Intravital imaging, however, has its own limitations. Intravital imaging of liver inflammation has been accomplished in mouse models of heat-induced liver damage[3,4,27], but this work requires surgical procedures in order to visualize the liver.

This is exceedingly difficult and requires a great deal of expertise. For these reasons, we decided to use zebrafish larvae as a tool to study SI in the intact liver.

Advantages of zebrafish and confocal microscopy as an approach to studying SI

Zebrafish are vertebrates, and as such, their immune cells and chemokines have greater homology to humans than worm and drosophila models. The zebrafish liver is fully functional and metabolically active by 5 days post-fertilization (dpf)[81], although it is still undergoing morphogenesis at this developmental stage. Therefore, experiments can be designed and executed within a week, saving valuable time and resources. Females can lay 50-100 embryos per mating, so it is relatively easy to obtain enough animals for a complete experiment with one or two breeding pairs. Zebrafish larvae are optically transparent, precluding the need for time-intensive dissection techniques for imaging. Optical transparency can be maintained indefinitely by working with zebrafish larvae from the AB *casper* background, which produce no melanocytes or iridophores due to null mutations in the *roy* and *nacre* genes[132]. Wild-type AB larvae also remain optically transparent until at least 8dpf with the application of N-phenylthiourea (PTU) to the embryo water, which inhibits pigment formation.

Our spinning-disc confocal microscope enables us to take high-resolution images of the liver without breaching the epithelium. Although widefield microscopy is more common for such studies, confocal microscopy allows imaging with higher resolution. With this increase in resolution it is possible to see morphologic changes in hepatocytes and subcellular structures such as nuclei.

Transgenic reporter lines allow us to study SI in vivo

Since it is ultimately leukocytes that respond to inflammatory signals, we decided to use transgenic reporter lines for neutrophil (*TG(lysc:PM2-mKate2)* and *TG(mpx:PM2-mKate2)*) and macrophage (*TG(mpeg1:eGFP))* populations to count the number of leukocytes present in the liver. To my knowledge, only one other group has

used this approach to assay liver inflammation in a model of hepatocellular carcinoma[76], and none have tried it for drug-induced models of SI. For assays of leukocyte recruitment to be robust, the inflammatory signal should originate from one region of the embryo (i.e. an amputated tailfin or from the injection of bacteria into the otic cavity). This is important because *in vivo* leukocyte recruitment data can be noisy without a highly localized inflammatory signal. The ability to exert spatiotemporal control over the tissue damage is also crucial because we need to be able to induce damage at a consistent larval age. To study SI in the absence of epithelial barrier breach, we utilized a pharmacologic approach to induce SI in the zebrafish liver. This presented a technical challenge for our approach because most drug-based methods of inducing SI in the zebrafish liver (like acetaminophen, alcohol, and heavy metal toxicity) affect multiple organ systems in the zebrafish larvae. Therefore, we sought out to find a way to generate tissue damage in only the zebrafish liver without causing damage to other systems in the larvae that could alter leukocyte recruitment.

Drawbacks of current drug-induced liver injury-based studies on SI

Since there are so many advantages to using the zebrafish liver for intravital imaging, it is no surprise that many studies have been conducted using the zebrafish liver as a model system. Researchers studying drug toxicity have developed high-throughput methods to screen for the toxicity of many different compounds[81,133,134]. However, for the purpose of studying SI in the liver, there are limitations to these studies that I have been able to address in this project. Several studies on DILI and liver damage in response to environmental toxins have been conducted using widefield imaging and traditional molecular biology techniques[81,102,135–137]. With widefield imaging, liver damage can be assessed by measuring a reduction in liver size[102]. One limitation to these studies is that many of them start toxin and drug exposure at 3dpf, which is when the liver bud begins to develop. Therefore, it is difficult to determine

whether the reduction in liver size is due to actual liver damage or to inhibition of liver development using this technique alone. This is a major drawback because developmental delay of the liver bud could be mistaken for liver damage if using widefield microscopy, leading to misinterpretation of the data. Additionally, cytochrome P450 enzyme expression levels change during this developmental stage. Since these enzymes are critical to the animal's ability to metabolize drugs and modulate toxicity, it is difficult to know whether results obtained in larvae are relevant to those obtained in older animals.

For this reason, follow-up studies in adult zebrafish are typically necessary because of the technical challenges associated with histpathologic analysis of zebrafish larvae. I address this problem in two ways. First, noxious substances are applied to the zebrafish larvae after 5dpf, when the liver is fully functional and metabolically active. This ensures that the reduction in liver size is due to liver damage rather than developmental delay. The higher resolution capability of our confocal microscope allows for analysis of morphologic variations in damaged hepatocytes (which is described in more detail in subsequent chapters). Essentially, this allows us to observe liver damage prior to the reduction in liver size because we can observe the morphology of individual cells.

Some of the DILI studies in zebrafish have also attempted to address the question of inflammation in the liver. However, almost all of them rely on molecular biology techniques such as quantitative PCR to identify transcriptional changes in inflammatory genes[28,47,137] as opposed to quantifying the number of leukocytes in the liver.

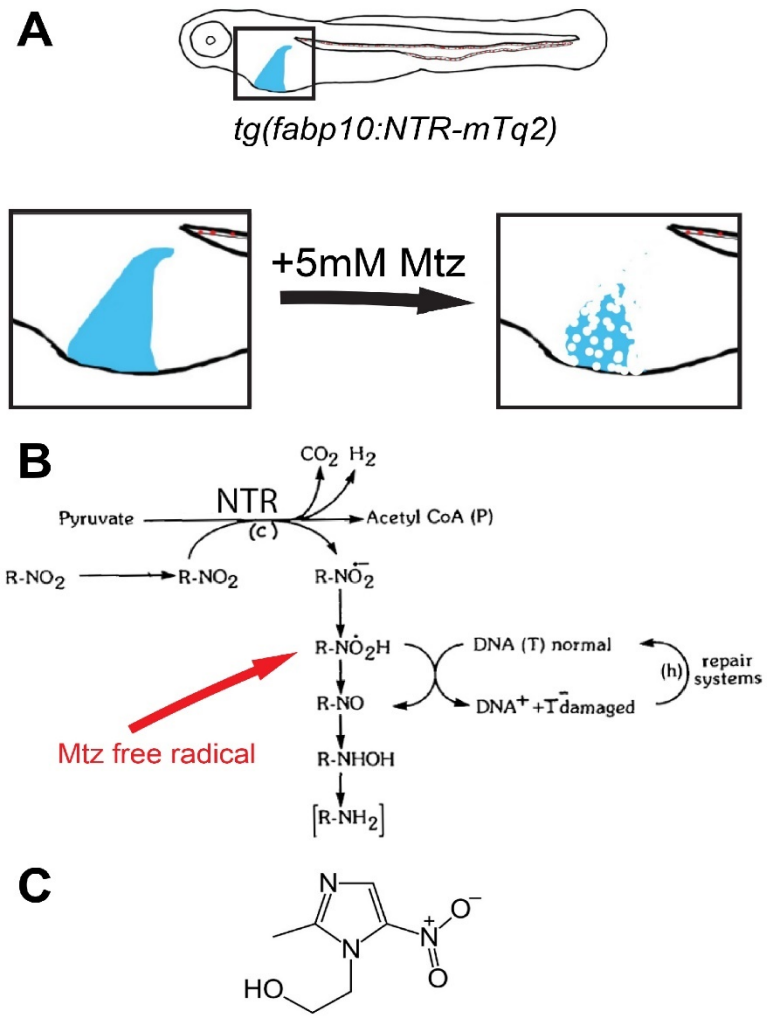

Figure 1.8: The NTR/Mtz system allows us to damage hepatocytes in a spatiotemporally controlled manner. A) Schematic showing Mtz-induced damage in only hepatocytes expressing *fabp10:NTR-mTq2*. B) NTR converts Mtz into a toxic free-radical and generates DNA damage. C) Structure of Mtz.

The NTR/Mtz system

The NTR/Mtz system allowed us to generate liver damage in a spatiotemporally controlled manner (Figure 1.8). The NTR/Mtz system has been used before in zebrafish to study the effects of specific cell types on certain processes, such as regeneration and development[104,138–141]. In the NTR/Mtz system, the bacterial enzyme NTR is expressed as a transgene in zebrafish using a promoter of interest (in our case, the hepatocyte-specific *fabp10* promoter), usually fused with a fluorescent

fusion protein. NTR is not expressed in vertebrates in nature and has no effect on the animal on its own. However, when the NTR-expressing zebrafish larvae are bathed in Mtz, NTR converts Mtz into a toxic free radical that induces oxidative stress in the NTR-expressing cell[142]. Neighboring cell types are unaffected by this process, so this system was ideal for our study.

The NTR/Mtz system has enabled us to address several questions relating to SI that were otherwise difficult to answer. As previously discussed, prior work in our lab has shown that DAMPs are insufficient to induce leukocyte recruitment to the site of a tailfin amputation, and that inflammatory lipids are sufficient to recruit leukocytes. It is also unclear whether cell death causes leukocyte recruitment to the site of tissue injury via DAMP release, or whether leukocytes are recruited to the damaged tissue with non-canonical signals and cause tissue damage themselves. Therefore, the main goal of this study was to determine which signals are responsible for recruiting leukocytes to the liver during NTR/Mtz-mediated liver damage. Since we had both neutrophil and macrophage reporter lines available to us for this study, and since neutrophils and macrophages play different roles in SI, we also sought to determine which cell type(s) are active in the damaged liver and the timecourse in which leukocyte subpopulations travel to the liver. The final goal of this study was to identify how hepatocytes were damaged/killed and to identify the predominant form of cell death in the liver. My hypothesis was that neutrophils would be recruited to the liver early (~24hrs) during Mtz application by signals other than DAMPs and worsen liver damage, and that macrophages would be recruited to the liver after neutrophils to promote healing and resolution of inflammation.

CHAPTER 2: MATERIALS AND METHODS

Plasmid construction

Standard molecular biology procedures were used to create entry clones and expression plasmids. The NTR construct[103,104,139] was c-terminally fused to the cyan fluorescent protein mTurquoise2 (mTq2). The mKate2 (mK2*)* and *PM2-mK2* DNA fragments were created as previously described (Enyedi et al.). To create plasmids for transgenesis the DNA fragments were cloned into the pDONR221 backbone vector and recombined with the *lysc* or *fabp10* promoter and the SV40 polyadenlyation sequence into the pDestTol2GC2 backbone vector using the Tol2kit system.

Zebrafish husbandry

Casper [132], *AB wild-type*, and transgenic zebrafish strains were maintained using standard rearing conditions with the approval of the Institutional Animal Care and Use Committee (IACUC). Zebrafish larvae were raised in E3 medium (5mM NaCl, 0.17mM KCl, 0.33mM CaCl2, 0.33mM MgSO4). For liver inflammation assays, larvae were raised until 5dpf in E3, at which time they were fed standard >50um larval food (from the aquatics facility at Memorial Sloan Kettering Cancer Center) daily until 24 hours prior to imaging (7-9dpf for the purposes of this study).

Generation of transgenic lines

~25pg of the *TG(*f*abp10:NTR-mTq2)*, *TG(lysc:PM2-mK2)*, or *TG(mpx:PM2-mK2)*, plasmid and transposase mRNA in 0.1M KCl was injected into the cytosol of single-cell stage *casper* embryos. Larvae were raised to adulthood and founders identified by mating adults with *casper* adults. F1 progeny were screened for expression of the transgene construct by the presence of either mTq2, eGFP, or mK2 (depending on the desired transgene). F1 progeny were raised to sexual maturity. Experiments were performed on progeny of F1s that were either outcrossed to *casper* adults or to the transgenic line of choice (depending on the experimental objective).

TG(mpeg1:eGFP) adults in the *AB wild-type* background were a gift from David Tobin's laboratory.

Metronidazole exposure

Larvae in the *casper* background were reared until 5dpf in E3, at which point they were sorted for expression of the desired transgene(s) as indicated. Larvae were then transferred into a new dish containing E3 and fed standard >50μm larval food. Larvae were transferred to 5mM Mtz (Acros Organics) in 0.2% DMSO in E3 for the appropriate length of time (i.e. larvae to be imaged at the 24hr time point were placed in 5mM Mtz 24hrs prior to imaging, etc.) (Figure 2.1). Controls were placed in 0.2% DMSO for 48hrs starting at 6dpf. Since the larval food fluoresces strongly in the

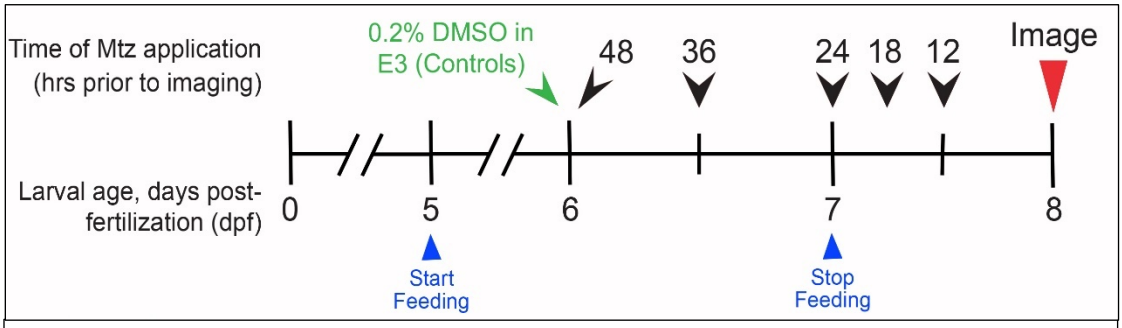

Figure 2.1: Timing of Mtz application and feeding. 5mM Mtz is applied at various time points prior to imaging, corresponding with the desired length of Mtz exposure. For example, larvae in the 48hr Mtz group have been exposed to 5mM Mtz starting at 6dpf until they are imaged at 8dpf. All larvae are imaged at 8dpf.

TRITC channel and the larval gut lies in close proximity to the liver, larvae were starved for 24hrs prior to imaging to prevent intestinal fluorescence from interfering with liver imaging. All larvae were imaged at 8dpf regardless of when Mtz was applied, with the exception of the larvae imaged after a 24hr recovery period (which were 9dpf) and the larvae imaged after a 48hr recovery period (which were 10dpf). Experiments conducted using the *TG(mpeg1:eGFP)* transgenic line in the AB background were performed as described, except 0.2mM N-phenylthiourea (PTU) was

added to the E3 starting at 1dpf until imaging to inhibit melanin synthesis. See Appendix A for detailed experimental procedures.

Fluorescent dye labeling

TG(fabp10:NTR-mTq2; casper) larvae were reared and treated with 5mM Mtz as described above. Immediately prior to imaging, larvae were placed in E3 medium containing 0.2% DMSO and the specified fluorescent dye. Dye concentrations and incubation times are listed in Table 2.1 below:

Table 2.1: Fluorescent Reporter Dye Concentrations and Incubation Times

Fluorescent Dye	Final concentration (in E3)	Incubation time (min)
SYTOX Green (Invitrogen)	0.2uM	20
CellROX Orange (Invitrogen)	2.5uM	30

After incubation with the fluorescent dye, larvae were washed 3 times with 0.2mg/mL Tricaine in E3, embedded, and imaged.

Confocal microscope

Experiments were performed at room temperature (~26°C) on a Nikon Eclipse FN1 microscope equipped with a 25x Apochromat LWD NA 1.1 water immersion

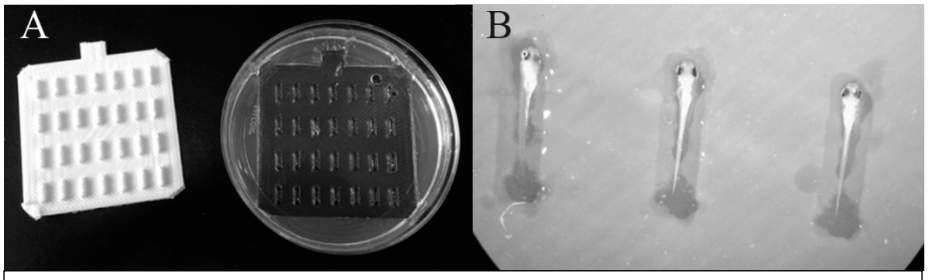

Illustration 2.1: Embedding of larvae for confocal imaging. A) A custom 3D-printed form (left) was used to make a mold using 2% agarose (right). B) Larvae were positioned in the slots with the ventral surface facing up so that the liver would be accessible to the microscope objective.

objective lens, a Yokogawa CSU-X1 Spinning Disk unit, an Andor iXon3 897 EMCCD camera, 405 nm, 488 nm, and 561 nm diode laser lines (Andor Revolution XD). Liver inflammation experiments were performed on 8-10dpf larvae anesthetized in 0.2mg/ml Tricaine (Sigma) for 20min prior to imaging. Larvae were immobilized by embedding them in custom agarose molds with the ventral surface facing upward (to position the liver as close to the confocal objective as possible) (Illustration 2.1). Molds were prepared with 2% agarose dissolved in E3, the larvae positioned in the desired orientation in their individual slots and embedded in 2% low-melting point agarose dissolved in E3. After the agar solidified, the imaging dish was covered in ~2-3mL 0.2mg/mL Tricaine in E3 to prevent the larvae from desiccating during imaging and to ensure that they remained anesthetized during the entire imaging process. Imaging with the *TG(lysc:PM2-mK2)* or *TG(mpx:PM2-mK2)* transgenic lines (in which neutrophils are labeled with mK2) crossed with the *TG(fabp10:NTR-mTq2)* line, or *TG(fabp10:NTR-mTq2; casper)* larvae with the fluorescent dye CellROX Orange (CRO) was performed using the 561nm laser with a 620/30 bandpass filter (to capture mK2/orange fluorescence) and the 405nm laser with a 435/40nm bandpass filter (to visualize mTq2 fluorescence in hepatocytes). Imaging with *TG(mpeg1:eGFP; fabp10:NTR-mTq2)* larvae and *TG(fabp10:NTR-mTq2; casper)* larvae labeled with SYTOX Green (SG) dye was performed using the 488nm (with a 535/40 bandpass filter) and the 405nm (with a 435/40nm bandpass filter) laser to visualize macrophages, SG, and the *NTR-mTq2* construct, respectively. TG(hsp70:cpla2-mK2; fabp10:NTR-mTq2) larvae were imaged on the confocal microscope with the 561nm and 405nm lasers.

Confocal images were captured as z-stack images with a resolution of 2um per field of view at the desired time point (the height of the z-stack varies depending on

liver size and position). NIS-Elements software (Nikon) was used to acquire the images.

Widefield Fluorescence microscopy

Experiments were performed at room temperature (~26°C) on a Nikon Eclipse Ti inverted microscope, equipped with a 20x Plan Apochromat NA 0.75 and a 10x Plan Apochromat NA 0.45 air objective lens (Nikon), an Andor Clara CCD camera and a motorized stage. Green and red fluorescence was excited with a LED light source (Lumencor) using the bandpass filters 475/28 and 549/15, respectively. For eGFP measurements the 470/40 excitation filter was used together with a multispectral dichroic (Chroma, 59022 bs) and the 525/50 emission filter set (Chroma). The far-red mK2 fluorophore was imaged with the 572/35 excitation filter combined with the previously mentioned dichroic and the 632/60 emission filter set (Chroma).

To image leukocytes in the transgenic fish, 20-25 anesthetized 8dpf larvae were aligned and embedded on a coverglass dish (Matek Corporation) with the left side of the animal touching the coverglass. The larvae were anesthetized with 0.2mg/mL of Tricaine 20min prior to alignment. The larvae were immobilized in 1% low-melting agarose with 0.2mg/mL Tricaine dissolved in 5mM Mtz in E3. A Z-stack of red or green fluorescence images (with images in the Z-plane spaced apart 20um and spanning 80um) was acquired every 5min on the above described widefield microscope over the course of 4hrs with the 10X objective to follow leukocyte migration in the liver.

Image processing and analysis of leukocytes and fluorescent dyes in zebrafish livers (confocal images)

All image processing tasks were completed using the programs Prism, Autoquant X, Microsoft Excel, and the programming language R. Data sets were analyzed by two independent researchers to ensure reproducibility. Presented figures

and graphs are from the analysis conducted by the first author of this manuscript. Results from the second author were consistent within 20% of the results from the first author. Files were randomly blinded prior to analysis by either researcher using a custom R script to maintain objectivity during analysis. The custom script automatically exports a master key of the original file names along with the new blinded image numbers. Blinded images were opened in Autoquant X as maximum intensity projections of the z-stacks and visually analyzed for morphology score (see Table 2.2 for scoring criteria). Morphology scores for each image were recorded in a Microscoft Excel spreadsheet and re-organized into a contingency plot. Data was then copied into a Prism file for graphical representation and statistical analysis of the data. Morphology scores were presented as percentages of all of the images within one treatment category, with the absolute number of livers indicated numerically on the graph.

The liver images were cropped using the free-hand region-of-interest tool in Autoquant X. The 3D objects counter tool was used to quantify the number of leukocytes or fluorescently-labeled cells using fluorescence- and size-based thresholds (see Table 2.3). To calculate the minimum intensity threshold, cropped images were viewed using the slice viewer tool. An area without bright objects in the given channel was selected in a random slice and the average intensity for that channel was measured. This background fluorescence was recorded and multiplied by 5. This multiplier was selected based on imaging non-labeled *TG(fabp10:NTR-mTq2; casper)* larvae that had been treated with Mtz and suffered liver damage. Multiplying background fluorescence by 5 was the smallest multiplier that would allow for detection of fluorescent signal while excluding signal from auto-fluorescent cell debris.

Images were visually inspected slice-by-slice through the entire z-stack. Objects detected by Autoquant were deleted if they did not lie at least partially (for leukocytes, 20% of the object was inside the liver) or entirely (for cells labeled with fluorescent dye) within the liver margin. Results were exported as a Microsoft Excel file and recorded using MS Excel. Results of the MS Excel files were copied into a Prism file and plotted into dot plots (leukocyte or fluorescently-labeled cells) or

Table 2.2: Damage Score Criteria for Liver (Confocal Imaging)

Morphology Score	Criteria
No/Mild Damage	Liver is large (~200-250um at widest point) with a clearly defined margin. Hepatocytes look small (~15um in diameter) with uniform size and at least 90% of cells maintaining cell-cell contact with neighboring cells. Sinusoids are visible in the images as clear regions flanked by healthy-looking hepatocytes (Figure 3.1A). In some instances, areas of cytoplasmic clearing will be present within the cell.
Moderate Damage	The liver starts to lose its overall shape and the liver margin becomes disrupted. There may be fewer hepatocytes, but overall liver volume will be similar to that in "mild" damage because the hepatocytes become enlarged at this stage. Sinusoids will not be visible and enlarged cells will often have regions of cytoplasmic clearing. 10-65% of hepatocytes will have lost contact with neighboring cells. After the initial hepatomegaly, cells shrink and begin to resemble popcorn (termed "popcorn cells"; these structures tend to be autofluorescent and are likely cell corpses). (Figure 3.1A).
Severe Damage	Severely damaged livers will be significantly smaller in size than controls and show reduced mTq2 fluorescence. At this stage, there should be fewer rounded cells and more popcorn cells. A liver is rated as "severely" damaged when fewer than 40% of the hepatocytes appear to be intact and when at least half of the cells in the image are popcorn cells. Occasionally the liver will look so damaged that it is difficult to observe the liver margin (there will be a cluster of cells that are grouped together but do not necessarily come into contact with one another) (Figure 3.1A).

contingency tables (morphology scores) as indicated. Objects labeled by Autoquant X were visually inspected to ensure that the object's morphology was consistent with the

structures that I wanted to label. For example, since I wanted to count necrotic nuclei, structures had to meet the minimum size of 50μm^3 and have a round morphology.

Table 2.3: Image Analysis Parameters for Confocal Liver Imaging		
Reporter/Fluorescent Dye (object)	Minimum intensity threshold (arbitrary units)	Minimum volume (um^3)
lysc:PM2-mK2, *mpx:PM2-mK2*, and *mpeg1:eGF* (leukocyte count)	Background fluorescence X 5	70
CellRox Orange (ROS)	Background fluorescence X 5	10
Sytox Green (necrosis)	Background fluorescence X 3	50
TUNEL TMR Red (apoptosis)	Background fluorescence X 5	10

TUNEL staining

The *in situ* Cell Death Detection Kit, TMR Red (Sigma-Aldrich) was used to identify apoptotic cells via the TUNEL assay. 8dpf *TG(fabp10:NTR-mTq2; casper)* larvae that had been reared in either 0.2% DMSO or 5 mM Mtz for 24-48 hours were euthanized and fixed in 4% paraformaldehyde overnight at 4°C. Larvae were rinsed 3 times in phosphate-buffered saline/0.1% tween (PBST) for 5 min. Larvae were dehydrated by subsequently incubating them for 5 min in each of the following solutions: (i) 25% methanol (MeOH)/75% PBST, (ii) 50% MeOH/50% PBST, (iv) 75% MeOH/25% PBST, and (v) 100% MeOH. Larvae were placed in fresh 100% MeOH and stored at -20°C for a minimum of 12 hours. Larvae were rehydrated by subsequently incubating them for 5 min in each of the following solutions: 75% methanol (MeOH)/25% PBST, 50% MeOH/50% PBST, 25% MeOH/75% PBST. Larvae were washed 3 times with PBST, incubated in a 10μg/ml solution of Proteinase K for 15 min, and washed 3 more times with PBST. For permeabilization, larvae were incubated in a 1:1 mixture of acetone:ethanol for 7 min at -20°C, and were then washed 3 times with PBST. Positive controls were created by incubating control larvae in TURBO DNase (4U/ml—10U/ml in 50 mM Tris-HCL, pH 7.5, 1 mg/ml BSA) for 2 hours at room temperature. For each reaction, 5μl TUNEL enzyme

solution was added to 45µl TUNEL label solution and applied to the larvae. Samples were placed overnight in a humidified chamber at 37°C, washed 3 times with PBST, and mounted for confocal imaging.

RNA-seq of Zebrafish Larval Hepatocytes

TG(fabp10:NTR-mTq2; fabp10:PM2-eGFP-P2A-mK2) larvae were reared to 5dpf as described above. Larvae were treated with 5mM Mtz starting at 6dpf. At 8dpf larvae were euthanized on ice for 20min. Larvae were then dissociated by incubating in 0.25% Trypsin-EDTA during simultaneous mechanical disruption of the embryos by pipetting (see Appendix B for detailed protocol). Hepatocytes were sorted using fluorescence-assisted cell sorting (FACS) by expression of three fluorescent proteins (mTq2, eGFP, mK2) to ensure that the sorter returned a pure population of hepatocytes. mRNA was extracted using the PicoPure™ RNA Isolation Kit by Arcturus® and submitted to the Integrated Genomics Core at MKSCC, where it was tested for quality and amplified using SMARTer RNA amplification. The sample was then sequenced using the HiSeq RNA-seq platform by Illumina. Data files were analyzed by the MSKCC bioinformatics core.

Statistical analysis

Statistical analysis was performed using Prism. Leukocyte/fluorescently labeled cell counts in each experimental condition were compared to the 0.2% DMSO in E3 controls using an unpaired, two-tailed t-test with Welch's correction (to account for the fact that each experimental condition is not expected to have the same standard deviation). Error bars are presented as standard error of the mean. Morphology scores were analyzed via one-way ANOVA across all of the experimental conditions using a confidence interval of 0.99.

CHAPTER 3: RESULTS

The NTR/Mtz-system induces selective damage in the larval zebrafish liver.

To adapt the NTR/Mtz system for my study, I created a transgenic line in the *casper* background expressing the *NTR-mTq2* fusion protein under the hepatocyte-specific *fabp10* promoter. *Casper* zebrafish originate from *AB wt* zebrafish and contain null mutations in the genes *nacre* and *roy*, inhibiting both melanocyte and iridophore development [132]. In order to ensure that the liver was fully functioning and metabolically active, Mtz was added no earlier than 5dpf. Characteristic morphologic features of the liver, such as hepatic sinusoids and small, uniformly-sized hepatocytes, became apparent using a spinning disc confocal microscope by 5dpf (Figure 3.1A).

To induce liver damage, 6dpf *TG(fabp10:NTR-mTq2; casper)* larvae were bathed in 5mM Mtz 12-48hrs prior to imaging (Figure 2.1). This resulted in morphologically-identifiable liver damage starting at 24hrs after Mtz exposure. The first visible signs of damage were disruption of hepatic sinusoids, hepatocyte enlargement and swelling, and loss of contact with neighboring cells (Figure 3.1A, Table 2.2). The proportion of livers with moderate damage increases significantly starting ~24hrs post Mtz exposure and progresses until the majority of livers are either moderately- or severely-damaged (Figure 3.1B). Hallmarks of severe damage included loss of overall liver architecture with significant shrinkage of the entire organ, hepatocyte enlargement, and the presence of small, shrunken-looking structures with mTq2 fluorescence that may be cell corpses (Figure 3.1A). These features became most prominent at 48hrs post-Mtz application. Furthermore, I observed that morphological evidence of liver damage occurs prior to significant reduction in liver volume (Figure 3.1B&C). I observed little/no overall physical malformation in 8dpf Mtz-treated larva relative to controls (Figure 3.1D).

Figure 3.1: The NTR/Mtz system induces damage in the larval zebrafish liver.

(A) Confocal images of 8dpf zebrafish larval livers exposed to either 0.2% DMSO (controls) or 5mM Mtz for 24hrs or 48hrs. Top row: Control livers. *NTR-mTq2* fluorescence and *PM2-eGFP* fluorescence are shown in a single slice in the left and center columns, respectively. Maximum intensity projection with both channels is shown in the right column. Sinusoids are seen as channels without eGFP and mTq2 flanked by cells with increased eGFP fluorescence at the edge of the sinusoid. The panels show healthy hepatocellular membranes with a high degree of cell-cell contact and organization around the sinusoids. Second row: Moderately damaged liver from larva exposed to 5mM Mtz for 24hr. Hepatocytes show rounding, reduced cell-cell contact, increased cytoplasmic clearing (insets), and reduced size. Sinusoids are less visible. Third row: Moderately damaged liver from larva exposed to 5mM Mtz for 48hr. A few shrunken cells are visible in this image (inset), although at this stage they represent a minority of the cells in the liver. Bottom row: Severely damaged liver from larva exposed to Mtz for 48hr. The liver has lost much of its overall organization and is reduced in size. Shrunken cells are present in abundance (inset). All scale bars = 50μm. **(B)** The proportion of moderately- to severely-damaged livers increases with increasing Mtz exposure. Bars show percentage of livers in each condition that belong to each damage score. Absolute number of livers in each group is indicated by the white or black numbers. **(C)** Liver volume decreases when livers are severely damaged. Mean values for each group are indicated above the dot plots in brackets. ***T-test $p < 0.0005$. **(D)** Whole larvae exposed to 5mM Mtz for 48hrs (right) have reduced liver (red arrows) and swim bladder size (blue arrows) relative to untreated (left) larvae.

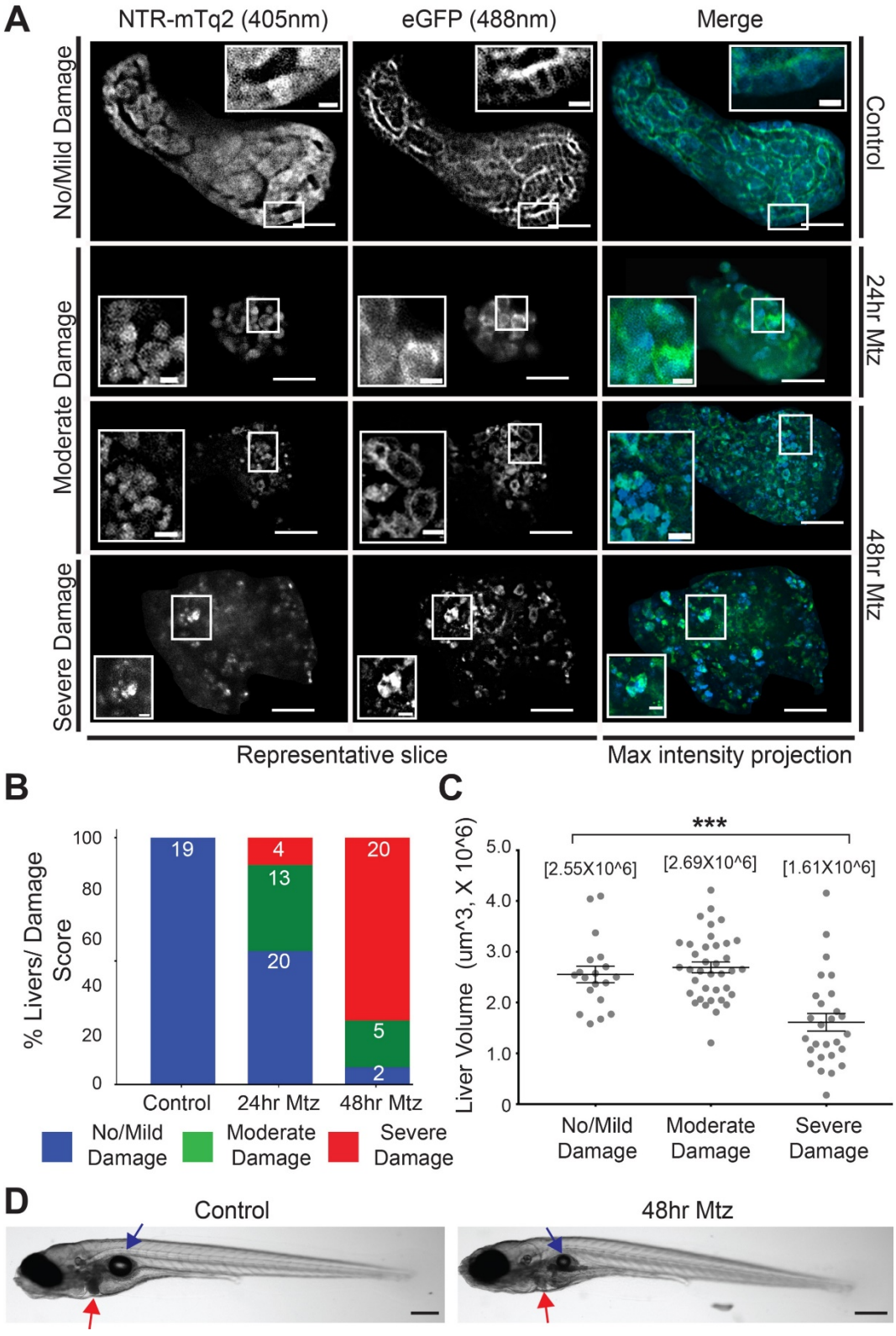

Figure 3.1: The NTR/Mtz system induces damage in the larval zebrafish liver (legend on preceding page).

The NTR/Mtz system induces oxidative stress in hepatocytes.

According to previous reports, the NTR/Mtz system causes tissue damage when NTR converts Mtz into a free radical and induces the production of cytotoxic reactive oxygen species (ROS) in NTR-expressing cells[103,104,139]. To determine whether this is the case in our system, we decided to investigate changes in gene regulation using RNA-seq to determine which molecular pathways and inflammatory signals are differentially expressed. I dissociated *TG(fabp10:NTR-mTq2; fabp10:PM2-eGFP-P2A-mK2)* larvae after exposing them to 5mM Mtz for

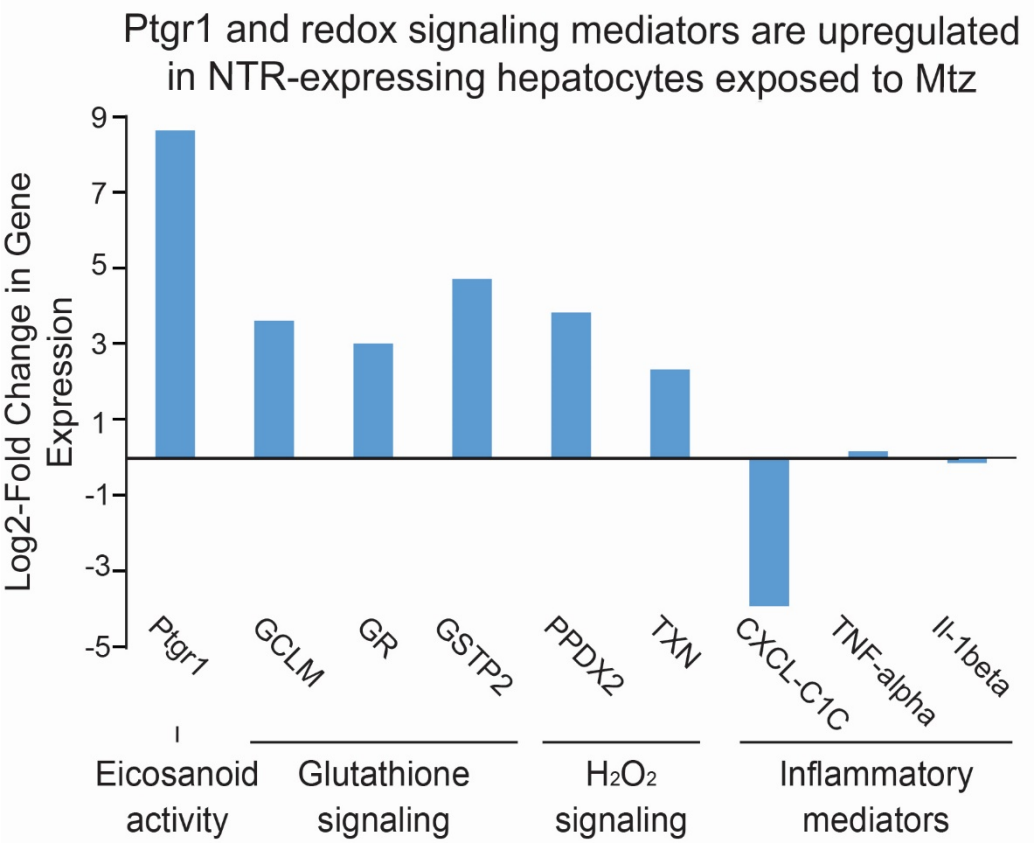

Figure 3.2: RNA-seq analysis shows upregulation of redox signaling and downregulation of inflammatory mediators. RNA-seq of FAC-sorted hepatocytes revealed involvement of the GSH and H_2O_2 redox pathways. Canonical SI mediators TNF-α and IL-1β showed no difference in gene expression, and the chemokine CXCL-C1C (which induces neutrophil chemotaxis) was strongly downregulated. This analysis was performed using the Zv9 genome alignment from Ensemble.

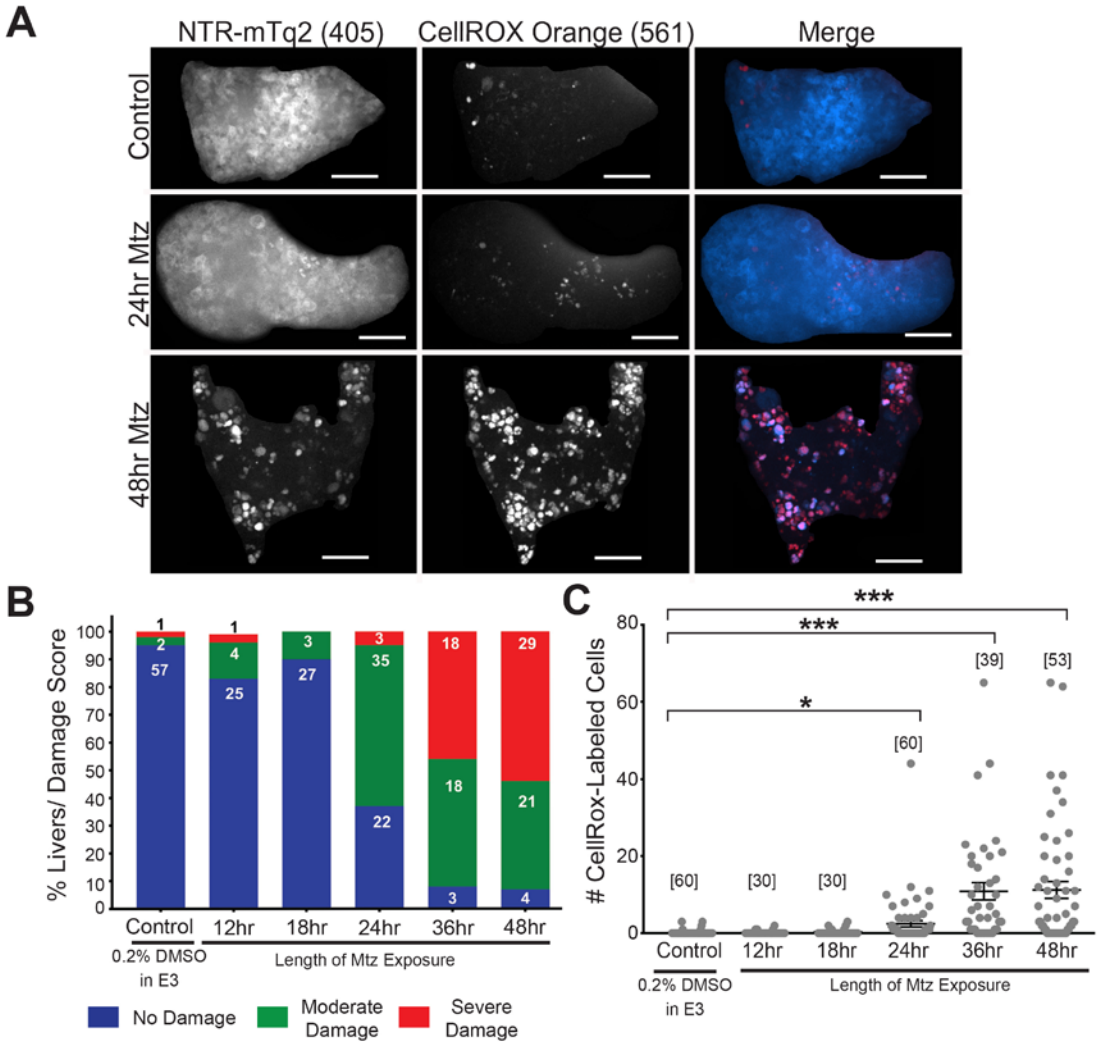

Figure 3.3: ROSs accumulate in livers damaged by the NTR/Mtz system. **(A)** Confocal images of 8dpf zebrafish larval livers exposed to either 0.2% DMSO (controls) or 5mM Mtz for 24 or 48hrs and incubated in the live-imaging dye CellROX Orange. Images are maximum intensity projections of z-stacks that have been deconvolved, autoscaled, and cropped so only the liver shows. Scale bars = 50µm. **(B)** The proportion of moderately- to severely-damaged livers increases with increasing Mtz exposure. Bars show percentage of livers in each condition that belong to each damage score. Absolute number of livers in each group is indicated by the white or black numbers. **(C)** Mtz-treated livers accumulate ROSs starting at 24hr Mtz exposure. The number of animals used for each group are indicated above the dot plots in brackets. T-test. * $p < 0.05$. *** $p < 0.0005$.

48hrs. mRNA was then extracted from FAC-sorted hepatocytes and submitted for RNA-seq as described in Chapter 2. Several genetic pathways relating to glutathione (GSH) synthesis and recycling were upregulated, as well as pathways involved in H_2O_2 and ROS neutralization (Figure 1.5 and Figure 3.2). Notably, many of the upregulated genes are from the KEAP1/NRF2-mediated antioxidant signaling pathway, which is described in more detail in Chapter 1.

Since antioxidant pathways were strongly upregulated in this system, I hypothesized that the NTR/Mtz system induces liver damage by producing ROSs and causing free radical DNA damage. I used CellROX Orange (CRO), a live imaging dye that becomes fluorescent upon binding to ROSs, to label cells experiencing oxidative damage. *TG(fabp10:NTR-mTq2; casper)* larvae treated with either Mtz or 0.2% DMSO and were incubated in CRO immediately prior to imaging. After 24hrs Mtz exposure, the *TG(fabp10:NTR-mTq2; casper)* larvae showed a significant increase in CRO labeling relative to untreated controls (Figure 3.3).

It is important to note that analysis of fluorescent dye labeling presents technical challenges that must be taken into consideration prior to analysis. After several experiments using fluorescent live-imaging dyes, I found it difficult to identify proper minimum fluorescence intensity thresholds in order to automate quantification using the software Autoquant. I treated *TG(fabp10:NTR-mTq2; casper)* larvae with either Mtz or 0.2% DMSO for 48hrs and imaged them in the mK2 (561nm) and eGFP (488nm) channels on our confocal microscope. I observed that larvae with liver damage auto-fluoresce in the 561nm channel (Figure 3.4), which also detects mK2 and CRO. In the 488nm channel, however, autofluorescence decreased after 48hrs of Mtz exposure (Figure 3.4).

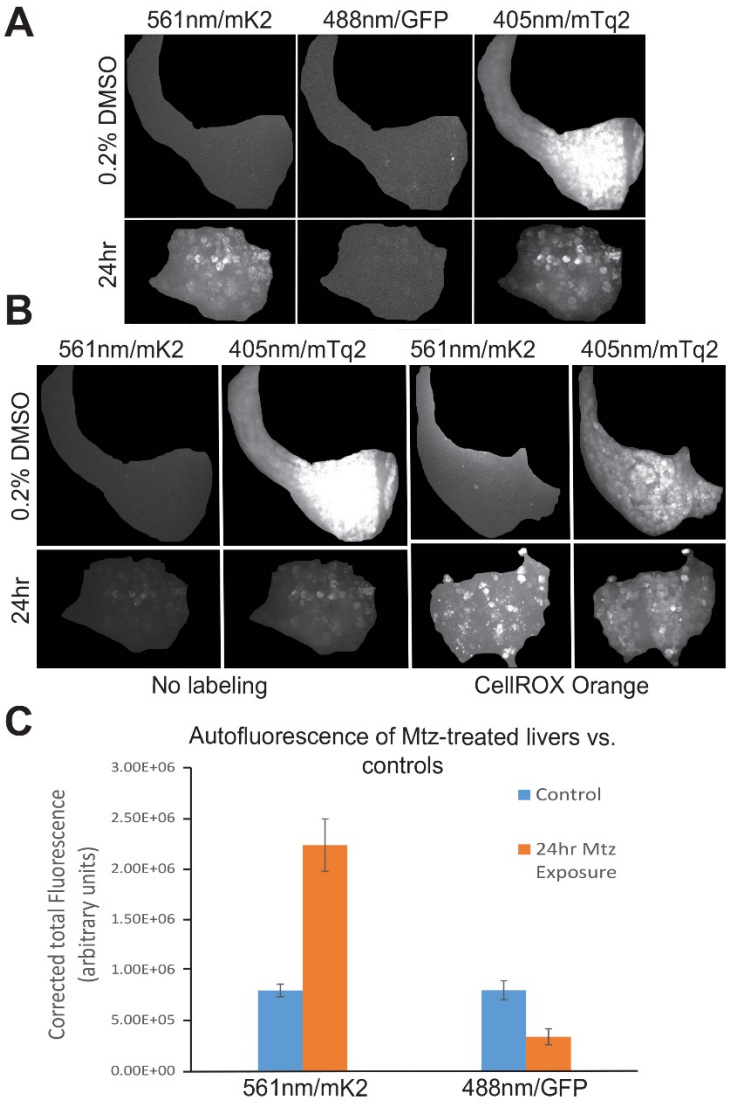

Figure 3.4 Autofluorescence in the 561nm/mK2 channel (previous page). **(A)** *TG(fabp10:NTR-mTq2; casper)* livers treated with 5mM Mtz for 24hrs (bottom) show autofluorescence in the 561nm/mK2 channel relative to controls (top). Images are maximum intensity projections of z-stacks that have been deconvolved, autoscaled, and cropped so only the liver shows. **(B)** Autofluorescence in *TG(fabp10:NTR-mTq2; casper)* livers treated with 5mM Mtz for 24hrs (bottom, left two panels) does not compare significantly to the mK2 fluorescence seen in *TG(fabp10:NTR-mTq2; casper)* livers treated with 5mM Mtz for 24hrs that have been labeled with CRO (bottom, right two panels). Images are maximum intensity projections of z-stacks that have been cropped so only the liver shows. Fluorescence was adjusted to be the same among all images captured in the mK2 channel and separately adjusted to be the same among all images captured in the mTq2 channel. **(C)** Corrected total fluorescence of autofluorescence present in *TG(fabp10:NTR-mTq2; casper)* livers after 24hrs 5mM Mtz exposure. Calculations were made based on fluorescence measurements taken in ImageJ.

After testing several different minimum fluorescence intensity thresholds, we found that multiplying the background fluorescence of each image by 5 allowed us to capture signal in the 561nm channel without including this autofluorescence (and therefore preventing the counts from being artificially high). Please note that this background multiplier is specific to our imaging system and may need to be modified for other microscopes. We found this technique to be useful while analyzing images captured in the 561/620nm excitation/emission spectra because it effectively excluded background signal in a consistent fashion.

The NTR/Mtz system induces cell death by apoptosis.

To determine how the NTR/Mtz system induces liver damage, we used the TMR Red TUNEL kit from Sigma to learn whether Mtz-treated *NTR-mTq2* hepatocytes die via apoptosis. The TUNEL kit labels nicked DNA, a process that occurs when DNA in apoptotic cells undergoes fragmentation[143]. TUNEL staining differs from the live imaging protocol in that the larvae must first be fixed in 4% PFA and permeabilized to allow the DNA-labeling enzymes to penetrate the liver (detailed in Chapter 2). The labeling and washing process can change the morphology of the liver and surrounding tissues. Additionally, fixation reduces mTq2 fluorescence. Therefore, I was unable to analyze these images for liver damage.

I anesthetized *TG(fabp10:NTR-mTq2; casper)* larvae that had been treated with Mtz or 0.2% DMSO for 24 or 48hrs, and euthanized them by placing them on ice for 20min. This was followed by an overnight incubation in ice-cold 4% PFA. I observed little-to-no labeling in the control animals but extensive labeling in larvae treated with Mtz (Figure 3.5). In my hands, the number of apoptotic cells did not change between the 24hr and 48hr groups.

The NTR/Mtz system also induces necrotic cell death.

To determine whether necrosis is present in *TG(fabp10:NTR-mTq2; casper)* larvae that had been treated with Mtz, I labeled the larvae with SG and imaged them intravitally. SG, which fluoresces upon binding to double-stranded DNA (dsDNA), is

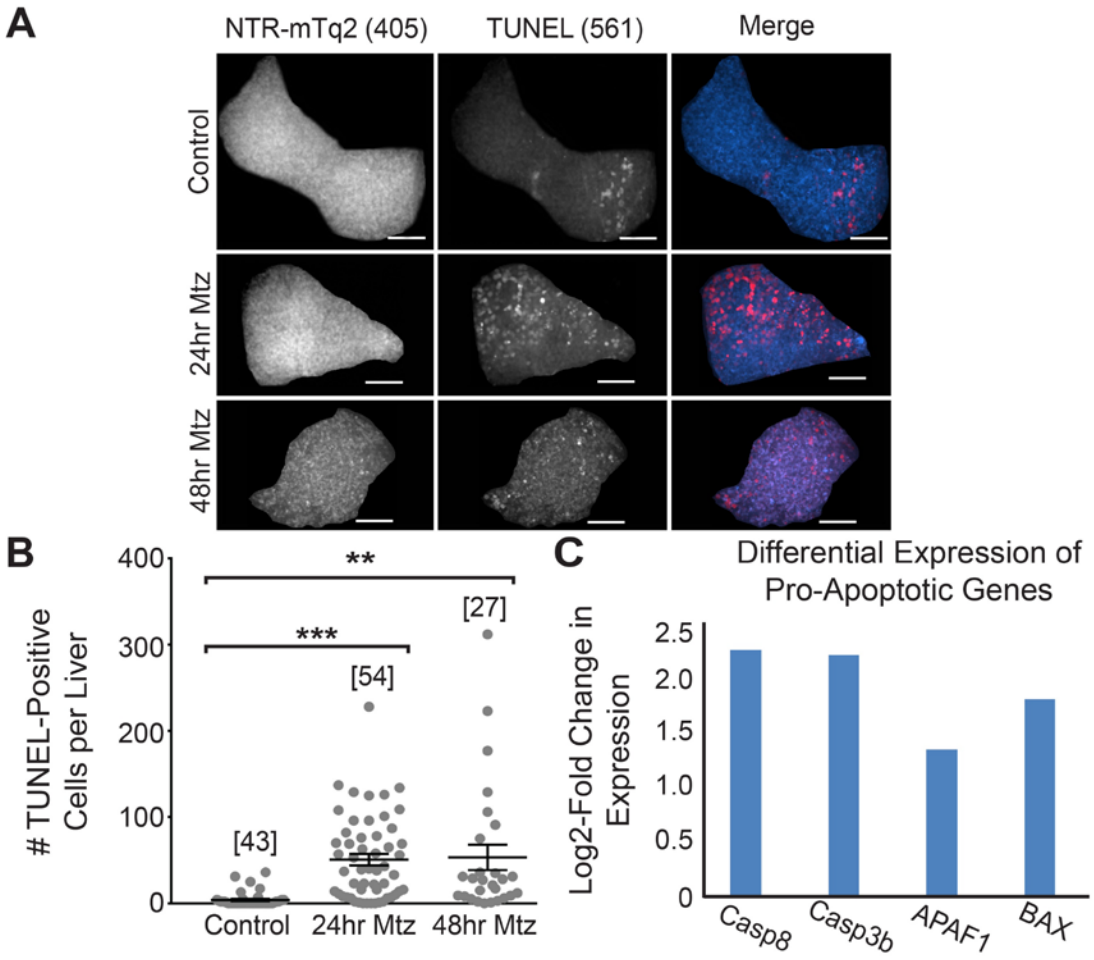

Figure 3.5: The NTR/Mtz system causes apoptosis in *TG(fabp10:NTR-mTq2; casper)* larvae. **(A)** Larvae were fixed in 4% PFA and labeled with the TMR Red TUNEL kit. Images shown are maximum intensity projections of livers captured in a z-stack with our spinning disc confocal microscope. Top: Control liver reared in 0.2% DMSO in E3 shows little/no TUNEL labeling. Middle: Liver from larva exposed to 5mM Mtz for 24hrs. Liver shows significant labeling with SO, indicating cellular necrosis. Bottom: Liver from larva exposed to 5mM Mtz for 48hrs. The degree of apoptosis in 48hr-exposed larvae is similar to that of 24hr-exposed larvae. Images have been deconvolved for clarity. Scale bars = 50µm. **(B)** Quantitative analysis of apoptosis. Number of animals per condition is indicated above the plot in brackets. T-test. ** $p < 0.005$. ***$p < 0.0005$. **(C)** RNAseq data showing significant upregulation of pro-apoptotic genes.

impermeable to intact cellular membranes. Therefore, cells labeled with SG must have a permeabilized plasma membrane, which is a hallmark of necrotic cell death[120]. I observed that livers treated with SG showed limited hepatocellular necrosis after ~24hrs Mtz exposure (Figure 3.6A&B), and that necrosis increased as the length of Mtz exposure increased.

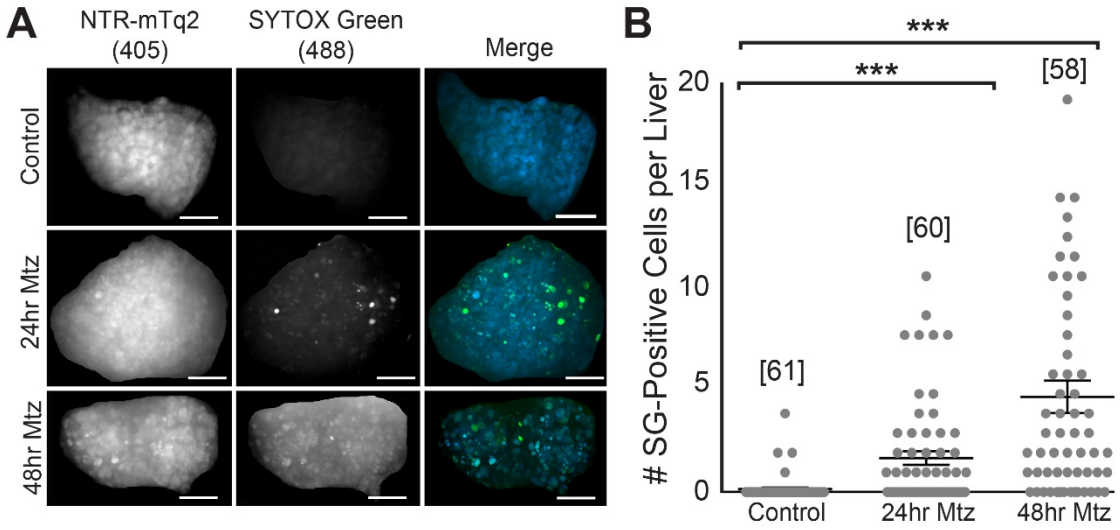

Figure 3.6: Necrosis is present in Mtz-treated livers. **(A)** *TG(fabp10:NTR-mTq2; AB wt)* livers treated with 5mM Mtz for 24hrs show SG labeling. Images are maximum intensity projections of z-stacks that have been autoscaled and cropped so only the liver shows. Scale bars = 50μm. **(B)** SYTOX Green-labeled structures appear 24hrs after Mtz exposure and increase 48hrs after Mtz exposure. Number of animals per experimental condition are indicated above the dot plot in brackets. T-test. *** $p < 0.0005$.

Leukocytes are recruited to the liver during NTR/Mtz-induced liver damage.

Our primary motivation for adapting the NTR/Mtz system was to study sterile inflammatory processes in the absence of integumental damage. Therefore, we crossed three transgenic reporter lines (*TG(lysc:PM2-mKate2)* and *TG(mpx:PM2-mKate2)* in the *casper* background to label neutrophils and *TG(mpeg1:eGFP)*, in the *AB wt* background, to label macrophages) with the *TG(fabp10:NTR-mTq2)* transgenic line to determine whether leukocytes are recruited to the liver during NTR/Mtz-induced liver damage.

Figure 3.7: *Lysc*$^{+}$ neutrophils are not recruited to the liver, but hepatocytes contain mK2-positive inclusions. **(A)** *TG(lysc:PM2-mK2; fabp10:NTR-mTq2)* livers treated with 5mM Mtz do not show increased neutrophil recruitment to the liver. Small mK2-positive vesicles are visible in the samples (white arrow). Scale bars = 50μm. **(B)** 5X Inset shows close-up of neutrophil and an inclusion-containing hepatocyte. Scale bar = 10μm. Images are maximum intensity projections of z-stacks that have been deconvolved, autoscaled, and cropped so only the liver shows. **(C)** Leukocytes are not recruited to the liver even though the larvae have increased liver damage after Mtz exposure. **(D)** Quantification of neutrophil recruitment to the liver after treatment with Mtz (left). Number of animals for each condition are shown above the dot plot in brackets. Quantification of small, mK2-positive inclusions present in the liver (right). Number of animals for each condition are shown above each dot plot in brackets. T-test. * $p < 0.05$; ** $p < 0.005$.

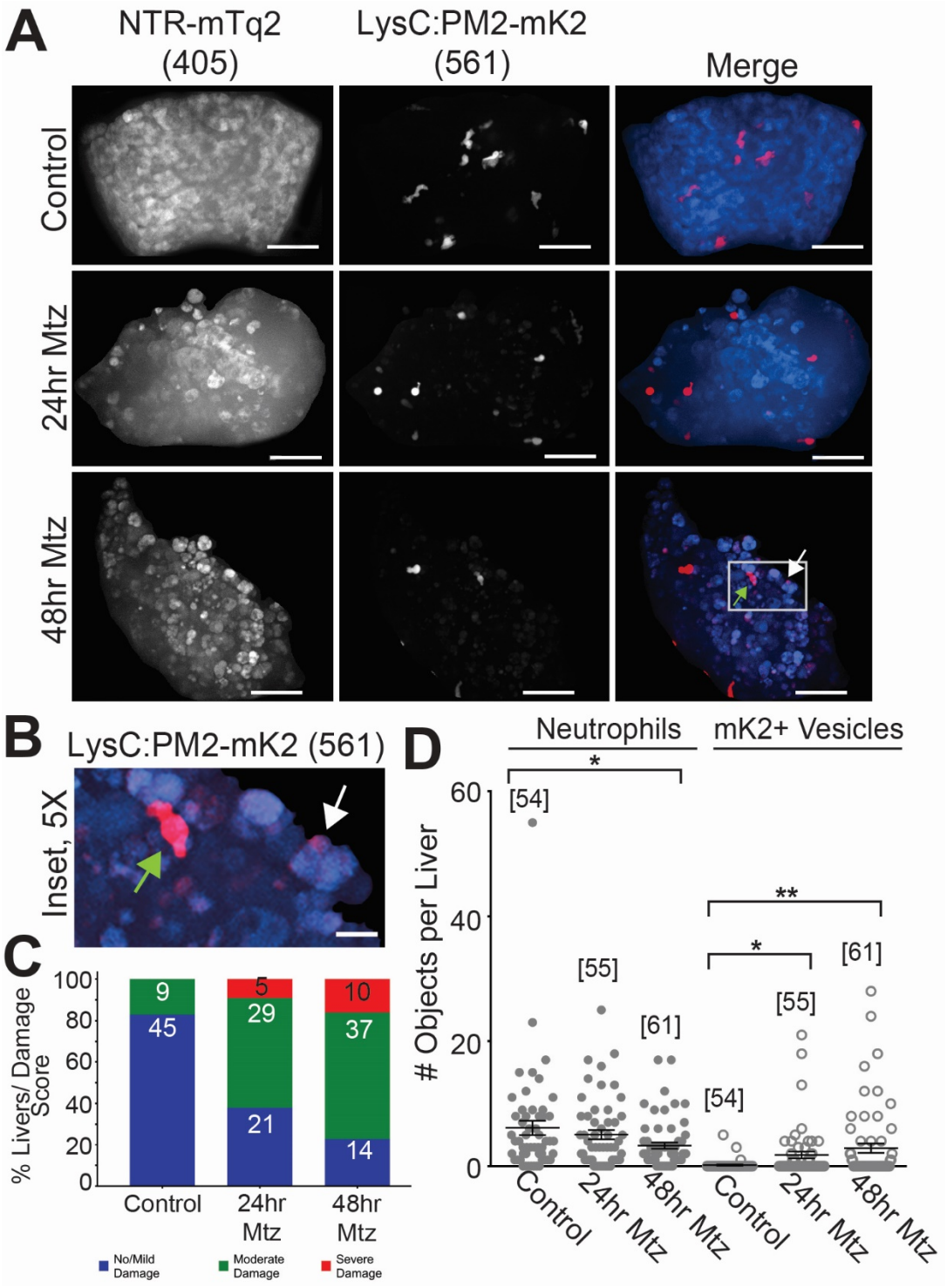

Figure 3.7: *Lysc*$^{+}$ neutrophils are not recruited to the liver, but hepatocytes contain mK2-positive inclusions (legend on preceding page).

In the initial experiments using the *lysc* transgenic reporter, I observed no increase in neutrophil recruitment (Figure 3.7A&B) after 48hrs exposure to 5mM Mtz. Instead, we found that there was an increase in the number of small, rounded, mK2-positive inclusions in many of the hepatocytes (Figure 3.7B, white arrow). The lack of neutrophil recruitment raised several questions, as the finding was contrary to my initial expectations. To address the concern that Mtz may inhibit neutrophil chemotaxis, I imaged *TG(LysC:PM2-mK2; fabp10:PM2-eGFP -P2A-mTq2)* larvae that had been exposed to Mtz for 48hrs and compared the number of neutrophils with

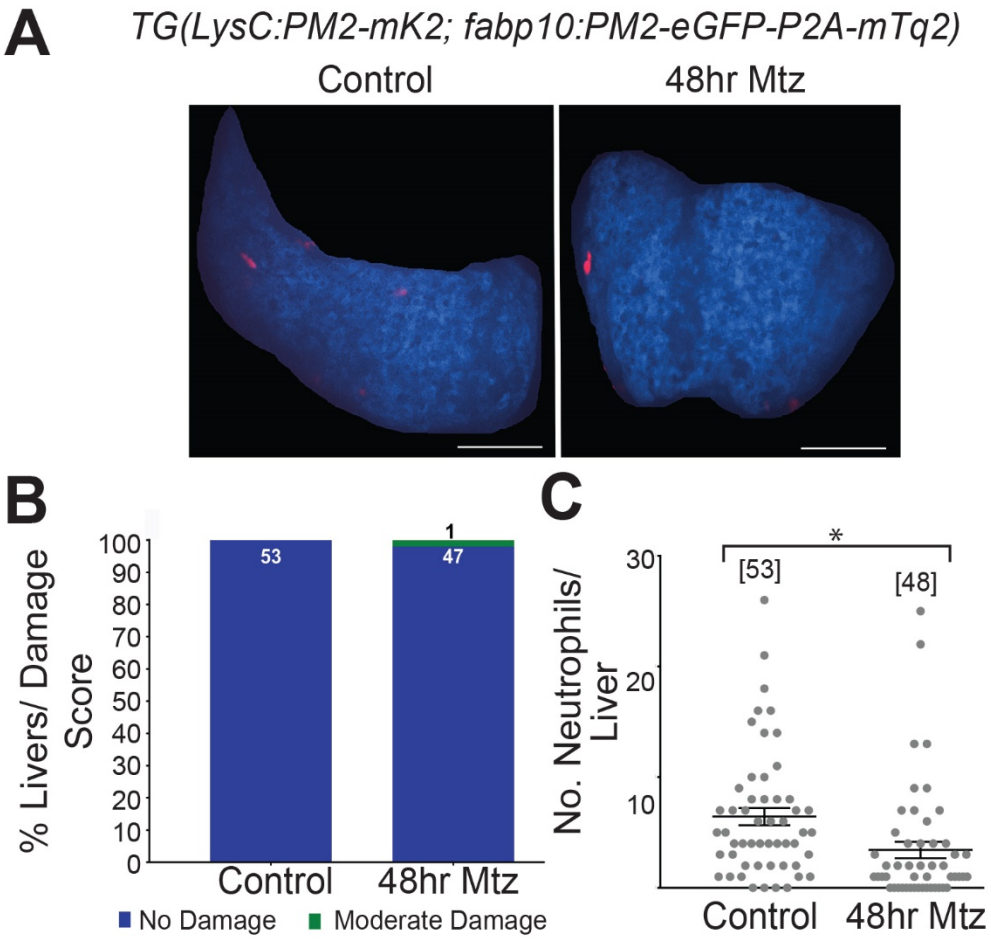

Figure 3.8: Livers without NTR show a reduction in *lysc*$^{+}$neutrophils after Mtz exposure. **(A)** *TG(lysc:PM2-mK2; fabp10:PM2-eGFP-P2A-mTq2)* larvae exposed to Mtz for 48hrs show no changes in liver morphology **(B)** and a decrease in leukocyte recruitment to the liver. **(C)** Quantification of *lysc*$^{+}$ neutrophils in the liver. Mean values for each condition are indicated above the dot plot in brackets. T-test. * $p < 0.05$.

that in a control group (Figure 3.8). We found that there is a significant reduction in *lysc*$^{+}$ neutrophils in the liver after 48hr Mtz exposure. This raised the concern that Mtz could inhibit neutrophil development. Therefore, I imaged the caudal hematopoietic niche (CHT) of *TG(lysc:PM2-mK2; fabp10:NTR-mTq2)* larvae using widefield microscopy (Figure 3.9).

There was a statistically significant reduction in *lysc*$^{+}$ neutrophils in the CHT between the Mtz-treated and control *TG(lysc:PM2-mK2; fabp10:NTR-mTq2)* larvae, but the difference between the means of the control and Mtz-treated group was not large enough to account for the reduction seen in Figure 3.8. To determine if *mpx*$^{+}$ and *mpeg1*$^{+}$ development was suppressed during Mtz exposure, *TG(mpx:PM2-mK2; fabp10:NTR-mTq2)* and *TG(mpeg1:eGFP; fabp10:NTR-mTq2)* larvae were also imaged in the CHT after being exposed to Mtz or 0.2% DMSO for 48hrs. The mean neutrophil counts in each of these reporter lines were unchanged (Figure 3.9). Imaging the livers of *TG(mpx:PM2-mK2; fabp10:NTR-mTq2)* larvae showed that *mpx*$^{+}$ neutrophils were increased in the liver after 48hrs Mtz exposure (Figure 3.10A-D). Increasing Mtz exposure was also associated with an increase in mK2^{+} neutrophil inclusions within hepatocytes. Since I initially expected neutrophils to arrive to the liver earlier (i.e. at 24hrs) during Mtz-induced damage, I decided to repeat this experiment with *TG(mpeg1:eGFP; fabp10:NTR-mTq2)* larvae to determine whether *mpeg1*$^{+}$ macrophages would arrive later in the inflammatory process as I originally predicted.

I found that macrophages were recruited to the liver after 24hrs of Mtz exposure (Figure 3.11). Macrophages that are recruited to the liver associate with damaged hepatocytes. Figure 3.11A&B shows macrophages surrounding hepatocytes which have been damaged after Mtz exposure.

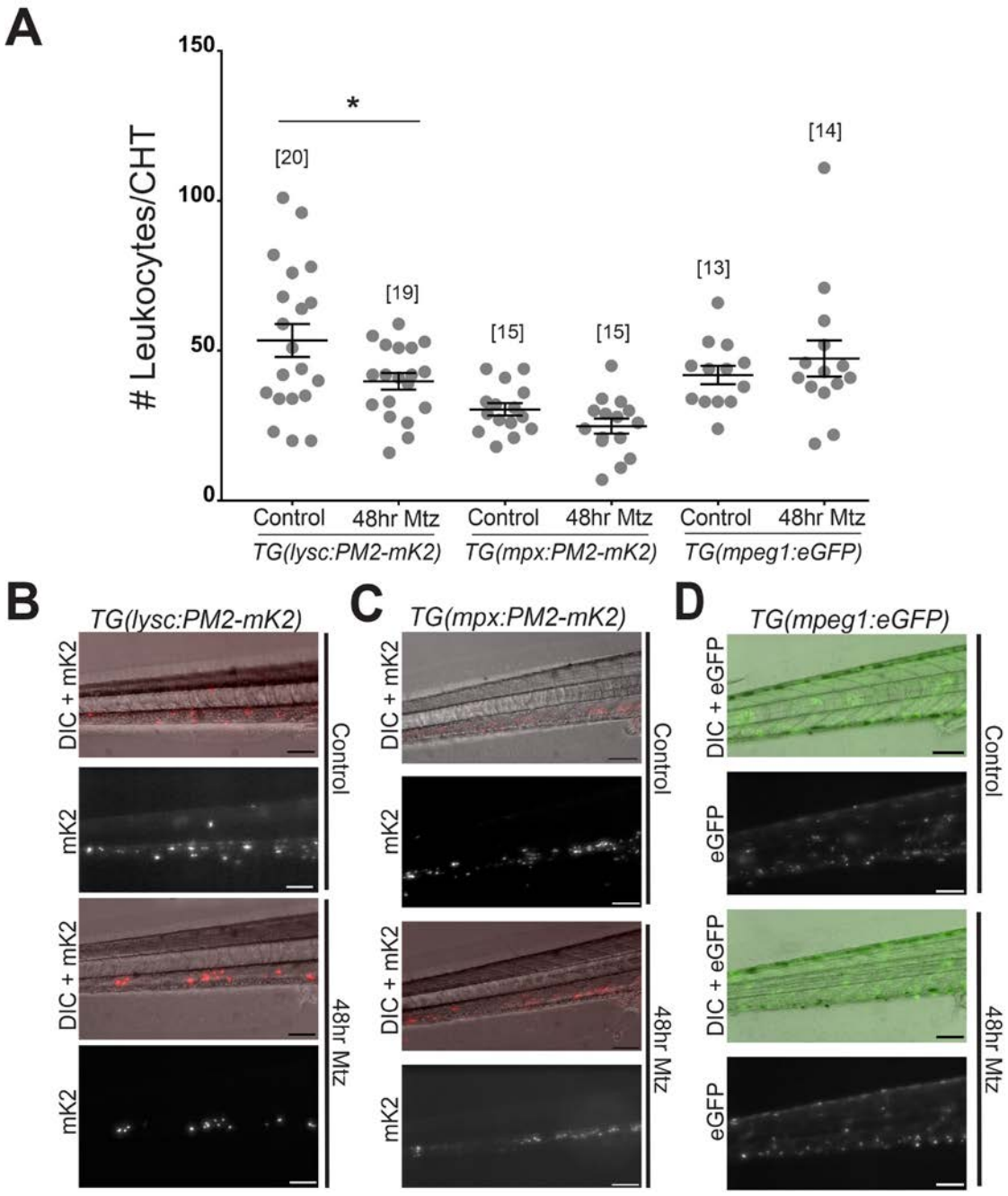

Figure 3.9 Mtz does not affect development of leukocyte subpopulations. **(A)** Leukocytes in the caudal hematopoietic niche (CHT) treated with either 0.2% DMSO or 5mm Mtz-treated larvae were quantified. A reduction in neutrophils is seen in the *lysc*$^{+}$ neutrophil, but there are no significant differences between Mtz-treated larvae and their respective controls in the *mpx*$^{+}$ and *mpeg1*$^{+}$ leukocytes. T-test. * $p < 0.05$. **(B-D)** Widefield maximum intensity projections of the CHT of *TG(lysc:PM2-mK2)* **(B)**, *TG(mpx:PM2-mK2)* **(C)**, and *TG(mpeg1:eGFP)* **(D)** leukocyte reporters. Scale bars = 100μm.

Figure 3.10: *Mpx*$^{+}$ neutrophils are recruited to the liver during Mtz exposure. **(A)** *Mpx*$^{+}$ neutrophils are recruited to the liver during NTR/Mtz-induced damage. *TG(mpx:PM2-mK2; fabp10:NTR-mTq2)* larvae were exposed to 5mM Mtz for 24 or 48hrs prior to live imaging. Intact leukocytes (green arrow) are visible within the liver and were quantified using the software Autoquant. Confocal microscopy enabled us to visualize small, rounded objects labeled with mK2 (white arrows) that appeared to be contained within, or sometimes adjacent to, hepatocytes. Scale bars = 50μm. **(B)** Inset is 5X magnification of the region in part **(A)** that is outlined with a grey box. Scale bar = 10μm. **(C)** Liver damage increases with increasing Mtz exposure. **(D)** Quantification of macrophage recruitment to the liver. Neutrophils and mK2^{+} inclusions are Mean values are increased in the 48hr group. Number of animals is shown for each condition above the dot plot in brackets. T-test. * $p < 0.05$. *** $p < 0.0005$.

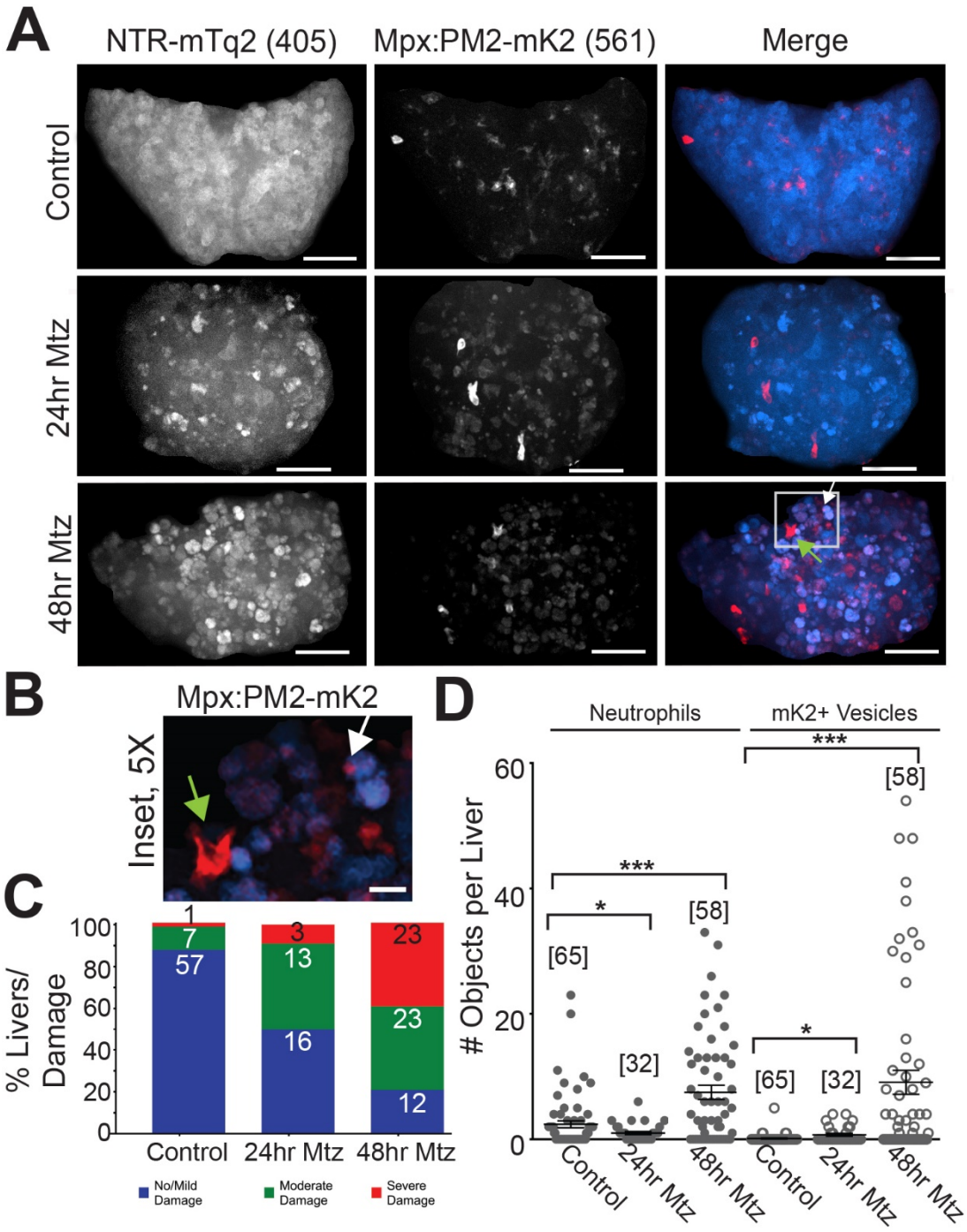

Figure 3.10: *Mpx*$^{+}$ neutrophils are recruited to the liver during Mtz exposure (legend on preceding page).

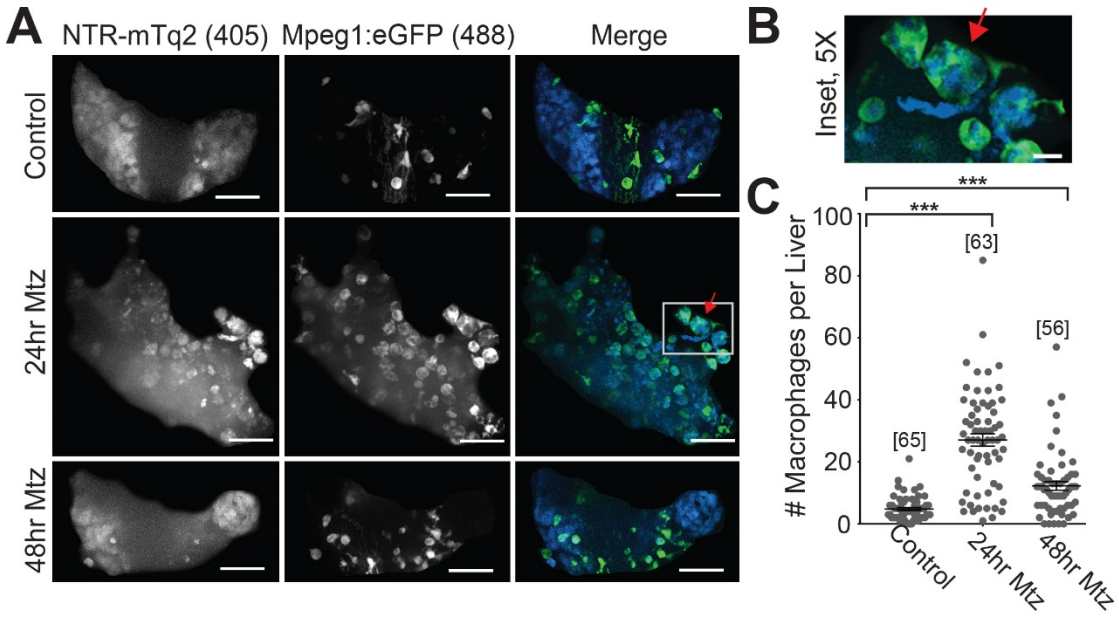

Figure 3.11: Macrophages are recruited to the liver during Mtz exposure. **(A)** *TG(mpeg1:eGFP; fabp10:NTR-mTq2)* larvae show robust macrophage recruitment after 24hrs Mtz exposure. Macrophages appear to phagocytose injured or dead hepatocytes (red arrow). Images are maximum intensity projections of z-stacks that have been deconvolved, autoscaled, and cropped so only the liver shows. Scale bar = 50 µm. **(B)** 5X inset of the area indicated by the gray box in part **(A)**. Scale bar = 10µm. **(C)** Quantification of macrophage recruitment to the liver. Number of animals for each condition are indicated above the dot plot in brackets. T-test. * $p < 0.05$. *** $p < 0.0005$.

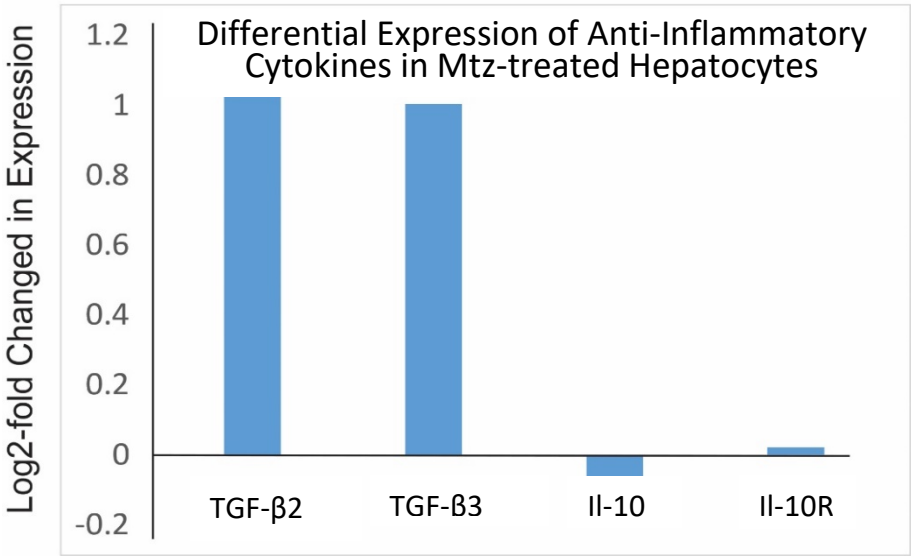

Figure 3.12: The anti-inflammatory cytokine TGF-β is upregulated in Mtz-treated hepatocytes. Two zebrafish isoforms of TGF-β show differential expression in Mtz-treated larvae. In contrast, IL-10 shows no differential expression.

Suspecting that Mtz may be responsible for an anti- inflammatory response in the liver, I decided to image *TG(lysc:PM2-mK2; fabp10:NTR-mTq2)* larvae both after 24hrs Mtz exposure and after 24hrs Mtz exposure followed by a 24hr recovery period (Figure 3.13). In this experiment I did not observe an increase in neutrophil recruitment after the recovery period. Since the *mpx*$^{+}$ neutrophils were seen in the liver after 48hrs, but not 24hrs, of Mtz exposure, I repeated the experiment using 9 and 10dpf *TG(lysc:PM2-mK2; fabp10:NTR-mTq2)* larvae that were exposed to Mtz for 48hrs. These larvae were allowed to recover for 24 or 48hrs, respectively (Figure 3.14) and labeled with SG prior to imaging.

In this experiment, 8dpf larvae treated with Mtz for 48hr were the most severely damaged group (Figure 3.15D) but did not show increased *lysc*$^{+}$ neutrophil recruitment compared to the 8dpf control group (Figure 3.15B). The severity of liver damage corresponds with a significant increase in SG labeling (Figure 3.15C); however, the number of SG-labeled cells between the 24 and 48hr exposure groups was practically unchanged (Figure 3.15C), even though the 48hr exposure group suffered much worse liver damage (Figure 3.15D).

The addition of recovery time after 48hrs Mtz exposure resulted in robust neutrophil recruitment (Figure 3.15). 9dpf larvae given a 24hr recovery period showed greater *lysc*$^{+}$ neutrophil recruitment to the liver than either the 9dpf control group or the 9dpf 48hr Mtz exposure group without a recovery period (Figure 3.15B). The 10dpf Mtz-treated group also showed greater neutrophil recruitment after a 48hr recovery period. These cohorts show that liver damage is most severe in the 48hr Mtz exposure group (Figure 3.15D). In both groups, the recovery group was found to have greater damage than the control group, but less damage than the 48hr Mtz group. In the 9dpf larvae group, the amount of SG labeling increased in both the 48hr Mtz

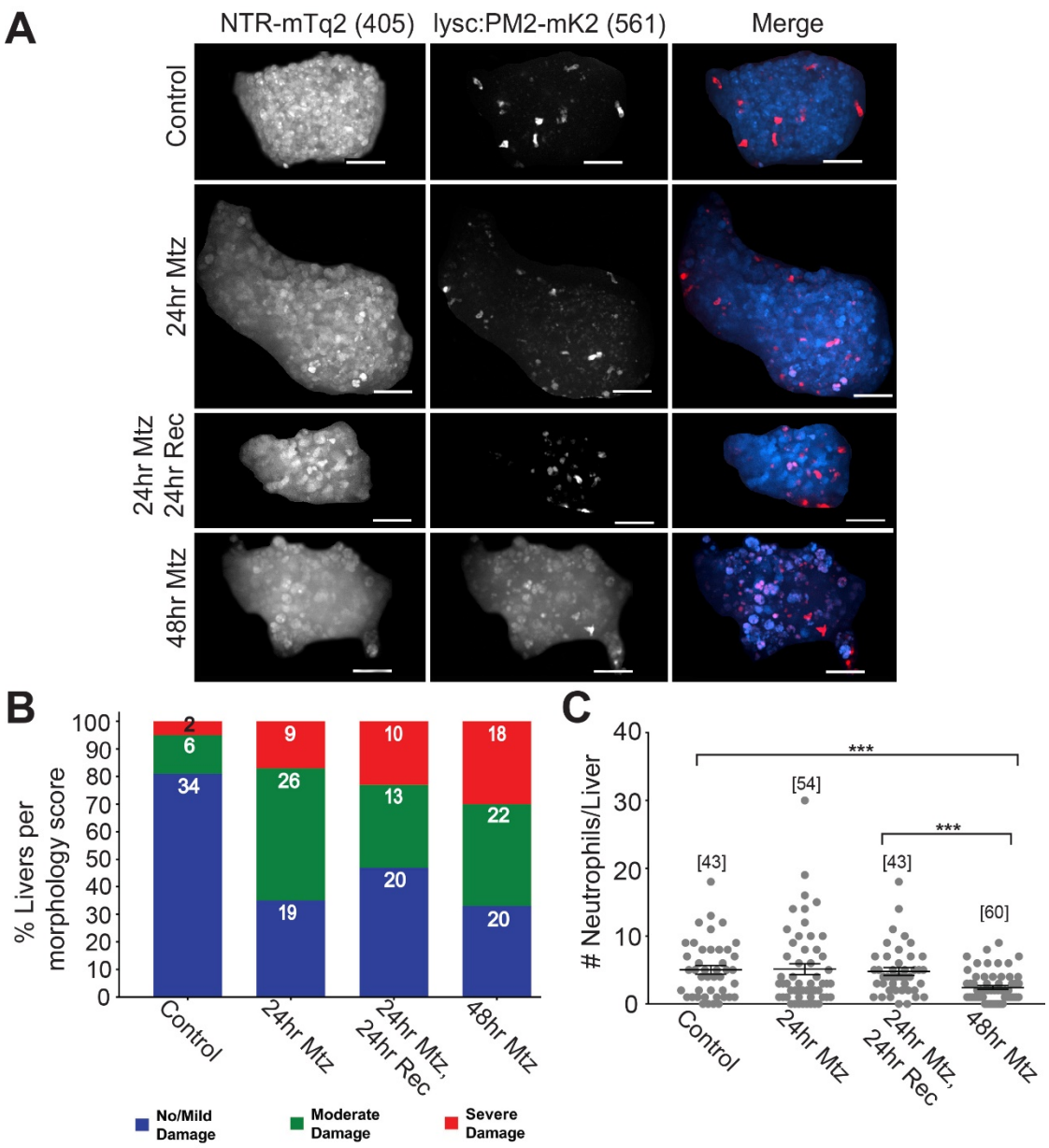

Figure 3.13: Removal of Mtz after 24hr Mtz exposure does not induce neutrophil recruitment into damaged livers. **(A)** Representative maximum intensity projections of zebrafish livers at 10dpf with fluorescent neutrophils after indicated times of Mtz exposure and recovery in the *TG(lysc:PM2-mK2)* reporter line. Scale bars = 50µm. **(B)** Quantification of morphological phenotypes by damage score. Numbers within bars indicate number of animals per group. **(C)** Number of neutrophils in the liver at indicated times of Mtz exposure in *TG(lysc:PM2-mK2)* reporter line. Square brackets indicate the number of animals per condition. Error bars, SEM. ***t-test $p < 0.0005$. Rec = Recovery.

exposure and in the 48hr Mtz exposure with the 24hr recovery period compared to controls (Figure 3.15C). The recovery group has the most SG-labeled cells, coinciding with the influx of neutrophils seen in this group. Concerned that the increase in SG labeling could be due to neutrophilic cell death (as opposed to hepatocellular cell death), I counted the number of SG^+ neutrophils in each liver and deducted them from the total SG count in the livers. The 10dpf larvae exposed to Mtz for 48hrs and given a 48hr recovery period showed the greatest degree of leukocyte recruitment out of all the groups (Figure 3.15B).

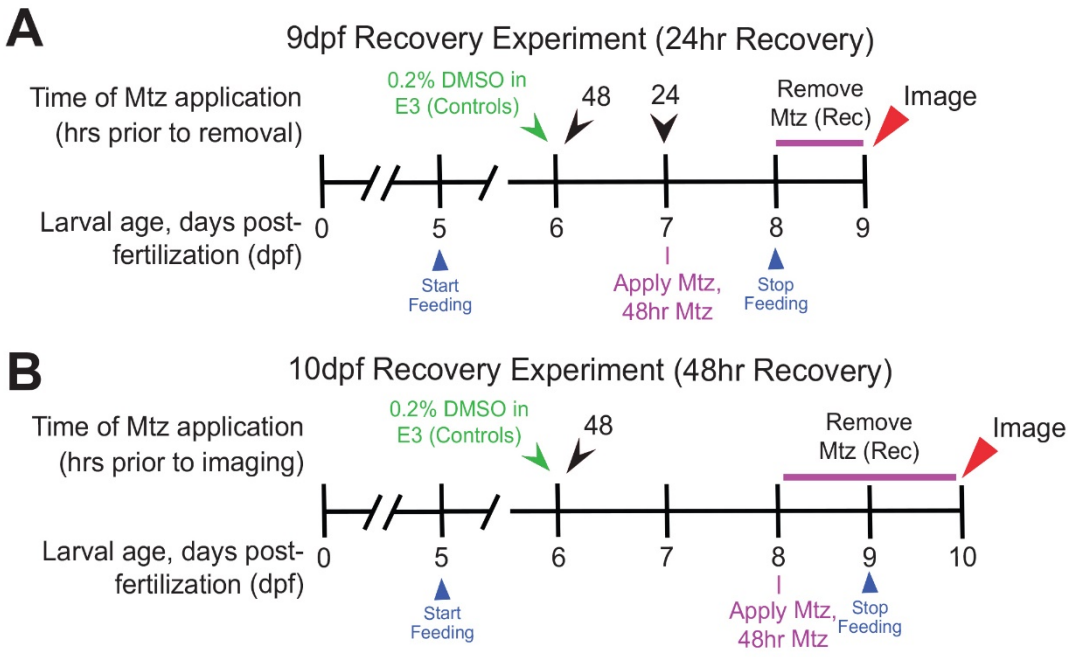

Figure 3.14: Schematic of recovery experiments performed with 9dpf (A) and 10dpf (B) larvae.

Figure 3.15: Removal of Mtz after 48hr Mtz exposure induces neutrophil recruitment into damaged livers. **(A)** Representative maximum intensity projections of zebrafish livers at 10dpf with fluorescent neutrophils after indicated times of Mtz exposure and recovery in the *TG(LysC:PM-mK2)* reporter line. Scale bars, 50nm. **(B)** Number of neutrophils in the liver at indicated times of Mtz exposure and recovery in the *TG(LysC:PM-mK2)* reporter line. Square brackets indicate the number of animals per condition. Error bars, SEM. T-test. *** $p < 0.001$. **** $p < 0.0001$. **(C)** Number of SG-positive hepatocytes in the liver at indicated times of Mtz exposure. Square brackets indicate the number of animals per condition. Error bars, SEM. T-test. * $p < 0.05$. ** $p < 0.01$. *** $p < 0.001$. **(D)** Quantification of morphological phenotypes by damage score. Numbers within bars indicate number of animals per group.

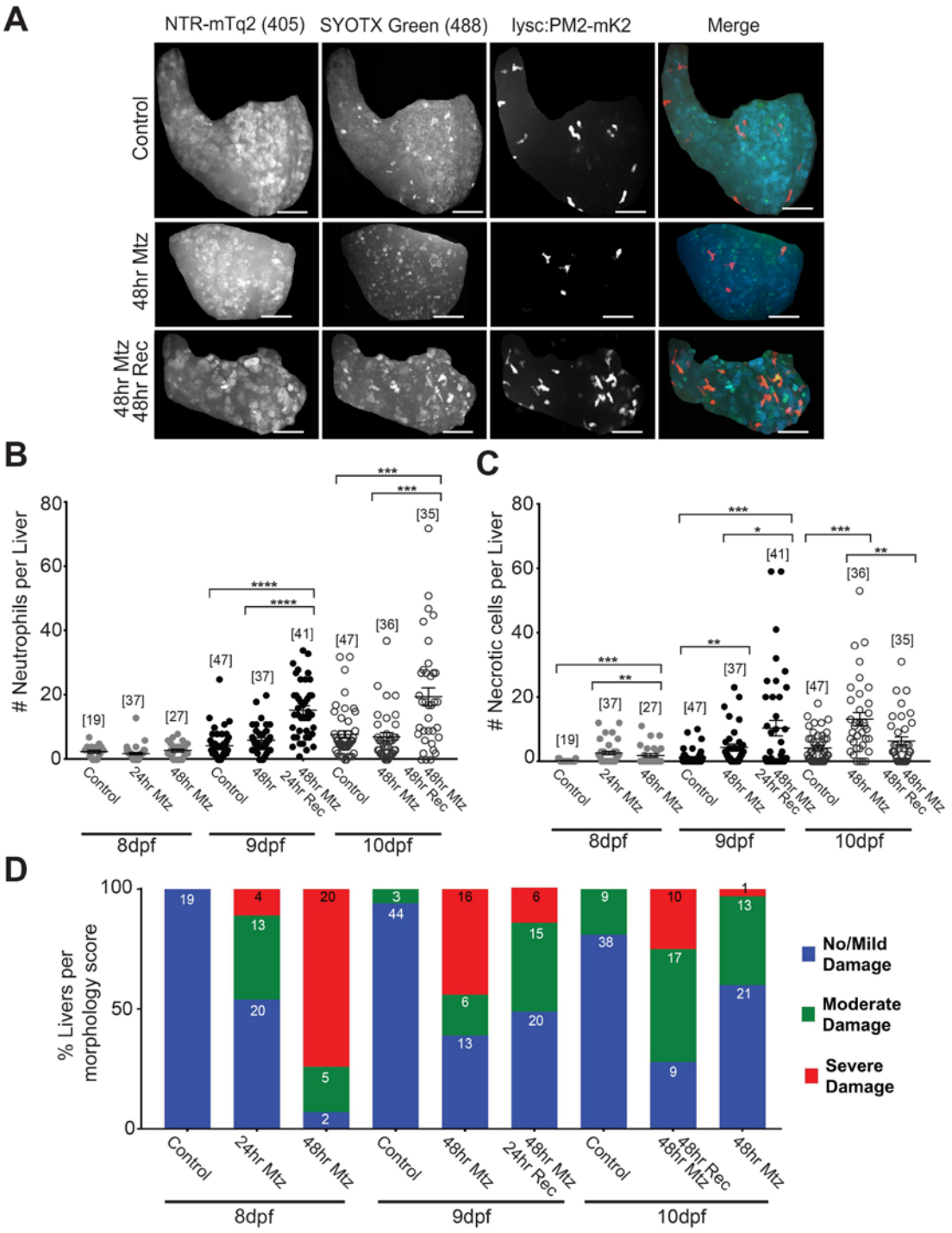

Figure 3.15: Removal of Mtz after 48hrs of Mtz exposure induces neutrophil recruitment into damaged livers (legend on preceding page).

CHAPTER 4: DISCUSSION

The NTR/Mtz system as a tool for inducing liver damage

The purpose of this project was to identify the signals that direct leukocyte trafficking during SI without breaching the epithelial barrier. To accomplish this, I needed to induce spatiotemporally-controlled liver damage so leukocytes would be preferentially trafficked to the liver. The larval zebrafish liver is an ideal system in which to study SI because it is a well-defined, fully functioning organ at 8dpf that is small enough to be imaged in a single confocal image field. Damaging the liver while sparing other tissues in the larvae presented a technical challenge, as zebrafish larvae are quite small and available systems (which rely heavily on drug toxicity) have systemic off-target effects. The NTR/Mtz system enabled us to reliably damage the liver while preserving surrounding tissues.

Mechanism of action of the NTR/Mtz system

The NTR/Mtz requires the use of both genetic and pharmacologic tools. NTR, an enzyme normally found in bacteria[103,104], converts the otherwise harmless antibiotic Mtz into a toxic free radical[142]. This free radical is then capable of inducing DNA damage and oxidative stress in the NTR-expressing cell. Since this system has been used in the liver by another group[102–104], I chose to express *NTR-mTq2* under the hepatocyte-specific *fabp10* promoter[102,136].

The NTR/Mtz system is a reliable way with which to induce selective liver damage

The NTR/Mtz system provided a way to initiate liver damage and inflammation in a spatiotemporally controlled manner without breaching the epithelial barrier. To measure SI we decided to count the number of leukocytes in the livers of *TG(fabp10:NTR-mTq2)* larvae that had been exposed to Mtz. Several leukocyte reporter lines were already in use by other members of the lab, which I could easily cross with *TG(fabp10:NTR-mTq2)* larvae. Since the liver is relatively large and well

demarcated, the liver margin served as a natural region of interest for leukocyte quantification. Our lab has extensive experience using leukocyte chemotaxis to assay inflammation. Such intravital imaging experiments have a certain amount of background noise, which is reduced if special care is taken to ensure that only one part of the larva is damaged. Inducing damage in only hepatocytes improves this intravital assay because it reduces the possibility that damage to other organs/epithelium (and therefore inflammatory signals) could interfere with our results.

Although there are many advantages to the NTR/Mtz system, there are also caveats to this approach. The NTR/Mtz system has been reported to induce mainly apoptotic cell death[104]. Although this was supported by my own data, I also observed necrosis in Mtz-treated *TG(fabp10:NTR-mTq2)* larvae. Because of this, it is difficult to draw definitive conclusions about the precise mechanism by which leukocytes are recruited to the liver. Pharmacologic inhibitors to prevent apoptosis are available, but necrosis cannot be pharmacologically inhibited (with the exception of necroptosis). To circumvent this problem, we conceived novel approaches to induce purely apoptotic or purely necrotic cell death in the zebrafish liver.

Alternative genetic approaches to induce liver damage

We considered multiple ways with which we could induce necrosis and/or apoptosis in the liver. In a prior study, researchers showed that overexpression of mixed-lineage kinase like (*MLKL*) domain is sufficient to induce necrosis/necroptosis. I was able to replicate this finding in both HeLa cells and zebrafish embryos (data not shown). *MLKL* forms pores in the plasma membrane of cells upon stimulation of the necroptosis pathway (and/or overexpression), inducing necrotic cell death via necroptosis. Due to the toxicity of *mK2-MLKL*, I decided to use a conditional expression system to generate larvae that would express *mK2-MLKL* only in the liver. A *TG(hsp70:Cre)* line was already present in lab, so I attempted to create a

TG(fabp10:loxp-mTq2-stop-loxp-mK2:MLKL) transgenic line to cross with the *TG(hsp70:Cre)* line. I identified an F0 animal that produced *TG(fabp10:loxp-mTq2-stop-loxp-mK2:MLKL)* progeny, but I was unable to demonstrate that the *TG(hsp70:Cre)* line was capable of recombination. Unfortunately, that line did not have a fluorescent protein reporter expressed under the *hsp70* promoter, so I was unable to determine whether that line expressed functioning *Cre*. Although I was unable to complete this tool, it may be worth revisiting since there are few practical ways of inducing necrosis. The conditionally-expressed *mK2-MLKL* approach could theoretically work, and if successful, could be of immense benefit to the field.

In addition to the inducible necrosis construct, we conceived a strategy to develop a zebrafish line capable of inducing only apoptosis in the liver. Since *Caspase 9* (*Casp 9*) overexpression has been shown to cause apoptosis[110], we aimed to use conditional overexpression (i.e. the *Cre-lox* system) to induce apoptosis in hepatocytes. As discussed above with the *mK2-MLKL* construct, I created a *fabp10:loxp-mTq2-stop-loxp-mK2-MLKL* transgene. I planned to generate a transgenic line with this construct and mate the F1 adults with the *TG(hsp70:Cre)* line to conditionally express apoptosis. I stopped work on this, however, when it became clear that the *TG(hsp70:Cre)* line was unreliable. As with the *mK2-MLKL* construct, this approach can theoretically work and would prove useful to the field.

Attempts at using other drug-based approaches to induce SI

I made several attempts to induce liver damage in 5-8dpf zebrafish larvae using paracetamol (APAP) and alcohol (EtOH) as described in prior studies[12,22,81,144]. Despite multiple attempts to optimize these experiments, I did not observe liver damage in response to either substance at high concentrations. The concentration of APAP and EtOH was sufficient to kill roughly 50% of the treated larvae at 8dpf, but the larvae (both deceased and survivors) did not show obvious signs of liver damage.

Without further experimentation I cannot comment on how or why this is the case, but it is important to note that there was a key difference in the timing of the drug application and imaging relative to other studies.

In previous studies larval livers were exposed to APAP or EtOH as early as 2-3dpf [81,133,145], whereas I exposed the livers to APAP and EtOH from 5-8dpf. I made this change for a few reasons. First, the liver bud begins to develop at around 3dpf and is not fully functional until roughly 5dpf[146]. I was concerned that the 2-3dpf larvae would be unable to properly metabolize APAP and EtOH, which could alter the experimental outcome. Drug metabolism is a critical step in the pathophysiology of APAP- and EtOH-induced hepatitis because liver damage is actually caused by the metabolites of APAP and EtOH, as opposed to the drugs themselves[84,147]. Zebrafish larvae do not have a fully functional liver prior to 5dpf[146]; therefore, I decided to apply the drug no earlier than 5dpf in order to mimic the effects of APAP and EtOH toxicity in adults as closely as possible. My other concern with the approaches used in younger larvae was that at 3dpf the liver is actively undergoing morphogenesis[146]. I was concerned that administering drugs to larvae that young would result in developmental delay of the liver, which would be substantially smaller than healthy livers. Since the most common way to assay liver damage is to image the larvae and measure reduced liver size/volume[12], developmental delay of the liver could essentially result in false positive results. Therefore, I relied on 5-8dpf and confocal imaging to avoid these pitfalls. Despite several attempts at optimization of APAP and EtOH, I was unable to induce liver damage or SI using either APAP or EtOH.

Confocal imaging produced high-resolution intravital images

Benefits of confocal imaging

The lab's spinning disk confocal microscope offers a major advantage to this project. This microscope allowed us the option of observing morphological changes

individual cells prior to the development of severe damage. It could image individual hepatocytes greater detail than a widefield microscope. On a widefield microscope, the most reliable way to look for liver damage is to quantify changes in liver size. With the confocal microscope, however, I observed that reduction in liver size was most pronounced with severely damaged livers and virtually nonexistent in mild or moderately damaged livers. Based on my data, it is important to detect liver damage before the livers become severely damaged. Many processes we observed took place in moderately-damaged livers that were similar in size to control livers. For example, moderately-damaged livers showed extensive CRO labeling (Figure 3.3) and macrophage infiltration (Figure 3.10). We were also able to identify $mK2^{+}$ inclusions in hepatocytes, which to my knowledge is a novel finding. Therefore, confocal microscopy increases the sensitivity of the damage score assay, providing better information on the relationship between liver damage and cell death or leukocyte recruitment.

Caveats of our confocal imaging system

Every imaging modality, including confocal microscopy, has limitations that are important to be aware of. After imaging several experiments with the CRO dye, I noticed that it could be difficult to visually distinguish between CRO-labeled structures and autofluorescent cellular debris. This became more challenging in animals with weaker CRO labeling because it was necessary to lower the minimum fluorescence intensity threshold in order to quantify these inclusions using Autoquant. This effectively increased the chance that autofluorescent debris would be read and counted as a CRO^{+} hepatocyte by the analysis software.

To overcome this issue, I improved the accuracy of the assay by accounting for each image's background intensity. I first imaged several Mtz-treated larvae in the 405nm, 488nm, and 561nm channels and determined that Mtz-treated livers have mild

autofluorescence in the 561nm channel but not the 488nm channel (Figure 3.4). To overcome this problem, I measured the background fluorescence of each image in the 561nm channel and multiplied that by a single number until Autoquant could no longer detect autofluorescent debris. For the 561nm channel a multiplier of 5 was enough to virtually eliminate autofluorescence in the quantitative analysis. The liver could then be visually inspected to confirm the presence of CRO labeling or autofluorescent cell debris, which has different morphology from the CRO^+ cells. Although there was no autofluorescence in the 488nm channel, the data were much cleaner after using a minimum intensity threshold calculated for each image by measuring the background fluorescence and multiplying it by 3. These parameters are specific to our microscope, so I highly recommend that anyone who tries this technique should first image unlabeled Mtz-treated larvae on their own system to determine whether a background fluorescence multiplier is necessary.

Mechanism of liver damage and cell death

The experimental results presented in this thesis are consistent with the mechanisms of NTR/Mtz-mediated cell death that have been described in other studies[104]. In my hands, experiments performed with TUNEL and fluorescent dye labeling revealed that apoptosis, necrosis, and ROSs are present in this system. Findings in prior studies suggest that hepatocellular damage in these larvae occurs via ROSs and free-radical damage, causing primarily apoptosis[142,148]. I was unable to definitively prove that ROSs or apoptosis cause liver damage, or to identify which signals cause leukocyte recruitment in this system. However, the pattern of leukocyte recruitment seen in my experiments poses interesting questions into which signals cause leukocyte trafficking to the liver.

Redox signaling may direct the progression of liver damage in the NTR/Mtz system

It is widely accepted that the NTR/Mtz system mediates tissue-specific ablation via free-radical DNA damage and oxidative stress[142]. The predominance of apoptotic cell death, the presence of ROSs, and the differential regulation of redox signaling enzymes in Mtz-treated livers support this hypothesis. Indeed, our RNA-seq data indicate that enzymes involved in the *NRF2*-mediated antioxidant response is highly upregulated in this system (Figure 3.2). Many of the upregulated genes (such as *GCL*, *Prdx1*, *Ptgr1*, and many others) are downstream of the *KEAP1*/*NRF2*-mediated response to oxidative stress[91,92,149]. These data have limited utility because the mRNA for RNAseq was extracted from FAC-sorted hepatocytes of larvae that had been treated with either Mtz for 48hrs or 0.2% DMSO in E3. Intravital imaging experiments showed that these conditions do not necessarily correspond with neutrophil recruitment to the liver, depending on the leukocyte reporter used (Figure 3.7, Figure 3.10, Figure 3.11). Given that the RNA-seq results were consistent with the mechanisms described in the literature[142], I hypothesized that the NTR/Mtz system was causing oxidative damage in NTR-expressing hepatocytes.

This conclusion was further supported by live-imaging *TG(fabp10:NTR-mTq2; casper)* zebrafish labeled with CRO, which showed that ROSs are present in Mtz-treated livers within 24hrs of Mtz exposure (Figure 3.3). At 24hrs, most of the livers were either undamaged or moderately-damaged. Except for the 48hr Mtz exposure group, it is difficult to make a direct comparison between this and the RNA-seq experiment, since the RNA-seq data was obtained from RNA collected from hepatocytes exposed to Mtz for 48hrs. However, CRO labeling is visible in the liver starting at 24hrs, and we know that CRO labeling continues until 48hrs Mtz exposure from the data shown in Figure 3.3.

The RNA-seq and CRO experiments showed that ROSs are present in the NTR/Mtz system, and that hepatocytes alter expression of redox signaling enzymes after Mtz treatment. However, these experiments do not prove that ROSs or redox signaling is responsible for the progression of liver damage in this system. In order to determine whether this is the case, it is necessary to perform experiments in which key redox signaling enzymes are perturbed. If inhibiting these enzymes causes worsened liver damage, one could conclude that ROSs cause liver damage and that redox enzymes work to neutralize damage-causing ROSs. If inhibiting these enzymes causes less severe liver damage one may conclude that it is not the ROSs themselves that directly induce cellular damage, but that damage could be a downstream response to signaling pathways that detect ROS. Increased CRO labeling in the liver upon redox signal inhibition would support the hypothesis that redox signaling neutralizes ROSs in hepatocytes.

Experiments in which *TG(lysc:PM2-mK2; fabp10:NTR-mTq2)*, *TG(mpx:PM2-mK2; fabp10:NTR-mTq2)*, or *TG(mpeg1:eGFP; fabp10:NTR-mTq2)* are treated with redox signaling inhibitors during Mtz exposure could yield valuable insights into the role of ROSs and redox signaling on leukocyte recruitment. Although there is evidence that leukocyte recruitment occurs in response to oxidative stress and tissue damage[7,29], the literature is unclear about whether leukocytes are attracted to the cellular damage or to signals produced by redox signaling enzymes. Increased leukocyte recruitment after inhibition of redox signaling inhibition would support the hypothesis that leukocytes are attracted to cells damaged by ROSs. Conversely, if leukocyte recruitment is decreased after inhibition of redox signaling, one could conclude that redox enzymes are capable of inducing inflammatory pathways in response to ROSs.

Pharmacologic inhibition is the most straightforward approach to answer these questions. Genetic knockouts of key redox enzymes (Figure 1.5) are embryonic lethal, and conditional knockout systems are unreliable in Zebrafish. Morpholino inhibition was ineffective because morpholino and mRNA phenotypes were lost after 4dpf (data not shown). Since two arms (GSH and *Prdx1*) of redox signaling are present, the inhibition of one arm (i.e. inhibition of GSH signaling alone) could cause compensatory increases in the activity of the other arm. Therefore, in order to ensure that ROS neutralization/signaling is completely blocked, it may be useful to apply multiple drugs to the fish (such as buthionine sulfoximine to inhibit GSH synthesis and Conoidin A to inhibit *Prdx1*). If leukocyte recruitment is reduced in response to pharmacologic redox inhibitors, it may be possible to identify the signaling enzyme(s) responsible. Pharmacologic inhibitors to many of the key redox enzymes are available, and could be used to determine whether inflammatory signaling is initiated by redox enzymes or a downstream pathway.

Apoptosis is the major form of cell death in the NTR/Mtz system

One of the goals of this project was to identify the types of cell death caused by the NTR/Mtz system. Another was to determine whether leukocytes would be recruited to the dead and dying cells. Previous studies showed that the NTR/Mtz system induces cell death via apoptosis, possibly through ROS and/or free radical-mediated DNA damage. To better understand this process, I turned to data from the RNA-seq experiment for evidence of apoptosis. Examination of the RNA-seq data showed that several pro-apoptotic genes, such as *Caspase 3* (*Casp 3*), *Caspase 8* (*Casp 8*), and *Casp 9,* were upregulated during Mtz exposure.

To verify whether apoptosis is present in the NTR/Mtz system, I labeled Mtz-treated, PFA-fixed larvae with the TMR Red TUNEL kit from Sigma. I found that Mtz-treated larvae underwent pronounced apoptosis after 24hrs Mtz exposure as

expected. Unfortunately, I was unable to draw a connection between liver damage and apoptosis. The damage score assay was specifically developed for use with live larvae, and is not useful in fixed larvae. The TUNEL protocol involved fixing, dehydrating, rehydrating, and two separate overnight incubations; consequently, the livers' morphology varied from that seen in live imaging (compare Figure 3.5 to Figure 3.1). Note that the overall shape of the liver in the TUNEL-labeled larvae was similar to that seen in intravitally-imaged livers, but finer details (such as cell swelling, sinusoids, etc) were lost (Figure 3.5). Furthermore, mTq2 fluorescence was greatly reduced in fixed larvae. These factors together prevented me from analyzing these livers for damage. Since I cannot make a reliable assessment on the degree of liver damage in these livers, I am currently unable to draw a direct correlation between liver damage and apoptosis.

Apoptosis is an important feature of the NTR/Mtz system. Canonically, apoptotic cell death has been considered an "immunologically silent" form of cell death that occurs in response to DNA damage, such as that seen in oxidative stress[1]. Cells with oxidative stress and/or DNA damage attempt to undergo apoptosis as a means to prevent necrotic cell death[41,52,113], which is cytotoxic to neighboring cells. In Mtz-treated livers TUNEL staining revealed an increase in apoptosis at 24hrs Mtz exposure, which coincides with macrophage infiltration in the liver. This could be explained by prior reports in the literature, which show that macrophages are recruited by "find me" signals produced by apoptotic bodies[50,113,118]. Treating *TG(mpeg1:eGFP; fabp10:NTR-mTq2)* larvae with a pan-caspase inhibitor such as zVAD-FMK during Mtz exposure should inhibit apoptosis[62,107,150]. If macrophage recruitment is reduced or prevented zVAD-FMK application, we could conclude that apoptosis is responsible for macrophage infiltration.

Even if apoptosis is responsible for the liver damage seen in this system, inhibiting apoptosis may not prevent liver damage and could actually worse it. Reports in the literature have documented that inhibition of apoptosis does not improve the progression of organ damage (as in the case of IRI), and may actually increase the amount of necrosis in the organ, worsening tissue damage[107]. In situations of oxidative stress, stressed cells attempt to mitigate damage by upregulating redox signaling enzymes. The cell has become so damaged that it will no longer divide; however, it will continue to fulfill its metabolic functions as much as possible until the source of the oxidative stress is removed[151,152]. Since the cell has been irreparably damaged, it will undergo apoptosis upon removal of the stressor. In theory, this process allows for the death and removal of damaged cells with as little inflammation as possible. If apoptosis is inhibited in situations of oxidative stress, the cell will no longer be able to undergo apoptosis when the oxidative stressor is removed. Eventually, the cell would succumb to necrosis.

Necrosis is a minor contributor to cell death in the NTR/Mtz system

Although apoptosis is the predominant form of cell death seen in these experiments, necrosis also contributes to the pathogenesis of Mtz-mediated liver damage. Our data show that necrotic cell death is present in low levels in the Mtz-treated liver (Figure 3.6) and that it is probably not widespread enough to account for the degree of tissue damage we observe. To better understand necrosis in the NTR/Mtz system, I used SG to label necrotic nuclei in live zebrafish larvae. SG labeling was significantly increased within 24hrs of Mtz exposure, and further increased at 48hrs of Mtz exposure. However, the number TUNEL-labeled nuclei outnumbered SG-labeled nuclei by roughly 10:1. An important feature to note is that SG does not specifically label hepatocytes; rather, it labels nuclei of any cells that have permeabilized plasma membranes (i.e. necrotic cells)[95]. Since the liver is

composed of multiple cell types, it is important to consider that some of the SG labeling may actually be of non-hepatocyte cells. During image analysis it became clear that a that some of the SG-labeled cells did not exist within hepatocytes. For example, SG was observed in some *lysc*$^{+}$ neutrophils (Figure 3.15A). When SG^{+} *lysc*$^{+}$ neutrophils were observed, the number of SG^{+} *lysc*$^{+}$ neutrophils was deducted from the total count of SG^{+} cells. Without other cell type-specific reporter lines (such as those available for hepatic stellate cells and endothelial cells) I am only able to quantify the number of SG^{+} cells within the liver parenchyma that are not neutrophils. Understanding how non-hepatocyte cells in the liver respond to hepatocellular damage is important because some cell types (especially hepatic stellate cells) have been documented to undergo inflammatory and fibrotic changes in response to damage signals. Therefore, further experimentation is needed better understand necrosis in non-hepatocyte cell populations in the NTR/Mtz system.

In the data discussed thus far, it seems unlikely that primary necrosis (i.e. pathological necrosis by an otherwise intact hepatocyte) contributes significantly to cell death in this system. Although there may be some primary necrosis in this system, some of the necrosis could be secondary necrosis of apoptotic bodies that were not cleared in a timely manner. Since one of the central paradigms of SI is that DAMP spillage from necrotic cells is responsible for recruiting neutrophils to the site of injury[3,7,23,53], these findings may indicate that the NTR/Mtz system is not the best tool with which to study SI. However, reports in the literature indicate that inhibition of apoptosis may result in increased necrosis as described. If this is true, applying pan-caspase inhibitors to the larvae during Mtz exposure ought to result in significantly more necrosis. Provided that DAMPs truly are responsible for driving SI, this should result in neutrophilic infiltration to the liver.

Inhibiting apoptosis may be useful for understanding necrosis in this system. However, the data presented in Figure 3.15 demonstrates that replacing Mtz with clean 0.2%DMSO in E3 for 24-48hrs after exposing the larvae to Mtz for 48hrs results in both an increase in neutrophils and SG^+ cells in the liver. Figure 3.15C shows that SG^+ cells are increased in the 9dpf group that had been exposed to Mtz for 48hrs and given a 24hr recovery time relative to 9dpf larvae exposed to Mtz for 48hrs alone. This occurs even though the livers had less severe damage than the 9dpf larvae exposed to Mtz for 48hrs without a recovery period (Figure 3.15D). In the 10dpf larvae exposed to Mtz for 48hrs and given a 48hr period of recovery, SG^+ cells were still significantly increased relative to 10dpf controls, but not relative to 10dpf larvae that were exposed to Mtz for 48hrs without a recovery period. Therefore, the addition of a 24hr recovery period could be sufficient to drive SI in the liver and enable researcher to study this process *in vivo*. Given the relationship between redox signaling, apoptosis, and necrosis, redox enzymes would be a reasonable place to start perturbation experiments. Two obvious experiments would be qRT-PCR of key redox and inflammatory mediators, in addition to pharmacologic perturbation of said mediators. For a more comprehensive understanding of differential gene expression, it would also be worth performing RNA-seq on *TG(fabp10:NTR-mTq2; casper)* larvae that had been given a 24hr recovery period after Mtz exposure or no recovery period, and compare those groups with the control group. This experiment could identify additional targets for perturbation and elucidate which signals are necessary for leukocyte recruitment to the liver.

Leukocyte recruitment to the liver

The main reason for attempting to induce necrosis and apoptosis in the liver was to cause SI. We would use it to test redox and inflammatory pathways to determine their role in SI. Although we eventually observed leukocyte infiltration in

all three of our leukocyte reporter lines, the process was not as straightforward as we originally expected.

Neutrophils are generally not recruited to the liver in the presence of Mtz

When I first began designing the assay for this experiment (i.e. quantifying the number of neutrophils or fluorescently-labeled cells in each liver), it was with the expectation that neutrophil recruitment would occur as a result of pro-inflammatory signals being released from hepatocytes prior to their death. In the initial experiments, I imaged larvae during continuous exposure to Mtz. I expected results from the *TG*(*lysc:PM2-mK2)* and *TG(mpx:PM2-mK2)* reporter lines to be similar because prior work showed that *lysc*- and *mpx*-driven reporters should label identical neutrophil populations[153,154].

In practice, I observed significant differences in behavior between the two lines. In the *lysc* reporter I saw no increase in neutrophil migration to the liver during Mtz exposure (Figure 3.15B). I also observed fewer *lysc*$^+$ neutrophils during Mtz exposure than in the control group (Figure 3.7D & Figure 3.13C) in more than one instance. In the *mpx* reporter line, however, I observed that *mpx*$^+$ neutrophils were recruited to the liver after 48hrs Mtz exposure (Figure 3.10). *Mpx*$^+$ neutrophil infiltration was most apparent when the livers were severely damaged. However, a linear regression analysis showed that the degree of liver damage is a poor predictor of leukocyte infiltration ($R^2 = 0.23$, data not shown).

I consistently observed small, round mK2$^+$ inclusions in hepatocytes in both reporter lines. Without further study I cannot identify the structures with certainty, but they resemble vesicules in structure and presumably obtain mK2$^+$ material from the neutrophil populations labeled by *lysc:PM2-mK2* and *mpx:PM2-mK2.* The mechanism of this activity is unclear. In the future, creating timelapse movies of Mtz-treated livers could capture the event(s) that lead to the development of mK2$^+$ inclusions in

hepatocytes. Initially, there was concern that these inclusions were not mK2$^+$, but instead contained autofluorescent substances such as lipofuscin. To ensure that this was not the case, I examined the images carefully in all three channels and discovered that the inclusions were only present in the 561nm/mK2 channel. Analysis of unlabeled, Mtz-treated *TG(fabp10:NTR-mTq2; casper)* larvae showed that damaged livers autofluoresce at a low level in the 561nm channel. Steps were taken to ensure that quantification of leukocytes and fluorescent dye-labeled livers was unaffected by this autofluorescence (see Chapter 2 for more details). This was mainly accomplished by multiplying the background fluorescence of each image either an integer multiplier. Therefore, the inclusions seen in *TG(lysc:PM2-mK2; fabp10:NTR-mTq2)* and *TG(mpx:PM2-mK2; fabp10:NTR-mTq2)* are unlikely to be an artifact of imaging or autofluorescence from dead cell corpses.

The discrepancy between the results of the *lysc* and *mpx* lines drew our attention, as we expected the two leukocyte reporters to behave the same way. I reasoned that this difference could be due to one of three reasons: (1) It is possible that our *lysc*$^+$ and *mpx*$^+$ neutrophil reporter lines vary slightly from those described in the literature. These transgenic lines were created by injecting single-cell stage *casper* embryos with the respective Tol2 constructs and transposase mRNA (see Chapter 2 for detailed protocol). It is possible that the *PM2-mK2* constructs were inserted into the genome in such a way that the expression of one of the constructs was changed by the surrounding non-coding DNA. (2) These results may be due to the reduction of *lysc*+ neutrophils observed in *TG(lysc:PM2-mK2; fabp10:PM2-eGFP-P2A-mTq2)* larvae after exposure to Mtz (Figure 3.8). That experiment should be repeated using the *mpx* reporter line to determine whether Mtz may have an effect on *mpx*$^+$ neutrophil infiltration into the liver. (3) Mtz may effect the development of *lysc*$^+$ neutrophils. The data shown in Figure 3.9 indicates that *lysc*$^+$, but not *mpx*$^+$, neutrophils are reduced in

the CHT after exposure to Mtz. The difference in means between control and Mtz-treated *lysc*$^{+}$ neutrophils is statistically significant, but smaller than one would expect based on the discrepancies shown in Figure 3.8 and Figure 3.9.

Mtz may have anti-inflammatory activity in the zebrafish liver

There has been at least one report that Mtz has anti-inflammatory properties[155]. This remains a possibility in the NTR/Mtz system, especially given the pattern of gene expression in our RNA-seq data. For example, several canonical mediators of SI such as *Il-1β*, *Cxcl-C1C*, and formylated peptides either demonstrated no differential expression in hepatocytes or were strongly downregulated. Certain anti-inflammatory mediators were upregulated. *Ptgr1*, a *NRF2*-dependent enzyme, was the most strongly upregulated gene in the analysis. *Ptgr1* hydrolyzes LTB_4, a potent neutrophil chemoattractant, into a biologically inactive molecule. Additionally, two isoforms of *Tgf-β*, which also has anti-inflammatory properties, are upregulated in zebrafish hepatocytes during Mtz exposure (Figure 3.12). Therefore, further characterization of the effects of Mtz on the zebrafish liver is needed to better understand the system and results obtained using the *lysc*$^{+}$ neutrophil reporter. An RNA-seq or qRT-PCR experiment comparing *TG(lysc:PM2-mK2; fabp10:PM2-eGFP-P2A-mTq2)* livers treated with Mtz or 0.2% DMSO in E3 would be very important for this system.

Neutrophil recruitment occurs after Mtz has been removed from the bathing medium

After reviewing the above experiments, I suspected that Mtz may have anti-inflammatory effects on *lyc*$^{+}$ neutrophils, or perhaps inhibit their development. I decided to image Mtz-treated larvae after removing Mtz from the bathing medium to see whether SI could be initiated in the absence of Mtz. To do this, I reared larvae to 6dpf and exposed them to Mtz for 48hrs. They were given either a 24hr or 48hr recovery period in 0.2% DMSO in E3 and imaged at 9dpf and 10dpf, respectively. Figure 3.15 shows that *lysc*$^{+}$ neutrophils infiltrate the damaged liver robustly after a

recovery period. The 9dpf larvae given 24hrs to recover after 48hrs Mtz exposure had greater leukocyte recruitment than the 9dpf larvae without a recovery period. The same trend was observed in the 10dpf larvae that were either given a 48hr recovery period after 48hrs of Mtz exposure, or 48hrs of Mtz exposure without a recovery. The 24hr and 48hr recovery groups had less damage than the non-recovery groups in both the 9dpf and 10dpf larvae, showing that liver damage is not correlated to *lysc*$^{+}$ neutrophil recruitment.

To determine whether leukocyte recruitment and hepatocellular necrosis was correlated in these groups, I had incubated the larvae described above with SG and included SG in the imaging. I found that the 9dpf larvae with a 24hr recovery period had more leukocytes and significantly increased SG labeling relative to the 9dpf larvae without a recovery period. The 9dpf, 24hr recovery group also had less damage than the 9dpf larvae without a recovery. Without additional experiments to verify these observations I cannot make a concrete conclusion about this finding. However, in these larvae, necrosis does not necessarily correlate to the degree of liver damage (Figure 3.15C). This suggests that necrosis may not be responsible for liver damage. The 10dpf larvae with a 48hr recovery period had more leukocytes and less SG labeling than the 10dpf larvae without a recovery period. These data indicate that leukocyte recruitment does not necessarily correspond with increased SG labeling. At this time the mechanism by which neutrophils are recruited to the liver is unclear. One could argue that removal of Mtz causes neutrophil recruitment, which then cause liver damage and necrosis. On the other hand, Mtz removal could allow cells to undergo necrosis, which then drives neutrophil recruitment to the liver. It should be noted that although survival was not quantified in this experiment, roughly half of the larvae in the 24hr and 48hr recovery groups expired before they could be imaged. The significance of this observation is currently unclear. An experiment in which

leukocyte recruitment of shorter recovery groups (i.e. 12hrs, 6hrs, etc) would be useful for understanding this process. While this experiment does not directly support the hypothesis that neutrophils arrive to the liver via signals other than DAMPs, it also does not provide evidence to the contrary. I find it curious that the amount of necrosis in the liver does not necessarily correspond to the degree of inflammation. This should be followed up on because it is an important question in SI research.

Macrophages are recruited to the liver within 24hrs Mtz exposure

I expected that macrophages would be present in greater numbers after neutrophils had been recruited to the liver. My data, however, showed that there is a strong influx of macrophages at 24hr Mtz exposure without a recovery period. Macrophages are still present in the liver after 48hr Mtz exposure, but there are roughly twice as many per liver in the 24hr group. Invtravital timelapse images collected during this process showed that not only were macrophages engulfing hepatocytes, but that the macrophages were constantly moving around the damaged liver (data not shown).

Canonically, macrophages produce anti-inflammatory cytokines, including TGF-β and Il-10, upon engulfment of apoptotic cell corpses[3,5,7]. I do not have any data to directly show that macrophages enter the liver to engulf apoptotic hepatocytes. However, this is a possibility given that they enter the liver while the liver is undergoing apoptosis; that is, they are observed as having engulfed hepatocytes or apoptotic bodies, which is reported in the literature. Canonically, macrophages are recruited to apoptotic cell corpses upon release of “find me” signals such as sphingosine 1-phosphate[117] and engulf apoptotic cells with “eat me” signals present on the outer membrane of the apoptotic cells[108]. Therefore, it is possible that the macrophages could be contributing to anti-inflammatory signals in the liver that suppress neutrophil recruitment.

The results from the macrophage recruitment experiment were consistent with my observations from prior experiments. However, more work is needed to verify the mechanism by which macrophages are recruited to the liver and determine the role of macrophages in the liver during this process. To verify that macrophages are recruited to the liver by apoptotic cells, an experiment in which a pan-caspase inhibitor such as zVAD-FMK is applied to *TG(mpeg1:eGFP, fabp10:NTR-mTq2)* larvae. If macrophages are recruited by "find me" signals from apoptotic hepatocytes, there should be fewer macrophages in the liver when an apoptosis inhibitor is applied. If macrophages are recruited to the liver as a means to engulf apoptotic cells and prevent apoptotic cells from progressing to secondary necrosis, knocking out the macrophage population in the larvae should theoretically result in increased necrosis and greater neutrophil recruitment. This could be accomplished by injecting macrophage-depleting drugs, such as clodronate liposomes[29], into the larvae. Finally, the *TG(mpeg1:eGFP)* line is in the *AB wt* background instead of the *casper* background. In order to image *AB wt* larvae, it is necessary to rear them in a solution of PTU to inhibit the development of melanocytes and iridophores. PTU is highly toxic and may have off-target effects. Therefore, it should be tested in larvae in the *casper* background to determine whether it influences the leukocyte recruitment assay readout.

The use of the NTR/Mtz system for studies on SI

My original hypotheses were that neutrophils would arrive to the liver by non-DAMP signals and directly cause liver damage, and that macrophages would be recruited to the liver after this in order to promote healing and resolution of the inflammatory process. In terms of leukocyte recruitment, I observed that macrophages were recruited earlier than *mpx*$^{+}$ neutrophils during Mtz exposure, whereas *lysc*$^{+}$ neutrophils were not recruited to the liver at all during Mtz exposure. I observed that

not only did neutrophils infiltrate into the liver after the macrophages had arrived, but also that their presence in the liver did not correspond to either an increase in hepatocellular necrosis or worsened liver damage. In our transgenic lines, I observed that experiments performed with *lysc*$^{+}$ neutrophils showed different results than the experiments performed with the *mpx*$^{+}$ neutrophils. Further work with the *lysc* reporter revealed that Mtz may have an anti-inflammatory effect on, or inhibit development of, *lysc*$^{+}$ neutrophils.

CHAPTER 5: CONCLUSION AND FUTURE DIRECTIONS

This project provides valuable insight into how cell death and leukocyte recruitment interact to generate SI. The NTR/Mtz system can be used to study several aspects of SI generated by tissue injury in the absence of epithelial barrier breach. For example, treating the larvae with Mtz without a recovery period can be used to study redox signaling, apoptosis, and macrophage recruitment. Allowing the larvae time to recover from Mtz toxicity could be used to study the pro-inflammatory aspect of the system, in which neutrophil recruitment and necrosis become prominent. Although I did not perform the recovery experiment with the *mpx* and *mpeg1* reporter lines, it would be useful to perform for two reasons. First, it would provide further insight as to whether *lysc*$^{+}$ and *mpx*$^{+}$ neutrophils have radically different behavior in this system. Second, an experiment with the *mpeg1* line would be useful to better understand which signals are needed for macrophages to arrive to, and stay in, the liver.

We expected that the NTR/Mtz system would most likely produce liver damage and inflammation via a combination of necrosis and apoptotic cell death. While useful, (since this probably mimics clinically relevant processes like APAP toxicity), it makes identifying individual signals from the different forms of cell death difficult. Developing and optimizing novel tools, such as the necroptosis and apoptosis tools discussed in the previous chapter, would be immensely valuable to the field of SI.

While the NTR/Mtz system has the potential to be a highly useful tool, further characterization of the effects of Mtz and PTU are required in order to fully understand the dynamics of these processes. Since pharmacologic perturbation remains the most promising tool to study several aspects of the anti-oxidant pathways, each drug that one uses to target an enzyme in the pathway should also undergo rigorous characterization. By rigorous characterization, I mean that every drug should be subjected to at least the following tests: 1) Titrate the drug of interest to find the

highest non-lethal dose at which the larvae can be subjected to; 2)Imaging the CHT of each leukocyte reporter used in the study to ensure that the drug does not alter the leukocyte population; 3) Imaging of each leukocyte reporter crossed with the *TG(fab10:PM2-eGFP-P2A-mTq2)* reporter line to determine whether the drug affects the number of leukocytes in the liver at baseline; 4) Experiments using Mtz and co-application of Mtz should include a separate control for the tested drug only; and 5) Tests 1 and 2 should be performed with the co-application of Mtz and the drug of choice to ensure that there are no synergistic effects of Mtz and the drug on the system in the absence of NTR. For drugs that produce interesting results, it would be necessary to validate the intravital data with orthogonal approaches, such as qRT-PCR and western blotting.

In summary, the NTR/Mtz system may be useful for studying SI. I was able to generate neutrophil recruitment to the liver under specific experimental conditions; however, with the data collected so far I am unable to draw conclusions on the mechanism by which this occurs. While obtaining mechanistic data on SI is important, it is more important to first perform a systematic series of control experiments on the effects of Mtz and PTU in all leukocyte reporters. Without these data it will be impossible to draw definitive conclusions about how the system induces SI, and whether it will provide meaningful results in future experiments.

APPENDIX A

Protocol for Metronidazole Exposure (for larvae requiring PTU)

- Collect *tg(mpeg1:eGFP) X tg(fabp10:NTR-mTq2)* or *tg(mpeg1:eGFP) X tg(fabp10:NTR-mK2)* larvae.
- 1dpf: place embryos in 0.2mM PTU in E3.
- 1-4dpf: Clean dishes and replace E3 with 0.2mM PTU as needed.
- 5dpf: Sort larvae for transgene expression. Feed larvae with a very small amount of 50µm larval food by dipping a 200µL pipette tip into the food and sprinkling it into the dish.
- 6dpf: From this point on all of the solutions should be dissolved in 0.2% DMSO in E3.
    - Make the following stock solutions (volumes will vary depending on the experiment):
        - 0.5L of 0.2% DMSO in E3: add 1mL DMSO to 499mL E3.
        - 100mL 10mM Mtz: add 0.1715g Mtz powder to 100ML 0.2% DMSO in E3. This is a 2X stock solution. 10mM Mtz can be stored at 4°C for up to 1 week; after that it needs to be made fresh. It is okay to leave at room temperature for 1-2 days, but after that it should be made fresh. It takes a little time to dissolve so it helps to stir it using the magnetic stir bars for ~10min.
        - 100mL 2X PTU: add 4mL 50X PTU to 96mL 0.2% DMSO in E3.
    - Separate larvae out into desired experimental groups (i.e. Controls, 24hr Mtz exposure, etc). Anesthetize the larvae in tricaine and place the

control group (and shorter timepoint groups) into 1X PTU in 0.2% DMSO in E3 and feed.

    - If imaging larvae exposed to Mtz for 48hrs, place the 48hr exposure group in 5mM Mtz. These larvae will also need PTU, so add equal volumes of 10mM Mtz and 2X PTU to a petri dish and then transfer the larvae to this dish and feed them.
    - Experimental groups requiring shorter Mtz exposure should be transferred to dishes containing the 5mM Mtz/PTU solution at the appropriate time. For example, the 36hr exposure group will be transferred 36hrs prior to imaging at 6dpf, the 24hr group will be transferred 24hrs prior to imaging at 7dpf, etc.

- 7dpf: Place larvae in dishes containing fresh 0.2% DMSO in E3 or the 5mM Mtz/PTU mixture as appropriate. Do NOT feed, as food in the intestines will become autofluorescent and interfere with imaging.
- 8dpf: Image larvae. For long-term live imaging (i.e. movies longer than 1hr or so) it is a good idea to put Mtz into the embedding agarose and bathing liquid. I add ~500uL 10mM Mtz and 20µL 20X Tricaine to 500uL 2% low-melting point agarose to make a 1% low-melting agarose with 5mM Mtz and 1X Tricaine. If bathing liquid is needed, use 5mM Mtz with the appropriate volume of Tricaine.

APPENDIX B

Protocol for Zebrafish Larval Dissociation using Trypsin

By Isabelle Kim (Richard White Lab, MSKCC), adapted by Michelina Stoddard

- Anesthetize larvae in 0.2mg/mL Tricaine in E3, place in Eppendorf tube, and euthanize at 4°C for 20min.
- Wash 3X with ice-cold FACS buffer (1mM $CaCl_2$ in PBS).
- Pre-warm ~2-3mL 0.25% Trypsin-EDTA for 5min at 37°C.
- Remove FACS buffer from Eppendorf tube and add 500uL pre-warmed 0.25% Trypsin-EDTA. Place the Eppendorf tube into a 37°C heat block for 15-20min, or until the larvae have completely dissociated. During the incubation, pipette up and down with a P1000 pipette every 5min. Dissociation is complete when the mixture is a homogenous dark brown, and the zebrafish's eyes are no longer visible floating in the suspension.
- Add 100uL Fetal Calf Serum (FCS) to the mixture to quench the reaction.
- Gently mix with a P200 pipette to break up any remaining chunks.
- Centrifuge at 1000Xg for 5min and gently remove supernatant with P1000 pipette.
- Resuspend contents in 1mL FACS buffer with 1:100 FCS added (make about 15mL).
- Filter through 40µm BD strainer into a 50mL Falcon tube with 4mL FACS buffer with FCS.
- Centrifuge 1000Xg for 5mmin, gently remove supernatant.
- Resuspend in 200µL FACS buffer with FCS (up to 500µL, if necessary) and strain through 40µm, blue-topped BD FACS tube (5mL).
- Place on ice and proceed with FACS operations.

REFERENCES

1. Guicciardi, M. E., Malhi, H., Mott, J. L. & Gores, G. J. Apoptosis and Necrosis in the Liver. *Compr Physiol* **3,** (2013).
2. Kalogeris, T., Baines, C. P., Krenz, M. & Korthuis, R. J. *Cell Biology of Ischemia/Reperfusion Injury*. *International Review of Cell and Molecular Biology* **298,** (Elsevier Inc., 2012).
3. Kubes, P. & Mehal, W. Z. Sterile Inflammation in the Liver. *Gastroenterology* **143,** 1158–1172 (2012).
4. McDonald, B. *et al.* Intravascular danger signals guide neutrophils to sites of sterile inflammation. *Science (80-.).* **330,** 362–366 (2010).
5. Chen, G. Y. & Nuñez, G. Sterile inflammation: sensing and reacting to damage. *Nat. Rev. Immunol.* **10,** 826–837 (2010).
6. Shen, H., Kreisel, D. & Goldstein, D. R. Processes of sterile inflammation. *J. Immunol.* **191,** 2857–63 (2013).
7. Van Golen, R. F., Reiniers, M. J., Olthof, P. B., van Gulik, T. M. & Heger, M. Sterile inflammation in hepatic ischemia/reperfusion injury: Present concepts and potential therapeutics. *J. Gastroenterol. Hepatol.* **28,** 394–400 (2013).
8. Woolbright, B. L. & Jaeschke, H. The impact of sterile inflammation in acute liver injury. **3,** 170–188 (2017).
9. Rock, K. L., Latz, E., Ontiveros, F. & Kono, H. The sterile inflammatory response. *Annu. Rev. Immunol.* **28,** 321–342 (2010).
10. Chong, Y. *et al.* Deaths in the United States, 1900-2013. *Natl. Cent. Heal. Stat.* (2015).
11. Hassan, K., Bhalla, V., El Regal, M. E. & Hesham A-Kader, H. Nonalcoholic fatty liver disease: A comprehensive review of a growing epidemic. *World J. Gastroenterol.* **20,** 12082–12101 (2014).
12. Howarth, D. L., Yin, C., Yeh, K. & Sadler, K. C. Defining hepatic dysfunction parameters in two models of fatty liver disease in zebrafish larvae. *Zebrafish* **10,** 199–210 (2013).
13. Ross, R. Atherosclerosis--An Inflammatory Disease. *N. Engl. J. Med.* **340,** 115–126 (1999).
14. Ross, R. Inflammation or Atherogenesis. *N. Engl. J. Med.* **340,** 115–126 (1999).
15. Shaukat, Z., Liu, D. & Gregory, S. Sterile inflammation in drosophila. *Mediators Inflamm.* **2015,** (2015).
16. Murphy, K., Travers, P. & Walport, M. *Janeway's Immunobiology*. (Garland Science, 2008).
17. Huang, C. & Niethammer, P. Tissue Damage Signaling Is a Prerequisite for Protective Neutrophil Recruitment to Microbial Infection in Zebrafish Article Tissue Damage Signaling Is a Prerequisite for Protective Neutrophil Recruitment to Microbial Infection in Zebrafish. *Immunity* **48,** 1006–1013.e6 (2018).
18. Enyedi, B., Jelcic, M. & Niethammer, P. The cell nucleus as a mechanotransducer of wound induced inflammation. *Cell* **in press,** 0–6 (2016).
19. Khoo, J. C., Miller, E., McLoughlin, P. & Steinberg, D. Enhanced macrophage uptake of low density lipoprotein after self- aggregation. *Arterioscler. Thromb. Vasc. Biol.* **8,** 348–358 (1988).
20. Reynolds, W. F. *et al.* Myeloperoxidase polymorphism is associated with gender specific risk for Alzheimer's disease. *Exp Neurol* **155,** 31–41 (1999).
21. Weiner, H. L. & Frenkel, D. Immunology and immunotherapy of Alzheimer's disease. *Nat. Rev. Immunol.* **6,** 404–416 (2006).
22. Williams, C. D. *et al.* Neutrophil activation during acetaminophen hepatotoxicity and repair in mice and humans. *Toxicol. Appl. Pharmacol.* **275,**

122–133 (2014).
23. Shichita, T. *et al.* MAFB prevents excess inflammation after ischemic stroke by accelerating clearance of damage signals through MSR1. *Nat. Med.* **23,** 723–732 (2017).
24. Wahli, W. & Michalik, L. PPARs at the crossroads of lipid signaling and inflammation. *Trends Endocrinol. Metab.* **23,** 351–363 (2012).
25. Yago, T. *et al.* Blocking neutrophil integrin activation prevents ischemia – reperfusion injury. *J. Exp. Med.* **212,** 1267–1281 (2015).
26. Andersson, U. & Tracey, K. J. HMGB1 is a therapeutic target for sterile inflammation and infection. *Annu. Rev. Immunol.* **29,** 139–162 (2011).
27. Liew, P. X. & Kubes, P. Intravital Imaging – Dynamic Insights into Natural Killer T Cell Biology. *Front. Immunol.* **6,** (2015).
28. de Oliveira, S. *et al.* Cxcl8 (IL-8) mediates neutrophil recruitment and behavior in the zebrafish inflammatory response. *J. Immunol.* **190,** 4349–59 (2013).
29. Kezić, A., Stajic, N. & Thaiss, F. Innate immune response in kidney ischemia/reperfusion injury: Potential target for therapy. *J. Immunol. Res.* **2017,** (2017).
30. Wang, J. & Kubes, P. A Reservoir of Mature Cavity Macrophages that Can Rapidly Invade Visceral Organs to Affect Tissue Repair. *Cell* **165,** 668–678 (2016).
31. Dal-Secco, D. *et al.* A dynamic spectrum of monocytes arising from the in situ reprogramming of CCR2 $^{+}$ monocytes at a site of sterile injury. *J. Exp. Med.* **212,** 447–456 (2015).
32. Tartey, S. & Takeuchi, O. Pathogen recognition and Toll-like receptor targeted therapeutics in innate immune cells. *Int. Rev. Immunol.* **36,** 57–73 (2017).
33. Heine, H. & Lien, E. Toll-like receptors and their function in innate and adaptive immunity. *Int. Arch. Allergy Immunol.* **130,** 180–192 (2003).
34. Kanwal, Z., Wiegertjes, G. F., Veneman, W. J., Meijer, A. H. & Spaink, H. P. Comparative studies of Toll-like receptor signalling using zebrafish. *Dev. Comp. Immunol.* **46,** 35–52 (2014).
35. Medzhitov, R. & Janeway, C. The Toll receptor family and microbial recognition. *Trends Microbiol.* **8,** 452–456 (2000).
36. Van Der Vaart, M., Spaink, H. P. & Meijer, A. H. Pathogen recognition and activation of the innate immune response in zebrafish. *Adv. Hematol.* **2012,** (2012).
37. Aderem, A. & Underhill, D. M. Mechanism of Phagocytosis in Macrophages. *Annu. Rev. Immunol.* **17,** 593–623 (1999).
38. Markiewski, M. M. *et al.* C3a and C3b activation products of the third component of complement (C3) are critical for normal liver recovery after toxic injury. *J. Immunol.* **173,** 747–54 (2004).
39. Jaeschke, H; woolbright, B. Injury By Targeting Reactive Oxygen Species. *Transpl. Rev.* **26,** 103–114 (2013).
40. CannistrÃ , M. *et al.* Hepatic ischemia reperfusion injury: A systematic review of literature and the role of current drugs and biomarkers. *Int. J. Surg.* **33,** S57–S70 (2016).
41. Turner, M. D., Nedjai, B., Hurst, T. & Pennington, D. J. Cytokines and chemokines: At the crossroads of cell signalling and inflammatory disease. *Biochim. Biophys. Acta - Mol. Cell Res.* **1843,** 2563–2582 (2014).
42. Monteiro, J. T. & Lepenies, B. Myeloid C-type lectin receptors in viral recognition and antiviral immunity. *Viruses* **9,** (2017).
43. Richardson, M. B. & Williams, S. J. MCL and Mincle: C-type lectin receptors that sense damaged self and pathogen-associated molecular patterns. *Front.*

Immunol. **5,** 1–9 (2014).
44. Yan, M., Huo, Y., Yin, S. & Hu, H. Mechanisms of acetaminophen-induced liver injury and its implications for therapeutic interventions. *Redox Biol.* **17,** 274–283 (2018).
45. Sarvestani, S. T. & McAuley, J. L. The role of the NLRP3 inflammasome in regulation of antiviral responses to influenza A virus infection. *Antiviral Res.* **148,** 32–42 (2017).
46. Pfeiler, S., Winkels, H., Kelm, M. & Gerdes, N. IL-1 family cytokines in cardiovascular disease. *Cytokine* 0–1 (2017). doi:10.1016/j.cyto.2017.11.009
47. Mehrdana, F., Kania, P. W., Nazemi, S. & Buchmann, K. Immunomodulatory effects of excretory / secretory compounds from Contracaecum osculatum larvae in a zebrafish inflammation model. 1–13 (2017).
48. Schaefer, L. Complexity of Danger : The Diverse Nature of Damage- associated Molecular Patterns *. **289,** 35237–35245 (2014).
49. Apetoh, L. *et al.* Toll-like receptor 4-dependent contribution of the immune system to anticancer chemotherapy and radiotherapy. *Nat. Med.* **13,** 1050–1059 (2007).
50. Elliott, M. R. *et al.* Nucleotides released by apoptotic cells act as a find-me signal to promote phagocytic clearance. *Nature* **461,** 282–286 (2009).
51. Brenner, C., Galluzzi, L., Kepp, O. & Kroemer, G. Decoding cell death signals in liver inflammation. *J. Hepatol.* **59,** 583–594 (2013).
52. Huebener, P. *et al.* The HMGB1/RAGE axis triggers neutrophil-mediated injury amplification following necrosis. *J. Clin. Invest.* **125,** 539–550 (2015).
53. Kataoka, H., Kono, H., Patel, Z. & Rock, K. L. Evaluation of the contribution of multiple DAMPs and DAMP receptors in cell death-induced sterile inflammatory responses. *PLoS One* **9,** (2014).
54. Yan, B. *et al.* Il-1β and Reactive Oxygen Species Differentially Regulate Neutrophil Directional Migration and Basal Random Motility in a Zebrafish Injury–Induced Inflammation Model. *J. Immunol.* **192,** 5998–6008 (2014).
55. Oka, T., Hikoso, S., Yamaguchi, O. & Taneike, M. Europe PMC Funders Group Mitochondrial DNA That Escapes from Autophagy Causes Inflammation and Heart Failure. **485,** 251–255 (2012).
56. Tian, J. *et al.* Toll-like receptor 9-dependent activation by DNA-containing immune complexes is mediated by HMGB1 and RAGE. *Nat. Immunol.* **8,** 487–496 (2007).
57. Galluzzi, L., Kepp, O. & Kroemer, G. Mitochondria: Master regulators of danger signalling. *Nat. Rev. Mol. Cell Biol.* **13,** 780–788 (2012).
58. Zhang, Y. K. J., Wu, K. C. & Klaassen, C. D. Genetic Activation of Nrf2 Protects against Fasting-Induced Oxidative Stress in Livers of Mice. *PLoS One* **8,** 1–10 (2013).
59. Garg, A. D., Krysko, D. V., Vandenabeele, P. & Agostinis, P. Hypericin-based photodynamic therapy induces surface exposure of damage-associated molecular patterns like HSP70 and calreticulin. *Cancer Immunol. Immunother.* **61,** 215–221 (2012).
60. Spisek, R. *et al.* Bortezomib enhances dendritic cell (DC)–mediated induction of immunity to human myeloma via exposure of cell surface heat shock protein 90 on dying tumor cells: therapeutic implications. *Blood* **109,** 4839–4845 (2007).
61. Liew, P. X., Lee, W. Y. & Kubes, P. iNKT Cells Orchestrate a Switch from Inflammation to Resolution of Sterile Liver Injury. *Immunity* **47,** 752–765.e5 (2017).
62. Angosto, D. *et al.* Evolution of inflammasome functions in vertebrates:

Inflammasome and caspase-1 trigger fish macrophage cell death but are dispensable for the processing of IL-1β. *Innate Immun.* **18,** 815–824 (2012).
63. Ghiringhelli, F. *et al.* Activation of the NLRP3 inflammasome in dendritic cells induces IL-1B-dependent adaptive immunity against tumors. *Nat. Med.* **15,** 1170–1178 (2009).
64. Jaeschke, H. & Woolbright, B. L. Current strategies to minimize hepatic ischemia-reperfusion injury by targeting reactive oxygen species. *Transplant. Rev.* **26,** 103–114 (2012).
65. Yago, T. *et al.* Complexity of the cell – cell interactions in the innate immune response after cerebral ischemia. *Toxicol. Appl. Pharmacol.* **1623,** 53–62 (2015).
66. Rouschop, K. M. A. Protection against Renal Ischemia Reperfusion Injury by CD44 Disruption. *J. Am. Soc. Nephrol.* **16,** 2034–2043 (2005).
67. Ergin, B., Heger, M., Kandil, A., Demirci-Tansel, C. & Ince, C. Mycophenolate mofetil improves renal haemodynamics, microvascular oxygenation, and inflammation in a rat model of supra-renal aortic clamping-mediated renal ischaemia reperfusion injury. *Clin. Exp. Pharmacol. Physiol.* **44,** 294–304 (2017).
68. Enyedi, B., Kala, S., Nikolich-Zugich, T. & Niethammer, P. Tissue damage detection by osmotic surveillance. *Changes* **15,** 1123–1130 (2013).
69. Gault, W. J., Enyedi, B. & Niethammer, P. Osmotic surveillance mediates rapid wound closure through nucleotide release. *J. Cell Biol.* **207,** 767–782 (2014).
70. Niethammer, P., Grabher, C., Look, A. T. & Mitchison, T. J. A tissue-scale gradient of hydrogen peroxide mediates rapid wound detection in zebrafish. *Nature* **459,** 996–9 (2009).
71. Pipalia, T. G. *et al.* Cellular dynamics of regeneration reveals role of two distinct Pax7 stem cell populations in larval zebrafish muscle repair. *Dis. Model. Mech.* **9,** 671–84 (2016).
72. Huttenlocher, A. & Poznansky, M. C. Reverse leukocyte migration can be attractive or repulsive. *Trends Cell Biol.* **18,** 298–306 (2008).
73. Mossman, B. T. & Churg, A. Mechanisms in the patheogenesis of asbestosis and silicosis. *Am J Rep* **157,** 1666–1689 (1998).
74. McDonald, B. & Kubes, P. Innate Immune Cell Trafficking and Function During Sterile Inflammation of the Liver. *Gastroenterology* **151,** 1087–1095 (2016).
75. Navab, M., Gharavi, N. & Watson, A. D. Inflammation and metabolic disorders. *Curr. Opin. Clin. Nutr. Metab. Care* **11,** 459–464 (2008).
76. Umemura, A. *et al.* Liver damage, inflammation, and enhanced tumorigenesis after persistent mTORC1 inhibition. *Cell Metab.* **20,** 133–144 (2014).
77. Wree, A., Mehal, W. Z. & Feldstein, A. E. Targeting Cell Death and Sterile Inflammation Loop for the Treatment of Nonalcoholic Steatohepatitis. *Semin Liver Dis* **36,** 27–36 (2016).
78. Vial, G., Dubouchaud, H. & Leverve, X. M. Liver mitochondria and insulin resistance. *Acta Biochim. Pol.* **57,** 389–392 (2010).
79. Lee, W. M. Drug-induced acute liver failure. *Clin. Liver Dis.* **17,** 575–586 (2013).
80. Ju, C. & Reilly, T. Role of immune reactions in drug-induced liver injury (DILI). *Drug Metab. Rev.* **44,** 107–115 (2012).
81. North, T. E. *et al.* PGE2-regulated wnt signaling and N-acetylcysteine are synergistically hepatoprotective in zebrafish acetaminophen injury. *Proc. Natl. Acad. Sci.* **107,** 17315–17320 (2010).
82. Sanz-Garcia, C. *et al.* Sterile inflammation in acetaminophen-induced liver

injury is mediated by Cot/tpl2. *J. Biol. Chem.* **288,** 15342–15351 (2013).
83. Qiu, Y., Benet, L. Z. & Burlingame, A. L. Identification of the hepatic protein targets of reactive metabolites of acetaminophen in vivo in mice using two-dimensional gel electrophoresis and mass spectrometry. *J. Biol. Chem.* **273,** 17940–17953 (1998).
84. Lawson, J. a, Farhood, a, Hopper, R. D., Bajt, M. L. & Jaeschke, H. The hepatic inflammatory response after acetaminophen overdose: role of neutrophils. *Toxicol. Sci.* **54,** 509–516 (2000).
85. Zhai, Y. *et al.* Cutting Edge: TLR4 Activation Mediates Liver Ischemia/Reperfusion Inflammatory Response via IFN Regulatory Factor 3-Dependent MyD88-Independent Pathway. *J Immunol* **173,** 7115–7119 (2004).
86. Aquilano, K., Baldelli, S. & Ciriolo, M. R. Glutathione: new roles in redox signaling for an old antioxidant. *Front. Pharmacol.* **5,** 1–12 (2014).
87. Ornoy, A., Livshitz, A., Ergaz, Z., Stodgell, C. J. & Miller, R. K. Hyperglycemia, hypoxia and their combination exert oxidative stress and changes in antioxidant gene expression: studies on cultured rat embryos. *Birth Defects Res. B. Dev. Reprod. Toxicol.* **92,** 231–9 (2011).
88. Cheng, M.-L. L., Lu, Y.-F. F., Chen, H., Shen, Z.-Y. Y. & Liu, J. Liver expression of Nrf2-related genes in different liver diseases. *Hepatobiliary Pancreat. Dis. Int.* **14,** 485–491 (2015).
89. Zhang, D. D. & Hannink, M. Distinct cysteine residues in Keap1 are required for Keap1-dependent ubiquitination of Nrf2 and for stabilization of Nrf2 by chemopreventive agents and oxidative stress. *Mol. Cell. Biol.* **23,** 8137–51 (2003).
90. Dodson, M., Redmann, M., Rajasekaran, N. S., Darley-Umar, V. & Zhang, J. KEAP1-NRF2 Signaling and Autophagy in Protection against Oxidative and Reductive Proteotoxicity. *Biochem J* **469,** 165–187 (2015).
91. Kansanen, E., Kuosmanen, S. M., Leinonen, H. & Levonenn, A. L. The Keap1-Nrf2 pathway: Mechanisms of activation and dysregulation in cancer. *Redox Biol.* **1,** 45–49 (2013).
92. Motohashi, H. & Yamamoto, M. Nrf2-Keap1 defines a physiologically important stress response mechanism. *Trends Mol. Med.* **10,** 549–557 (2004).
93. Dhanoa, B. S., Cogliati, T., Satish, A. G., Bruford, E. A. & Friedman, J. S. Update on the Kelch-like (KLHL) gene family. *Hum. Genomics* **7,** 13 (2013).
94. Itoh, K., Chiba, T., Takashi, S. & Et, A. An Nrf2/small Mad heterodimer mediates the induction of phase II detoxifying enzyme genes through antioxidant response elements. *Biochem. Biophys. Res. Commun.* **236,** 313–322 (1997).
95. Dunning, S. *et al.* Glutathione and antioxidant enzymes serve complementary roles in protecting activated hepatic stellate cells against hydrogen peroxide-induced cell death. *Biochim. Biophys. Acta - Mol. Basis Dis.* **1832,** 2027–2034 (2013).
96. Lennicke, C., Rahn, J., Lichtenfels, R., Wessjohann, L. a & Seliger, B. Hydrogen peroxide - production, fate and role in redox signaling of tumor cells. *Cell Commun. Signal.* **13,** 39 (2015).
97. Schofield, Z. V., Woodruff, T. M., Halai, R., Wu, M. C. & Cooper, M. A. Neutrophils--A Key Component of Ischemia-Reperfusion Injury. *SHOCK* **40,** 463–470 (2013).
98. Ishikawa, M., Numazawa, S. & Yoshida, T. Redox regulation of the transcriptional repressor Bach1. *Free Radic. Biol. Med.* **38,** 1344–1352 (2005).
99. Rajasekaran, N. S., Firpo, M. a, Milash, B. a, Weiss, R. B. & Benjamin, I. J. Global expression profiling identifies a novel biosignature for protein

aggregation R120GCryAB cardiomyopathy in mice. *Physiol. Genomics* **35,** 165–72 (2008).
100. Bagaitkar, J. *et al.* NADPH oxidase controls neutrophilic response to sterile in fl ammation in mice by regulating the IL-1 a / G-CSF axis. **126,** 2724–2734 (2015).
101. Igusa, Y. *et al.* Loss of autophagy promotes murine acetaminophen hepatotoxicity. *J. Gastroenterol.* **47,** 433–443 (2012).
102. Chlebowski, A. C., La Du, J. K., Truong, L., Massey Simonich, S. L. & Tanguay, R. L. Investigating the application of a nitroreductase-expressing transgenic zebrafish line for high-throughput toxicity testing. *Toxicol. Reports* **4,** 202–210 (2017).
103. Curado, S. *et al.* Conditional targeted cell ablation in zebrafish: A new tool for regeneration studies. *Dev. Dyn.* **236,** 1025–1035 (2007).
104. Curado, S., Stainier, D. Y. R. & Anderson, R. M. Nitroreductase-mediated cell/tissue ablation in zebrafish: a spatially and temporally controlled ablation method with applications in developmental and regeneration studies. *Nat. Protoc.* **3,** 948–954 (2008).
105. Chuang, D. Y., Simonyi, A., Kotzbauer, P. T., Gu, Z. & Sun, G. Y. Cytosolic phospholipase A plays a crucial role in ROS/NO signaling during microglial activation through the lipoxygenase pathway. *J.Neuroinflammation.* **12,** 199 (2015).
106. Wang, D. *et al.* p21WAF1 and hypoxia/reoxygenation-induced premature senescence of H9c2 cardiomyocytes. *Folia Histochem. Cytobiol.* **49,** 445–451 (2011).
107. Baskin-Bey, E. S. *et al.* Clinical trial of the pan-caspase inhibitor, IDN-6556, in human liver preservation injury. *Am. J. Transplant.* **7,** 218–225 (2007).
108. Ravichandran, K. S. Find-me and eat-me signals in apoptotic cell clearance: progress and conundrums. *J. Exp. Med.* **207,** 1807–1817 (2010).
109. Lalaoui, N., Lindqvist, L. M., Sandow, J. J. & Ekert, P. G. The molecular relationships between apoptosis, autophagy and necroptosis. *Semin. Cell Dev. Biol.* **39,** 63–69 (2015).
110. Druskovic, M., Suput, D. & Milisav, I. Overexpression of caspase-9 triggers its activation and apoptosis in vitro. *Croat. Med. J.* **47,** 832–840 (2006).
111. Galán, A. *et al.* Modulation of the stress response during apoptosis and necrosis induction in cadmium-treated U-937 human promonocytic cells. *Biochim. Biophys. Acta - Mol. Cell Res.* **1538,** 38–46 (2001).
112. Scaffidi, P., Misteli, T. & Bianchi, M. E. Release of chromatin protein HMGB1 by necrotic cells triggers inflammation. *Nature* **418,** 191–195 (2002).
113. Szondy, Z., Sarang, Z., Kiss, B., Garabuczi, É. & Köröskényi, K. Anti-inflammatory mechanisms triggered by apoptotic cells during their clearance. *Front. Immunol.* **8,** (2017).
114. Gamble, J. R. & Vadas, M. A. Endothelial adhesiveness for blood neutrophils is inhibited by transforming growth factor-β. *Science (80-.).* **242,** 97–99 (1988).
115. Wahl, S. M. *et al.* Transforming growth factor type beta induces monocyte chemotaxis and growth factor production. *Proc. Natl. Acad. Sci. U. S. A.* **84,** 5788–92 (1987).
116. Gardai, S. J. Recognition ligands on apoptotic cells: a perspective. *J. Leukoc. Biol.* **79,** 896–903 (2006).
117. Birge, R. B. *et al.* Phosphatidylserine is a global immunosuppressive signal in efferocytosis, infectious disease, and cancer. *Cell Death Differ.* **23,** 962–978 (2016).
118. Krahling, S., Callahan, M. K., Williamson, P. & Schlegel, R. A. Exposure of

phosphatidylserine is a general feature in the phagocytosis of apoptotic lymphocytes by macrophages. *Cell Death Differ.* **6,** 183–189 (1999).
119. Szondy, Z., Sarang, Z., Kiss, B., Garabuczi, É. & Köröskényi, K. Anti-inflammatory mechanisms triggered by apoptotic cells during their clearance. *Frontiers in Immunology* (2017). doi:10.3389/fimmu.2017.00909
120. Chen, X. *et al.* Translocation of mixed lineage kinase domain-like protein to plasma membrane leads to necrotic cell death. *Cell Res.* **24,** 105–21 (2014).
121. Hildebrand, J. M. *et al.* Activation of the pseudokinase MLKL unleashes the four-helix bundle domain to induce membrane localization and necroptotic cell death. *Proc. Natl. Acad. Sci.* **111,** 15072–15077 (2014).
122. Dondelinger, Y. *et al.* MLKL Compromises Plasma Membrane Integrity by Binding to Phosphatidylinositol Phosphates. *Cell Rep.* **7,** 971–981 (2014).
123. Ghasemzadeh, M. & Hosseini, E. Intravascular leukocyte migration through platelet thrombi : directing leukocytes to sites of vascular injury. 1224–1235 (2015).
124. Singhal, R., Ganey, P. E. & Roth, R. a. Complement activation in acetaminophen-induced liver injury in mice. *J. Pharmacol. Exp. Ther.* **341,** 377–85 (2012).
125. Carbone, F., Nencioni, A., Mach, F., Vuilleumier, N. & Montecucco, F. Pathophysiological role of neutrophils in acute myocardial infarction. **2005,** 501–514 (2013).
126. Prabhu, S. D. & Frangogiannis, N. G. The Biological Basis for Cardiac Repair After Myocardial Infarction. *Circ Res* **119,** 91–112 (2016).
127. Marchetti, C. *et al.* Pharmacologic inhibition of the NLRP3 inflammasome preserves cardiac function after ischemic and non-ischemic injury in the mouse. *J Cardiovasc Pharmacol* **66,** 1–8 (2015).
128. Freeman, L. *et al.* NLR members NLRC4 and NLRP3 mediate sterile inflammasome activation in microglia and astrocytes. *J. Exp. Med.* **214,** 1351–1370 (2017).
129. Friedman, S. L. Hepatic Stellate Cells: Protean, Multifunctional, and Enigmatic Cells of the Liver. *New York* **88,** 125–172 (2010).
130. Giampieri, M. P., Jezequel, A. M. & Orlandi, F. The lipocytes in normal human liver. A quantitative study. *Digestion* **22,** 165–169 (1981).
131. Winau, F., Quack, C., Darmoise, A. & Kaufmann, S. H. Starring stellate cells in liver immunology. *Curr. Opin. Immunol.* **20,** 68–74 (2008).
132. White, R. M. *et al.* Transparent adult zebrafish as a tool for in vivo transplantation analysis. *Cell Stem Cell* **2,** 183–189 (2008).
133. Vliegenthart, A. D. B., Tucker, C. S., Del Pozo, J. & Dear, J. W. Zebrafish as model organisms for studying drug-induced liver injury. *Br. J. Clin. Pharmacol.* **78,** 1217–1227 (2014).
134. Nadanaciva, S. *et al.* Toxicity assessments of nonsteroidal anti-in fl ammatory drugs in isolated mitochondria , rat hepatocytes , and zebra fi sh show good concordance across chemical classes. *Toxicol. Appl. Pharmacol.* **272,** 272–280 (2013).
135. Cox, A. G. *et al.* Selenoprotein H is an essential regulator of redox homeostasis that cooperates with p53 in development and tumorigenesis. *Proc. Natl. Acad. Sci. U. S. A.* **113,** E5562–E5571 (2016).
136. Nissim, S. *et al.* Iterative use of nuclear receptor Nr5a2 regulates multiple stages of liver and pancreas development. *Dev. Biol.* **418,** 108–123 (2016).
137. Zhu, Q.-L. *et al.* Heat indicators of oxidative stress, inflammation and metal transport show dependence of cadmium pollution history in the liver of female zebrafish. *Aquat. Toxicol.* **191,** 1–9 (2017).

138. Gray, C. *et al.* Simultaneous intravital imaging of macrophage and neutrophil behaviour during inflammation using a novel transgenic zebrafish. *Thromb. Haemost.* **105,** 811–819 (2011).
139. Mathias, J. R., Zhang, Z., Saxena, M. T. & Mumm, J. S. Enhanced Cell-Specific Ablation in Zebrafish Using a Triple Mutant of Escherichia Coli Nitroreductase. *Zebrafish* **00,** 1–13 (2014).
140. Shimizu, Y., Ito, Y., Tanaka, H. & Ohshima, T. Radial glial cell-specific ablation in the adult Zebrafish brain. *Genesis* **53,** 431–439 (2015).
141. Siegerist, F., Blumenthal, A., Zhou, W., Endlich, K. & Endlich, N. Acute podocyte injury is not a stimulus for podocytes to migrate along the glomerular basement membrane in zebrafish larvae. *Sci. Rep.* **7,** 43655 (2017).
142. Edwards, D. I. Nitroimidazole drugs--action and resistance mechanisms. II. Mechanisms of resistance. *J. Antimicrob. Chemother.* **31,** 201–210 (1993).
143. Siegerist, F., Zhou, W., Endlich, K. & Endlich, N. 4D in vivo imaging of glomerular barrier function in a zebrafish podocyte injury model. *Acta Physiol.* **220,** 167–173 (2017).
144. Byun, J. S. & Yi, H. S. Hepatic Immune Microenvironment in Alcoholic and Nonalcoholic Liver Disease. *Biomed Res. Int.* **2017,** (2017).
145. Zhang, C., Ellis, J. L. & Yin, C. Inhibition of vascular endothelial growth factor signaling facilitates liver repair from acute ethanol-induced injury in zebrafish. *Dis. Model. Mech.* **9,** 1383–1396 (2016).
146. Matsumoto, K., Yoshitomi, H., Rossant, J. & Zaret, K. S. Liver organogenesis promoted by endothelial cells prior to vascular function. *Science (80-.).* **294,** 559–63 (2001).
147. Tuma, D. J. & Casey, C. A. Dangerous byproducts of alcohol breakdown--focus on adducts. *Alcohol Res. Health* **27,** 285–90 (2003).
148. Mugoni, V., Camporeale, A. & Santoro, M. M. Analysis of oxidative stress in zebrafish embryos. *J. Vis. Exp.* 1–11 (2014). doi:10.3791/51328
149. Cheng, M. L., Lu, Y. F., Chen, H., Shen, Z. Y. & Liu, J. Liver expression of Nrf2-related genes in different liver diseases. *Hepatobiliary Pancreat. Dis. Int.* **14,** 485–491 (2015).
150. Vojtech, L. N., Scharping, N., Woodson, J. C. & Hansen, J. D. Roles of inflammatory caspases during processing of zebrafish interleukin-1β in Francisella noatunensis infection. *Infect. Immun.* **80,** 2878–2885 (2012).
151. Ellett, F., Pase, L., Hayman, J. W., Andrianopoulos, A. & Lieschke, G. J. Mpeg1 Promoter Transgenes Direct Macrophage-Lineage Expression in Zebrafish. *Blood* **117,** 49–57 (2011).
152. Kim, H. C. *et al.* Oxidative damage causes formation of lipofuscin-like substances in the hippocampus of the senescence-accelerated mouse after kainate treatment. *Behav. Brain Res.* **131,** 211–220 (2002).
153. Forrester, A. M., Berman, J. N. & Payne, E. M. Myelopoiesis and myeloid leukaemogenesis in the zebrafish. *Adv. Hematol.* **2012,** (2012).
154. Hall, C., Flores, M., Storm, T., Crosier, K. & Crosier, P. The zebrafish lysozyme C promoter drives myeloid-specific expression in transgenic fish. *BMC Dev. Biol.* **7,** 1–17 (2007).
155. Al-Banna, N. A. *et al.* Impact of antibiotics on the microcirculation in local and systemic inflammation. *Clin. Hemorheol. Microcirc.* **53,** 155–169 (2013).